1970

Combined Differential Faraday Rotation And Differential Absorption Measurements Of The Ionosphere

Charles Edward Livingstone

Recommended Citation

Livingstone, Charles Edward, "Combined Differential Faraday Rotation And Differential Absorption Measurements Of The Ionosphere" (1970). *Digitized Theses*. 426.
https://ir.lib.uwo.ca/digitizedtheses/426

COMBINED DIFFERENTIAL FARADAY ROTATION AND DIFFERENTIAL ABSORPTION MEASUREMENTS OF THE IONOSPHERE

by

Charles Edward Livingstone

Department of Physics

Submitted in partial fulfillment
of the requirements for the degree of
Doctor of Philosophy

Faculty of Graduate Studies
The University of Western Ontario
London, Canada
August 1969

ABSTRACT

Differential Faraday rotation measurements were made at 40, 41 MHz using a continuous output polarimeter of the phase comparison type, and simultaneous differential absorption measurements were made using the ordinary and extraordinary mode amplitudes at 40 MHz.

Ionospheric electron contents were computed from an expansion of the Appleton-Hartree refractive index equation to second order in X as was the first nonlinear term of the expansion. Mean electron collision frequencies $\bar{\nu}$, $\bar{\nu}'$ were defined and computed using the amplitude and Faraday rotation data, as was a parameter sensitive to the relative heights of the electron density and absorption index centroids.

Three passes of satellite 1964, 64A/BE-B were examined in detail and, electron contents (using both first and second order theories), F region layer thickness changes, peak electron density changes, mean electron temperature changes, and the relative heights of the electron density and absorption index centroids were calculated over each pass. The maximum spatial

resolution of Faraday electron contents was also measured.

The first order Faraday theory was found to be inadequate in some cases for measurements of electron content irregularity intensities and horizontal scale sizes (as reported by Rao and Yeh, 1968).

Qualitatively increases in electron content were often associated with increases in F region thickness, decreases in peak electron density and decreases in F region electron temperature. The greatest changes in these parameters found in the three passes occurred on March 20, 1968 when an electron content increase of 7% was associated with an F region thickness increase by a factor of 2.1, a peak electron density decrease of 50%, and an electron temperature decrease of 20% over a horizontal distance of 72 km at F region altitudes.

The qualitative behavior of the ionosphere at such times is compatible with the theory of F region winds but there is insufficient data available from experiments of this kind to compute the required wind velocities without extensive model calculations.

The measured maximum spatial resolution for Faraday electron contents is ~ 1.4 km (at F region altitudes) with a safe estimate for normal interpretation of 2 km.

It is proposed that an ionosonde be acquired for use with experiments of this nature to provide much of the necessary auxiliary data required for F region wind velocity estimates.

ACKNOWLEDGEMENTS

The author would like to thank Dr. P. A. Forsyth, head of the Centre of Radio Science, for making available the facilities of the Centre and for his guidance as a member of the author's advisory committee. He would like to express his appreciation to Dr. J. A. Fulford for his advice on the design and construction of the receiving system used and for his criticism and advice as a member of the author's advisory committee, and he is indebted to Dr. D. R. Moorcroft for many helpful discussions of the theory involved in this work. He especially thanks his supervisor Dr. G. F. Lyon for his advice and guidance in formulating this problem and carrying it to completion. Many useful discussions with A. F. Dixon and Dr. F. H. Palmer are gratefully acknowledged. Many thanks are also due to his wife for helping with the preparation of the thesis diagrams and for her patience during the progress of this research, and to his mother for her assistance in typing the first draft of this thesis.

This work has been financed by the Defence Research Board of Canada, grant number 9511-58, with the author supported by a National Research Council scholarship.

TABLE OF CONTENTS

LIST OF FIGURES

CHAPTER 1

INTRODUCTION

(1.1) THE FARADAY EFFECT

In a neutral plasma containing a magnetic field the normal propagation mode refractive indices μ_x , μ_o (corresponding to left and right circular E.M. wave polarization for $\vec{k} \cdot \vec{H} > 0$), are unequal for waves whose propagation vector $\vec{k}$ has a component in the direction of the magnetic field $\vec{H}$ ($\vec{k} \cdot \vec{H} \neq 0$). If the wave source is linearly polarized and if $\vec{k} \cdot \vec{H} \neq 0$, the phase velocities $v_x = c/\mu_x$, $v_o = c/\mu_o$ (c is the speed of light in vacuo) of the normal modes are unequal and thus the wave's electric field vector (wave length λ) at some distance 's' along the propagation path will have rotated through an angle $\Omega = \frac{\pi}{\lambda} \int_0^s (\mu_x - \mu_o) ds$. This is the Faraday effect discovered in 1845 by M. Faraday and applied to ionic media in 1906 by H. A. Lorentz.

If both the wave source and the wave detector are linearly polarized, and if Ω , as seen at the detector, varies in time, the changes of the Faraday rotation angle in space and/or time will be observed as a time sequence of amplitude nulls.

The earth's ionosphere is such a plasma. Since the radio frequency refractive indices of the two ionospheric normal propagation modes are functions of the free electron and relatively heavy (as compared to the electrons) ion concentrations, the Faraday rotation of the wave polarization plane measured at the ground provides a measure of the free charge density along the propagation path. As the ionosphere is tenuous $N \sim 10^{15}/M^3$ (N is the approximate neutral particle number density at 300 km altitude) and weakly ionized $N_e, N_i \sim 10^{12}/M^3$; and as the earth's magnetic field intensity is small (B ~ 0.5 gauss); for radio wave frequencies greater than approximately 30 MHz, these radio frequencies are sufficiently different from the plasma resonance frequencies that:

(a) Only the effect of free electrons need be considered.

(b) The propagation paths are very nearly linear.

(c) The refractive index expressions may be used as first or second order expansions in the electron density and magnetic field intensity parameters X, Y_L.

As μ_x and μ_o are in principle different and as the ionosphere electron density-height profile has a pronounced peak, the ordinary, extraordinary mode propagation paths will in principle be different, although for sufficiently large wave frequencies their spatial separation will be small.

(1.2) THE EVOLUTION OF FARADAY ROTATION MEASUREMENTS OF THE IONOSPHERE TOTAL ELECTRON CONTENT

The regular, long period (~ 1 hr.) fading of radar transmissions scattered from the moon was first interpreted as a Faraday rotation phenomenon in 1954 (Murray and Hargreaves, 1954). Subsequent experiments using two frequencies (119, 120 MHz) led to the use of the differential polarization fading with the high frequency, quasi longitudinal approximations to the Appleton Hartree equation to measure the total electron content between the earth and the moon (Brown et al., 1956; Evans, 1957). The very slow polarization plane rotation rate and the moon scatter geometry, however, precluded observations of rapid variations in the total electron content of the ionosphere by this method.

With the launching of the first artificial satellite (1957 α 1) a transmitter was available for the first time which traversed the field of view of a ground observation point quickly and returned at short, regular intervals.

Faraday rotation angle measurements made with a single frequency transmission are ambiguous to the order $n\pi$. Several early attempts were made to minimise this ambiguity and so obtain reliable electron content measurements. These fall into two categories:

(a) total rotation angle estimates from ground rotation angle measurements (Bowhill, 1958; Blackband et al., 1959) and (b) total electron content estimates from rotation rate measurements (Aitchison and Weekes, 1959).

Since the satellite transmission frequencies used (20, 40 Mhz) were considerably lower than those employed in the moon-radar experiments (120 MHz), the application of the high frequency and linear ray path approximations developed for radar content measurements (Brown et al., 1956) were suspect.

In 1960 a data reduction method was developed which combined Faraday null measurements with ionosonde data in a model ionosphere ray trace computation to estimate the total electron content of the ionosphere, estimate ray refraction effects in the ionosphere and minimise the single frequency Faraday $n\pi$ ambiguity. A refinement of this approach (Garriot, 1960) employed the ray proximal point (point of closest approach to quasi transverse propagation) to minimise the $n\pi$ ambiguity and examined the contributions of the ordinary-extraordinary mode ray path splitting to the columnar integrated electron content.

The use of model ionosphere ray traces for ray refraction correction was later eliminated from Faraday rotation data reduction by a computation technique involving measurements at two widely spaced frequencies (Yeh, 1960; Yeh and Swenson, 1961).

Studies of the magnetic field dependence of (Yeh and Gonzalez, 1960; Roger, 1964) established the replacement of the ray path integral of the magnetic field parameter Y_L ,

$$(1\text{-}1) \qquad \tilde{M} = \frac{f \int N \sec(i) \, Y_L \, dh}{K_2 \int N \, dh}$$

by $\tilde{M} = |H| \cos(\theta) \sec(i)$ evaluated near h = 350 km in column integrated electron content computation from Faraday data.

The symbols used above are defined below.

f	is the wave frequency in Hz .
K_2	= 2.222 x 10^5 MKS is a constant.
h	is the height above the earth's surface in km.
θ	is the angle between the ray path and the earth magnetic field.
N	is the electron density $/M^3$.
i	is the angle between the ray path and the local earth normal.
H	is the strength of the earth magnetic field in AMP turns /M.
Y_L	$= \dfrac{K_2 H \cos(\theta)}{2\pi f}$.

The result of these studies was the general acceptance of the high frequency, linear ray path approximation of Browne et al. (1956) for Faraday electron content computations with signal frequencies greater than or equal to 40 MHz and satellite zenith angles less than 40°.

Total electron contents, measured simultaneously at the same ground station, using the three standard methods available in 1963;

(a) Single frequency Faraday rotation,

(b) Differential Doppler shifts,

(c) Hybrids of (a, b)

did not agree with each other to within the estimated experimental accuracies. To provide a basis for comparisons of contents derived from (a), (b), (c) an experiment was performed which employed all three simultaneously to transmissions from a single source and compared the results statistically as normalized to the method of greatest internal consistency (Garriot and de Mendonça, 1963). The result of greatest interest to this discussion was that the single frequency Faraday rotation technique over estimated the total electron content by approximately 10% as compared to differential Doppler dispersion measurements.

As early as 1960 some experimenters (Blackband, 1960; Little and Lawrence, 1960) advocated launching one or more satellites carrying two beacon transmitters with closely spaced frequencies (differential Faraday rotation measurements) as a means of eliminating the $n\pi$ rotation angle ambiguity. The satellites 1964, 64A/BE-B, 1965-32A/BE-C, in high and low inclination orbits respectively, carried continuous wave transmitters at 40, 41 MHz. Since their advent, differential Faraday rotation measurements have become a standard total electron content measurement method (Münther, 1966; Liszka, 1966; Rao, 1967; Rao and Yeh, 1968).

A second comparison of electron content measurements (Rao and Yeh, 1968) agrees in part with that of Garriot and de Mendonça (1963) in that the single frequency Faraday technique is less reliable than differential Doppler dispersion measurement by ~ 20%. In this experiment

(a) single frequency Faraday content measurements

(b) differential Faraday rotation measurements

(c) differential Doppler dispersion measurements

were made simultaneously using satellites BE-B, BE-C at times when the satellites arrived near the observation point within 20 minutes of each other. Detailed comparisons of the computed electron content profiles show good agreement between the differential Faraday and differential Doppler measurements of relative variations during a satellite pass and discrepancies of 5 to 10% in absolute content; but very poor correlations between single frequency Faraday results and either of the others.

Normally, Faraday rotation angle changes have been measured from the Faraday fading nulls of a linear dipole antenna. Thus the spatial resolution, of the computed electron contents, in the direction of satellite travel is, under ideal conditions, limited by the real time separations of the nulls. When the signal amplitude exhibits large amplitude scintillations, these can be in error by approximately 1/8 of a rotation. An early attempt to increase resolution by monitoring the relative phase of two circularly polarized antennas of opposite sense (Little and Lawrence, 1960) was defeated by the pulsed nature of the satellite transmissions then available. A later attempt to use the same method (Kushnir, 1966) was successful.

A second approach to the problem of increasing the Faraday electron content spatial resolution by increasing the data sampling rate involved the use of electronically rotated simple dipoles and measurements of the positions of the polarization nulls as compared to an antenna position marker (Rao, 1967).

(1.3) CHANGES IN ELECTRON DENSITY DISTRIBUTION CENTROID HEIGHT AND SOME PROPERTIES OF IONOSPHERIC ELECTRON CONTENT IRREGULARITIES

Although a spherically stratified ionosphere is so convenient for many model calculations, this condition is not normally found in practice. Local departures of the ionospheric electron density distribution from spherical stratification can take three basic forms:

(a) Large scale horizontal gradients ($\geqslant$ 600 km horizontal extent) (Roger, 1964; Lyon, 1965, Liszka, 1966; Munther, 1966; Rao, 1967; Rao and Yeh, 1968).

(b) Changes in shape of electron density profile and/or changes in electron density centroid height (Little and Lawrence, 1960; Yeh and Flaherty, 1966; Ross and Kuntman, 1967; Yuen, Roelofs and Young, 1969).

(c) Small scale gradients "irregularities" ($<$ 600 km horizontal extent) (Little and Lawrence, 1960; Kent, 1961; Singleton and Lynch, 1962; Titheridge, 1963; Roger, 1964; Liszka and Taylor, 1965; Titheridge, 1967).

We shall consider only the behaviour of electron density distribution and small scale irregularities [parts (b) and (c)].

(1.3.1) PROPERTIES OF THE ELECTRON DENSITY DISTRIBUTION

Little and Lawrence (1960), working with both ionosonde and Faraday rotation data in model ionosphere ray trace computations, found that for some satellite passes, the shape of the electron density distribution (the model) had to be altered during the course of the pass to fit all data. The best results were achieved when only the bottom side (below the F region peak) was adjusted.

Measurements of diurnal variation, seasonal variation, solar activity dependence and slab thickness of the ionosphere electron content as computed from Faraday data (Yeh and Flaherty, 1966) have suggested the use of an ionosphere electron density profile consisting of a diffusion-transport layer above a Chapman layer below the F region peak.

Such a model gives the best agreement between measured ionosphere slab thickness and F region temperature--it also has the property that a change in F region temperature produces a change in layer height which in turn (through $\bar{M}$) produces a change in the electron content as computed from Faraday data.

Investigations of ionospheric absorption of cosmic noise at 21, 25 MHz (Abdu, Degaonkar and Ramanathan, 1962; Degaonkar and Abdu, 1967; Abdu and

Degaonkar, 1967) have established a good statistical correlation between the ionosphere absorption coefficient "ρ" and the F region electron density N_F (in high sunspot number years the F region contribution to cosmic noise absorption at 25 MHz can be as high as 80%); and between absorption and F region temperature, $\rho \propto N_F T_e^{-3/2}$.

A combination of satellite Faraday rotation and differential Doppler dispersion measurements has been used to compute changes in the electron density profile centroid height (Ross and Kuntman, 1967). The magnetic field parameter $\bar{M}$ was calculated from a combination of Faraday and differential Doppler data, and the centroid height was inferred from the variations of $\bar{M}$ during a satellite pass. Relative height changes of 10% correlated with relative electron content variations of 10% in 20% of the records examined; centroid height changes of approximately 50 km can occur over less than 1° sub-satellite latitude for a satellite in a nearly polar orbit. This approach has very recently been extended by the use of ionosonde data to provide a correction to the total electron content computed from Faraday rotation measurements of geostationary satellite transmissions (Yuen, Roelofs and Young, 1969).

(1.3.2) PROPERTIES OF ELECTRON CONTENT IRREGULARITIES IN THE IONOSPHERE

Satellite radio frequency probe measurements of the properties of the ionospheric electron content irregularities have been performed and reported in the literature since 1960 (Little and Lawrence, 1960).

Those properties of particular interest here are: horizontal scale size, intensity (peak irregularity electron content as a fraction of the background), and height distributions.

For irregularities with horizontal scale sizes between 10 km and 400 km, Faraday rotation studies (Titheridge, 1963; Titheridge, 1968) have established that:

(a) 92% of the irregularities measured have columnar electron content between 0.1% and 10% of the ionospheric columnar electron content.

(b) The median values of electron content in each size interval in the range 10-400 km are proportional to the horizontal scale size of the irregularity.

(c) There is no statistically preferred size.

(d) There is no apparent elongation of these irregularities along the magnetic field lines.

(e) In the top-side ionosphere the number density of irregularities at a given height is proportional to the electron number density at that height.

(f) There is no apparent scale size-height relation.

In these investigations Titheridge used the amplitude null method of Faraday rotation measurement and thus the smallest measurable irregularity size is determined by the minimum Faraday null spacing at 20 MHz.

Observations of irregularities with horizontal scale sizes smaller than 10 km have been made by a number of experimenters using a wide variety of measurement techniques, two of which are: top-side sounder observations (Muldrew, 1963; Dyson, 1966) and amplitude scintillation measurements (Kent, 1961; Singleton and Lynch, 1961; Parkin, 1967; Kaiser and Predy, 1968; Allen, 1967).

A partial list of the properties of this group of irregularities is given below.

(a) Horizontal scale size $\gg$ 0.4 km (Singleton and Lynch, 1961; Parkin, 1967).

(b) Electron content enhancements range from $\sim$1% (Muldrew, 1963) to 25% (Booker, 1963--as quoted by Muldrew) of the background.

(c) The irregularities are field aligned with axial ratios ranging from 2:1 to 20:1 (Kent, 1961; Parkin, 1967) and a mean axial ratio of 6:1 [the mean axial ratio has been more recently estimated at 15:1 (Dixon, 1969)].

(d) Those electron density irregularities that produce scintillation on 40 MHz transmissions are most commonly found between approximately 200 km and 700 km (Dyson, 1967; Allen, 1967; Kaiser and Predy, 1968). The heights of most frequent occurrence lie between 350 km and 400 km (Kaiser and Predy, 1968; Allen, 1967).

(1.4) THE PRESENT INVESTIGATION

This experiment has been designed to achieve a three-fold objective:

(a) To obtain accurate total electron content measurements by applying differential Faraday rotation analysis to the 40, 41 MHz beacon transmissions of the satellite 1964-64A/BE-B as received in London, Ontario (43^{o}N, 81^{o}W).

(b) To determine experimentally the limit of horizontal, spatial resolution of Faraday electron content measurements at 40 MHz.

(c) To study changes in the electron density-collision frequency centroid height using amplitude measurements of the two circularly polarized components of the 40 MHz transmissions and the total Faraday rotation angles of the 40, 41 MHz transmissions.

To permit resolution of the Faraday $n\pi$ ambiguity, the changes in Ω were measured at two closely spaced frequencies (40, 41 MHz). To achieve the maximum possible spatial resolution, the changes in Ω were measured in terms of the relative phase of the two circular components of the incoming linearly polarized waves. That is, the suggestions of Little and Lawrence

(1960), and Kushnir (1966) were implemented. The equipment design used to achieve this yields the data required in part c as a by-product.

Electron content irregularities in the ionosphere have been observed with all horizontal scale sizes from 0.4 km to 1000 km (section 1.3.2). Since the two circularly polarized components of a linearly polarized wave propagate through the ionosphere along separate ray paths (section 1.1), the relative time displacements of the amplitude scintillations seen on the two components were used to estimate the ray path separations ($\geqslant$ 0.4 km) and thus the maximum spatial resolution of the Faraday electron contents in the direction of satellite travel.

Generalising the results of Abdu et al., and Yeh and Flaherty (section 1.3.1) it is in principle possible to estimate changes in electron density centroid heights from measurements of ionospheric absorption of VHF signals and of electron content.

When the results of Ross and Kuntman (section 1.3.3) are generalized, it is possible to use a combination of two measurements of the same ionospheric parameters--both dependent on the electron content but only one dependent on the electron density centroid height, to estimate changes in the centroid height during a satellite. In this experiment a mean collision frequency is defined and variations in its centroid heights are examined.

CHAPTER 2

THEORY AND EXAMINATION OF APPROXIMATIONS

(2.1) TABLE OF SYMBOLS

η - complex refractive index of a plasma containing a magnetic field.

μ, χ - real and imaginary parts of η .

ν - Appleton Hartree collision frequency [mean electron collision frequency (Ratcliff, 1959)].

θ - the angle between the signal ray path and the earthmagnetic field vector.

i - the angle between the signal ray path at some point in space and the earth normal through that point.

e - unit of electronic charge

m_e - mass of an electron

c - speed of light in vacuuo

ϵ_0 - dielectric permitivity of free space

$\vec{H}$ - the earth's magnetic field vector in amp turns

N - the ionosphere electron number density.

$\omega = 2\pi f$ - the wave angular frequency.

λ - the free space wavelength of an E. M. wave.

μ_0 - the magnetic permeability of free space.

$$K_1 = \frac{e^2}{\epsilon_0 m_e} = 3.218 \times 10^3 \text{ MKS}$$

$$K_2 = \frac{\mu_0 e}{m_e} = 2.222 \times 10^5 \text{ MKS}$$

$$X = \frac{K_1 N}{\omega^2}$$

$$Y_L = \frac{K_2 H \cos(\theta)}{\omega}$$

$$Y_T = \frac{K_2 H \sin(\theta)}{\omega}$$

$$Z = \frac{\nu}{\omega}$$

$$K = 0.0297 \text{ MKS}$$

(2.2) THE QUASI-LONGITUDINAL, HIGH FREQUENCY APPROXIMATION TO THE APPLETON-HARTREE REFRACTIVE INDEX EQUATION

The general Appleton-Hartree refractive index equation for an E. M. wave propagating in a neutral plasma containing a magnetic field is:

$$\eta^2 = (\mu + i\chi)^2 = 1 - \frac{X}{1 - iZ - \frac{1}{2}\frac{Y_T^2}{1-X-iZ} \pm \left[\frac{1}{4}\frac{Y_T^4}{(1-X-iZ)^2} + Y_L^2\right]^{\frac{1}{2}}} \tag{2-1}$$

As the complete expression is too complex to use comfortably in data reduction, it is in order to examine the relative magnitudes of each of the variables to simplify it to a manageable form.

Since the earth's ionosphere is tenuous and weakly ionized (section 1.1) and since the wave frequencies 40, 41 MHz are large $\nu \ll \omega$, or the term Z is effectively 0, in those parts of the ionosphere where the electron density is considerable, the refraction and absorption effects may be considered separately. If by $\nu \ll \omega$ we mean $\nu \lesssim 0.01\,\omega$, $\nu \lesssim 2.5 \times 10^6$/sec which corresponds to ionospheric heights of approximately 80 km (Thrane and Piggot, 1966) and ionospheric electron densities of the order of $10^9/M^3$ (a factor of ~ 1000 below F maximum). The ionosphere may be treated as a collisionless plasma for refraction effects.

For $\theta < 80^\circ$, $Y_T^4 \ll Y_L^2$, $Y_T^2 \ll 1$; the quasi longitudinal approximation is valid. At London, Ontario

(43°N, 81°W), and within the receiving cone for polarimeter output analysis, θ is smaller than 60°. Thus $\frac{Y_T^2}{Y_L} \leqslant \frac{K_2 H \sin^2(\theta)}{\omega \cos(\theta)} = 1.56 \frac{K_2 H}{\omega}$, for $\theta = 60^{\circ}$. From a 48 term spherical harmonic analysis of the earth's magnetic field, $\frac{K_2 H}{\omega} \leqslant .04$ at 100 km altitude, or $Y_T^2 \leq 0.062 Y_L$, or $Y_T^4 \ll Y_L^2$. As $Y_L \leq 0.04$, Y_T^2 is indeed much smaller than 1.0.

Thus, for computation of phase path lengths through the ionosphere η^2 may be considered real-- $\eta^2 \approx \mu^2$ and for sufficiently small X, μ becomes:

$$\text{(2-2)} \quad \mu_{\pm} = \sqrt{1 - \frac{X}{1 \pm Y_L}}$$

There are two normal propagation modes in the ionosphere at 40 MHz--the ordinary mode (+ sign) and the extraordinary mode (- sign) (Ratcliffe, 1959, p. 70, p. 75).

(2.3) FARADAY ROTATION

As was mentioned in section (1.1), the Faraday rotation of the polarization plane of a radio wave propagating through the ionosphere may be expressed as the difference of the phase paths of the two normal propagation modes, as measured from the source. This, in integral notation is:

$$\Omega = \frac{\pi}{\lambda} \int_0^s (\mu_o - \mu_x)\, ds \tag{2-3}$$

where the integral is computed along the mean ray path.

Upon insertion of the appropriate refractive index expressions (Equation 2-2) into (2-3) we have

$$\Omega = \frac{\pi}{\lambda} \int_0^s \left(\sqrt{1 - \frac{X}{1+Y_L}} - \sqrt{1 - \frac{X}{1-Y_L}} \right) ds$$

Expanding this integral as a power series in X, Y_L,

$$\Omega = \frac{\pi}{\lambda} \int_0^s X Y_L \left(1 + \frac{X}{2}\right) ds \tag{2-4}$$

plus terms of higher order in X, Y_L (also Yeh, 1960).

When $X \ll 1$, $Y_L \ll 1$ the higher order terms may be neglected. Under most ionospheric conditions $f_o F_2 < 11$ Mhz or $X_{MAX} < .073$ ("Canadian ionospheric data" 1968--Ottawa) and at London, Ontario $Y_{L\,MAX} \leq 0.04$. Thus, the approximation is valid.

If the condition $\frac{X^2}{2} \ll X$ holds, the first order Faraday rotation approximation is

$$\Omega = \frac{\pi}{\lambda} \int_0^s X Y_L\, ds \tag{2-5}$$

When the ray paths of the ordinary and extraordinary waves in the ionosphere are approximately linear and when the X^2 term in the expansion of may be neglected

(2-6) $\int_0^{h_s} N\,dh = \frac{\Omega f^2}{K \bar{M}}$, where $\bar{M}$

is defined in section 1.2, Equation (1-1).

This is the high frequency, linear ray path assumption of Browne et al. (1956). A ray trace computation--Appendix B--verifies the linear ray path assumption at 40 MHz for an undisturbed ionosphere under the conditions found on March 23, 1968 at London (f_oF_2 = 10.4 MHz) to within the computation error in the satellite slant range.

When Faraday rotation angle measurements are available at two frequencies, f and mf, the columnar electron content may be computed from the second order expansion of Ω in X, Y_L. Using Equation (2-4) and considering a plane stratified ionosphere, we have:

(2-7) $\int_0^{h_s} N\,dh = \frac{f^2}{K\bar{M}(m^2-1)}\left\{m^4\Omega(mf) - \Omega(f)\right\} = \frac{f^2}{K\bar{M}\rho(\Omega)}$

(Yeh, 1960, Yeh and Swenson, 1961). This result is more general than Equation (2-6) as it eliminates all terms in $\frac{1}{f^4}$, that is, the second order terms of the expansion of Ω in X. Thus in a spherically stratified ionosphere, and over a range of zenith angles for which the error in the plane ionosphere assumption is smaller than the error incurred in neglecting the second order terms, Equation (2-7) is applicable. Let us define a plane stratified ionosphere to be that portion of a spherically stratified ionosphere, over which the maximum error in the satellite slant range produced by the plane ionosphere assumption is of the order of 1% (the approximate expected error in the satellite slant range).

Then, if h_s is the mean satellite height above the earth's surface, and if ζ is the zenith angle of the satellite as seen from the receiving station, for a linear ray path in a plane stratified ionosphere, $R_p = \frac{h_s}{\cos(\zeta)}$. The satellite position, including the slant range R_s , is computed by an interpolation technique from orbital elements, provided by U.S.A.F.C.R.L., Boston, Massachussets. Our plane ionosphere criterion now becomes

$$\text{(2-8)} \qquad \frac{R_p - R_s}{R_s} \leqslant 0.01$$

which corresponds to satellite zenith angles lying within a zenith cone of half angle 30°. Relaxing this condition to $\frac{R_p - R_s}{R_s} \leqslant 0.02$ expands the half angle of the zenith cone to 35°.

When the two transmitted frequencies are closely spaced ($f_2 - f_1 \ll f_1 , f_2$), the ray paths are nearly identical if the high frequency approximation is valid, and the relations

$$\text{(2-9)} \quad \Omega_2 = (\Omega_2 - \Omega_1) \frac{f_1^2}{f_2^2 - f_1^2} , \quad \Omega_1 = (\Omega_2 - \Omega_1) \frac{f_2^2}{f_2^2 - f_1^2}$$

hold for the first order Faraday approximations. Now, comparing the measured changes in Ω_1 , Ω_2 on the ground, the total rotation angles Ω_{1T} , Ω_{2T} when the relative separation of Ω_1, Ω_2 is $n\pi$ are ambiguous to $\frac{n f_2^2 \pi}{f_2^2 - f_1^2}$, $\frac{n f_1^2 \pi}{f_2^2 - f_1^2}$ respectively where is an integer, and

$$(2\text{-}10) \quad \Omega_{1T} = \frac{n f_2^2 \pi}{f_2^2 - f_1^2} \qquad \Omega_{2T} = \frac{n f_1^2 \pi}{f_2^2 - f_1^2}$$

(At this point, the first and second order contents are equal.) This ambiguity is usually easily resolved. As the rotation angle coincidence conditions given in Equation (2-10) are strictly valid only for the first order Faraday computation, to make use of Equation (2-7) it is necessary to examine their relevance to the second order content calculation.

From Equations (2-4) and (2-6) the first order content overestimates the ionosphere total electron content by $\beta = \frac{f K_2}{2K\lambda} \int_0^{h_s} X^2 \, dh$. Applying the rotation coincidence conditions [Equation (2-10)] to the second order content Equation (2-7) we find that both the first and second order content estimates are identical at a coincidence point. As there is no physical reason for β to vanish at the point, we conclude that the conditions 2-10 are not applicable to the second order content calculations. Consider Equation (2-4) written in modified form with $\frac{\pi}{\lambda} \int_0^{s} X Y_L \, ds$ replaced by $\frac{K}{f^2} \breve{M} c_T = \frac{a}{f^2} c_T$

and $\frac{\pi}{2\lambda}\int_0^s x^2 Y_L \, ds$ replaced by $\frac{K \bar{M} K_2}{2 f^2 \omega^2}\delta = \frac{b}{f^4}\delta$, $\Omega = \frac{a}{f^2} C_T + \frac{b}{f^4}\delta$. Then for two frequencies, f_1 , f_2

$\Omega_1 = \frac{a}{f_1^2} C_T + \frac{b}{f_1^4}\delta$ and $\Omega_2 = \frac{a}{f_2^2} C_T + \frac{b}{f_2^4}\delta$

At an Ω_1 , Ω_2 coincidence point, we still have $\Omega_1 - \Omega_2 = n\pi$ and by analogy with the first order case we may write $\Omega_1 = \alpha n \pi$, $\Omega_2 = \gamma n \pi$ but due to the non "o" value of δ, $\alpha < \frac{f_2^2}{f_2^2 - f_1^2}$, $\gamma < \frac{f_1^2}{f_2^2 - f_1^2}$. It is evident, from the expressions for Ω_1 , Ω_2 that to produce a mathematical condition equivalent to (2-10) additional information is required (e.g., the shape of the electron density profile). However, as $\frac{b}{f^4}\delta \ll \frac{a}{f^2} C_T$ ($\frac{b}{f^4}\delta < 0.05 \frac{a}{f^2} C_T$ from the model), the parameters α , γ will not differ by more than 10% from their first order counterparts. Thus, if n is found from the first order case, and if the relative values of Ω are available at each point when $\Omega_1 - \Omega_2 = m\frac{\pi}{2}$ (m is an integer)

$\Omega_1^{(m+1)} - \Omega_1^{(m)} = \alpha\frac{\pi}{2}$, $\Omega_2^{(m+1)} - \Omega_2^{(m)} = \gamma\frac{\pi}{2}$

and the total Ω_1 , Ω_2 are known with reasonable accuracy for the entire record if mean values of α , γ are computed for the data.

Since Equation (2-7) is linear in Ω the use of the first order estimates of the total Ω_1 , Ω_2 may be used to compute the relative variations in $\int_0^{h_s} N dh$ for the pass and a correction for δ may then be computed to set the absolute value.

At a coincidence point $\Omega_1 = \alpha n \pi$, $\Omega_2 = \gamma n \pi$ where n, α, γ are known, solving for C_T we have

$$(2\text{-}7a) \quad C_T = \int_0^{h_s} N\,dh = \frac{f^2 n \pi}{K \bar{M}\,(m^2-1)} \left[m^4 \gamma - \alpha \right]$$

In addition to an error of β in the first order contents, a second error arises from the neglect of the second order terms in the derivation of Equations (2-10). This produces an over estimate of the total rotation angle by an amount $\delta\Omega$ determined by a comparison of Equations (2-10) with $\Omega_1 = \alpha n \pi$ and $\Omega_2 = \gamma n \pi$ (2-10a).

(2.4) THE MAXIMUM SPATIAL RESOLUTION OF FARADAY ELECTRON CONTENTS

For the case of a satellite transmitting a signal through an inhomogenous ionosphere to a ground station, the wave $\vec{E}$ as seen at the ground will be the resultant of the unscattered wave $\vec{E}$ and of all the electric fields of all waves scattered from electron density irregularities.

The observed Faraday rotation angle is the amplitude weighted mean of all polarization plane rotation angles of all the received waves.

The normal result at 40 MHz is that the perturbations of Ω due to waves scattered from electron density irregularities is small.

The ideal situation, then, is the case where the perturbation in the Faraday rotation angle due to scattering from ionospheric irregularities is small. This is the situation normally found in the ionosphere for 40 MHz transmissions.

From Fermat's principle, a ray path is defined as that propagation in path along which $\int_0^s \mu ds$ is stationary with respect to small variations transverse to $\vec{ds}$. Thus a ray may be considered to be the space grouping of all such paths of nearly equal phase-path length. Expressing this in terms of Fresnel zones, a ray will be defined to be a tube whose radius at range R is the radius of the first Fresnel zone ($r_F \approx \sqrt{\frac{R\lambda}{2}}$ for satellite transmissions). The condition that we have described previously corresponds to a single ray traversing the ionosphere. Because of the finite radius of a ray, the effective spatial resolution of the Faraday electron content determinations in the direction of satellite motion will be limited to distances of the order of one Fresnel zone radius.

For a satellite near the receiving station zenith, we expect to see a spatial resolution ranging from > .87 km near 200 km range to > 1.6 km near 700 km range which corresponds to the size of small irregularities found at these altitudes (section 1.3.2).

The ionosphere, as well as being inhomogenous (section 1.3.2) is also anisotropic (sections 1.1, 2.2, 2.3). Thus the two normal propagation modes traverse the ionosphere along different propagation paths. If the spatial resolution of the Faraday technique is considered in terms of the ordinary, extraordinary mode ray centers, near the ground station zenith, for a "quiet" inosphere (Appendix B), ray separations of the order of .2 km are computed at 200 km altitude and of the order of 0.05 km at 700 km altitude.

Combining the ray separations with the ray radius estimates, the maximum horizontal resolution of the Faraday electron contents will be of the order of 1 km to 2 km at F region altitudes. The ray paths sweep across the 350 km height shell at speeds of the order of 2 km/sec, this corresponds to phase scaling intervals of no less than 0.5 to 1.0 seconds.

(2.5) DIFFERENTIAL ABSORPTION

The design of the present experiment permits measurement of the ordinary and extraordinary mode amplitudes at 40 MHz as well as the Faraday rotation angles at 40, 41 MHz (section 1.4).

Let us now examine the Appleton-Hartree absorption index equation (Ratcliffe, 1959) to derive the absorption relations between the ordinary and the extraordinary propagation modes in the ionosphere.

When $\nu \ll \omega$ the absorption index is

$$(2\text{-}11) \qquad \kappa_{\substack{o\\x}} = \frac{\nu}{2c\,(1 \pm Y_L)} \left\{ \frac{1}{\mu_{\substack{o\\x}}} - \mu_{\substack{o\\x}} \right\}$$

where the subscripts o , x denote the ordinary, extraordinary modes respectively.

On application of the "quasi longitudinal" approximation this becomes:

$$\kappa_{\substack{o\\x}} = \frac{\nu X}{2c\,(1 \pm Y_L)^{3/2}\,(1 \pm Y_L + X)^{1/2}}$$

Expanding $\kappa_{\substack{o\\x}}$ as a power series in X, Y_L, ν (Jolley, 1961, p. 34), and applying the high frequency approximation (neglect all terms of order ≥ 3 in X, Y_L) we have

$$(2\text{-}12) \qquad \kappa_{\substack{o\\x}} = \frac{\nu X}{2c}\left(1 \pm 2Y_L + \frac{X}{2}\right)$$

Consider now the power input to the receiver from the ordinary and the extraordinary modes of a 40 MHz transmission.

$$P_o = \frac{\alpha P'}{R^2} f(\Omega, \eta, \xi)\, g_o(\varphi, \lambda, H)\, e^{-2\int_0^s \kappa_o\, ds} \qquad (2\text{-}13)$$
$$P_x = \frac{\beta P'}{R^2} f(\Omega, \eta, \xi)\, g_x(\varphi, \lambda, H)\, e^{-2\int_0^s \kappa_x\, ds}$$

where:

P_o, P_x are respectively the ordinary and extraordinary mode power inputs to the receiver.

α, β antenna system gains (including preamplifier gains and transmission line losses).

$\frac{P'}{R^2}$ is the power transmitted from satellite into the acceptance cone of the antenna (R is the satellite slant range).

Ω is the Faraday rotation angle at the ground.

η is the ray azimuth from geographic north.

ξ is the ray elevation angle.

φ, λ, H are the coordinates of a point in the ionosphere in N latitude, W longitude and height above the earth in km.

The function $f(\Omega, \eta, \xi)$ contains the antenna effect on the signal amplitude at the ground (Appendix A).
The functions g_o, g_x describe the diffraction patterns on the ground produced by small scale ($\sim$ 1 km) irregularities in the ionosphere.

If (a) the absorption within these irregularities does not differ appreciably from that of the quiet ionosphere, and (b) the back scatter efficiency of the irregularities is small (the peak electron density within the irregularity still leaves $X \ll 1$) the averages of g_o, g_x over the earth's surface is approximately 1.0. Thus the g_o, g_x functions may be neglected for suitably averaged data.

After removing the dependence of the received power on R, f, g_o, g_x we have

$$(2\text{-}14) \quad P_o' = \frac{\overline{P_o} \; R^2}{f(\Omega,\eta,\xi)} = \alpha p' e^{-\frac{1}{c}\int_0^s \nu X(1+\frac{X}{2}+2Y_L)ds}$$

$$(2\text{-}15) \quad P_x' = \frac{\overline{P_x} \; R^2}{f(\Omega,\eta,\xi)} = \beta p' e^{-\frac{1}{c}\int_0^s \nu X(1+\frac{X}{2}-2Y_L)ds}$$

If we define $\bar{\nu}$ and $\overline{\nu'}$ by

$$(2\text{-}16) \quad \bar{\nu} = \frac{\int_0^s \nu X(1+\frac{X}{2})ds}{\int_0^s X(1+\frac{X}{2})ds}$$

and

$$(2\text{-}17) \quad \overline{\nu'} = \frac{\int_0^s \nu X Y_L ds}{\int_0^s X Y_L ds}$$

we have two measures of an average collision frequency, one dependent on ν, X only and the other dependent on ν, X, Y_L .

By analogy with the definition of $\overline{M}$ (Equation 1-1) we may now interpret $\bar{\nu}$, $\overline{\nu'}$ as being collision frequencies at the height of the centroid of the absorption index profile. (The height of the center of an equivalent slab ionosphere which has constant absorption $\frac{d\chi}{dh} = 0$.)

From Equations (2-4), (2-14), (2-15), and (2-16) we have

$$(2\text{-}18)\quad \bar{\nu} = \frac{K_2 \bar{M}}{4 \sec(I)} \ln\left(\frac{\alpha\beta P'^2}{P_0' P_x'}\right) \frac{1}{\Omega}$$

From Equations (2-7), (2-14), (2-15), and (2-17) we have

$$(2\text{-}19)\quad \bar{\nu}' = \frac{K c f \pi^3}{K_1 K_2} \ln\left(\frac{\alpha P_x'}{\beta P_0'}\right) \rho(\Omega)$$

To examine the expected behaviour of $\bar{\nu}$ and $\bar{\nu}'$ in the ionosphere, consider the following model:

(a) The ionosphere is spherically stratified.

(b) The electron density profile above 140 km is that given in fig. 1 ("Satellite Environments Handbook" noon profile near sunspot maximum, with the total electron content adjusted to that of 1400 L.M.T. March 23, 1968 at London, Ontario; and the profile below 300 km adjusted to Ottawa ionosonde data 1400 L.M.T. March 23, 1968).

(c) The electron density profile below 140 km is that given in fig. 2 (Aikin and Blumle, 1968, fig. 1e).

(d) The electron and ion temperature profiles above 140 km is that shown in fig. 3 (Evans, 1967, fig. 6).

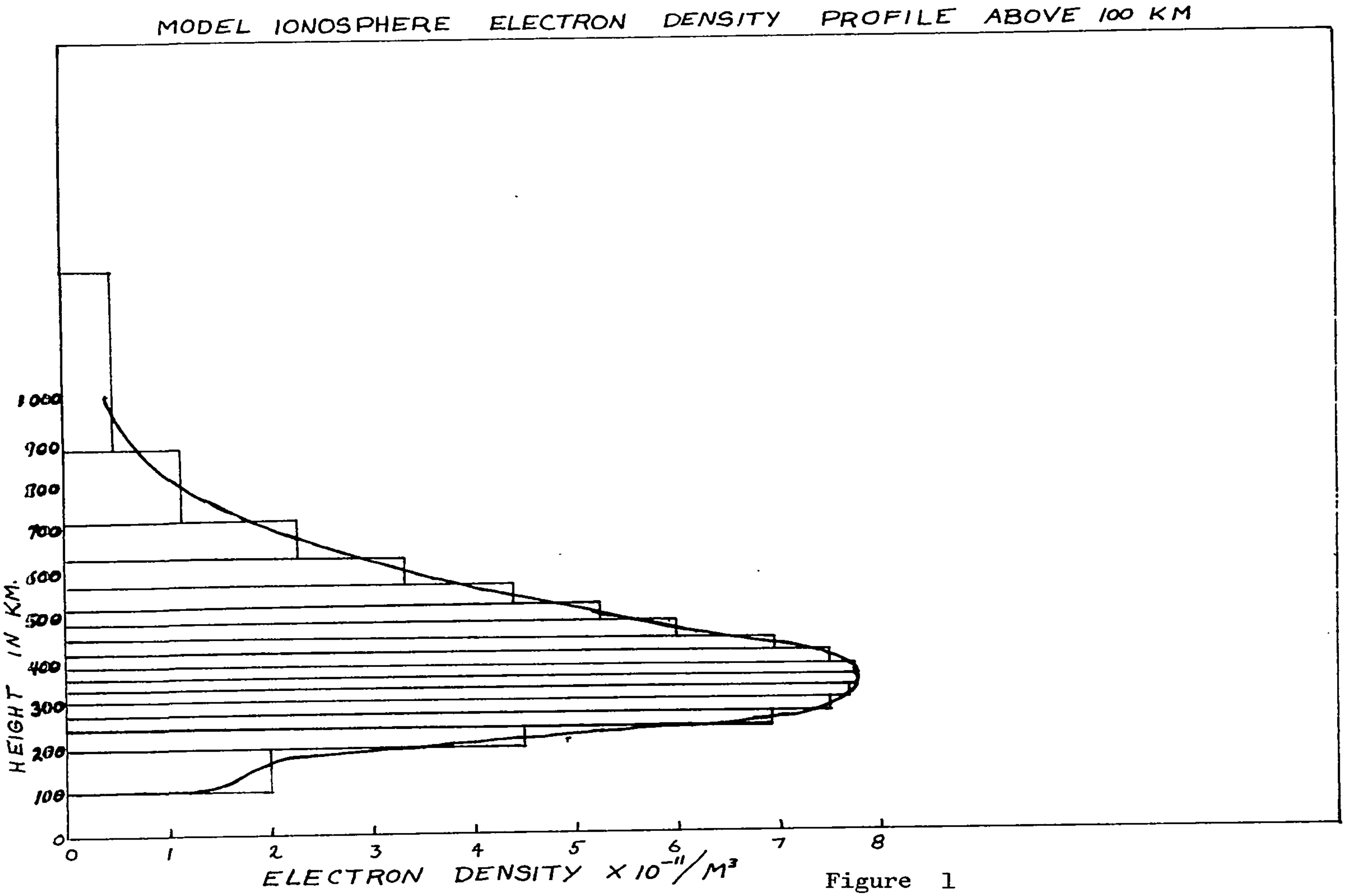
MODEL IONOSPHERE ELECTRON DENSITY PROFILE ABOVE 100 KM
HEIGHT IN KM.
1000
900
800
700
600
500
400
300
200
100
0
0
1
2
3
4
5
6
7
8
ELECTRON DENSITY X 10⁻¹¹/M³

Figure 1

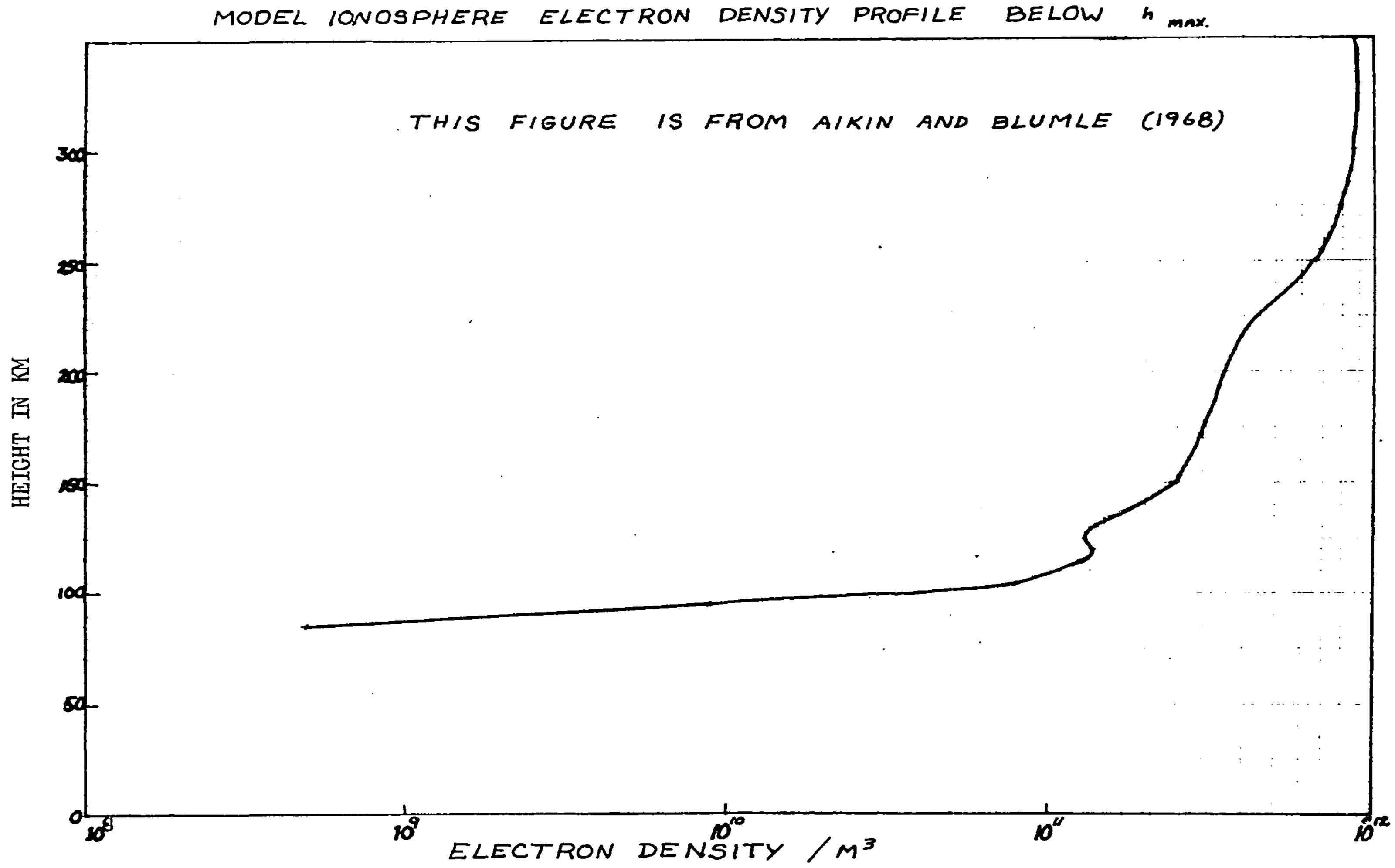

MODEL IONOSPHERE ELECTRON DENSITY PROFILE BELOW $h_{max.}$

THIS FIGURE IS FROM AIKIN AND BLUMLE (1968)

Figure 2

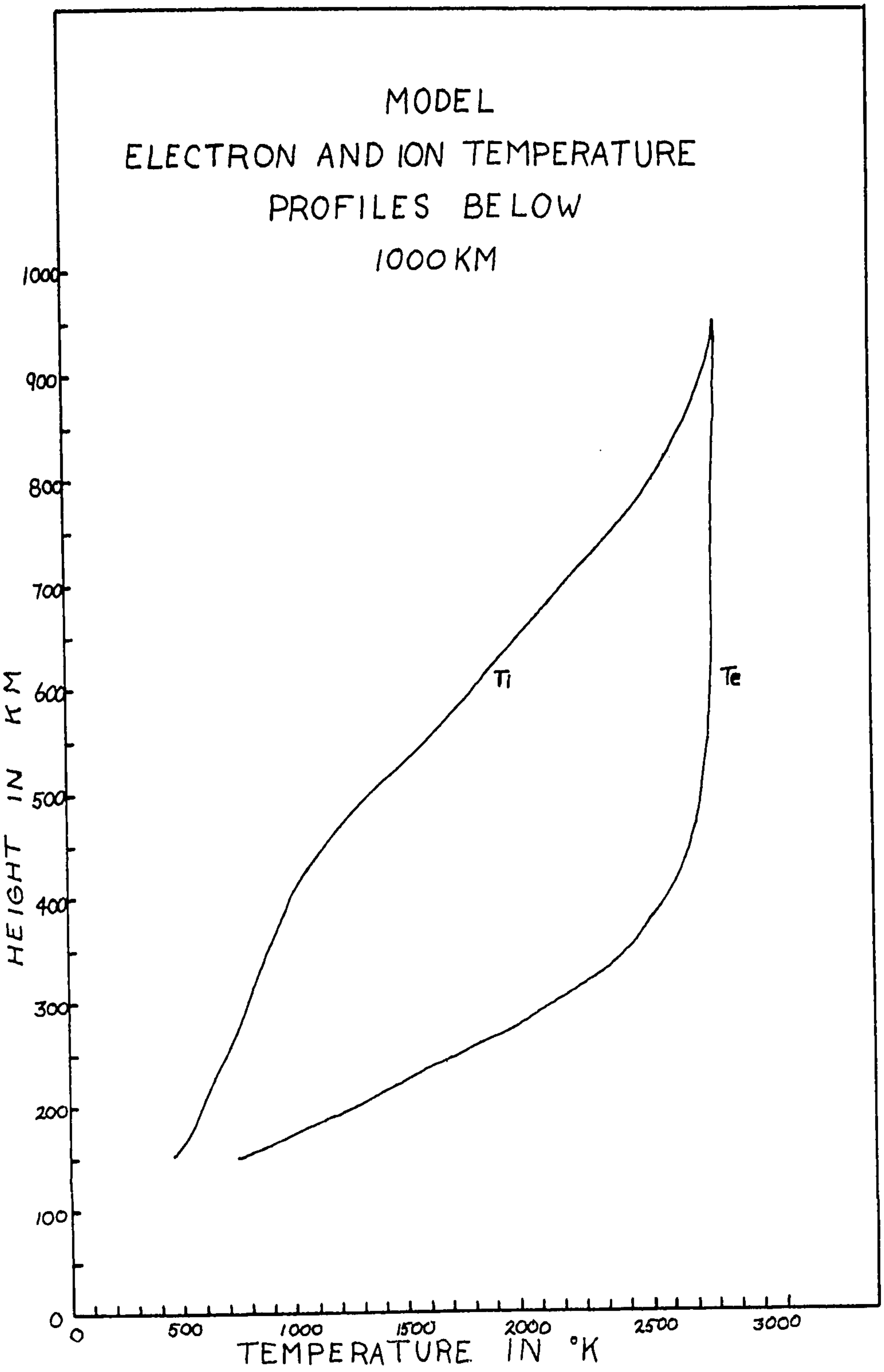
MODEL
ELECTRON AND ION TEMPERATURE
PROFILES BELOW
1000 KM
HEIGHT IN KM
0
100
200
300
400
500
600
700
800
900
1000
Ti
Te
0
500
1000
1500
2000
2500
3000
TEMPERATURE IN °K

Figure 3

(e) The electron collision frequencies below 140 km are those of Thrane and Piggot (1966).

Above 200 km electron-ion collisions predominate (Thrane and Piggot, 1966; Abdu et al., 1967). If the electrons and ions are in thermal equilibrium,

$$(2\text{-}20) \quad \nu_{ei} = [34 + 4.18 \log(T_e^3/N_e)]\, N_i / T_e^{3/2}$$

where T_e is the electron temperature in °K (Nicolet, 1959, as quoted by Abdu et al., 1967). N_e, N_i are the electron and ion number densities (for a neutral plasma, unless there are negative ions present).

If the electrons and ions are not in thermal equilibrium,

$$(2\text{-}21) \quad \nu_{ei} = [30 + 3.6 \ln(T_e \sqrt{\frac{T_i}{N_e}})\, N_i / T_e^{3/2}$$

where T_i is the ion temperature in °K (Thrane and Piggot, 1966). The electron collision frequencies for this model (2-20), (2-21) are plotted in fig. 4 above 140 km and the collision frequency data of Thrane and Piggot is plotted in fig. 4 below 140 km.

Since X_{MAX}, $Y_{L\,MAX}$ are both less than .04, the absorption coefficient, κ, is given by $\kappa = \frac{1}{2c}\int_0^s \nu X\, ds$ (ν is in/sec) to first order. The model altitude dependence of κ is displayed in fig. 5. The mean collision frequency for the model corresponds to an

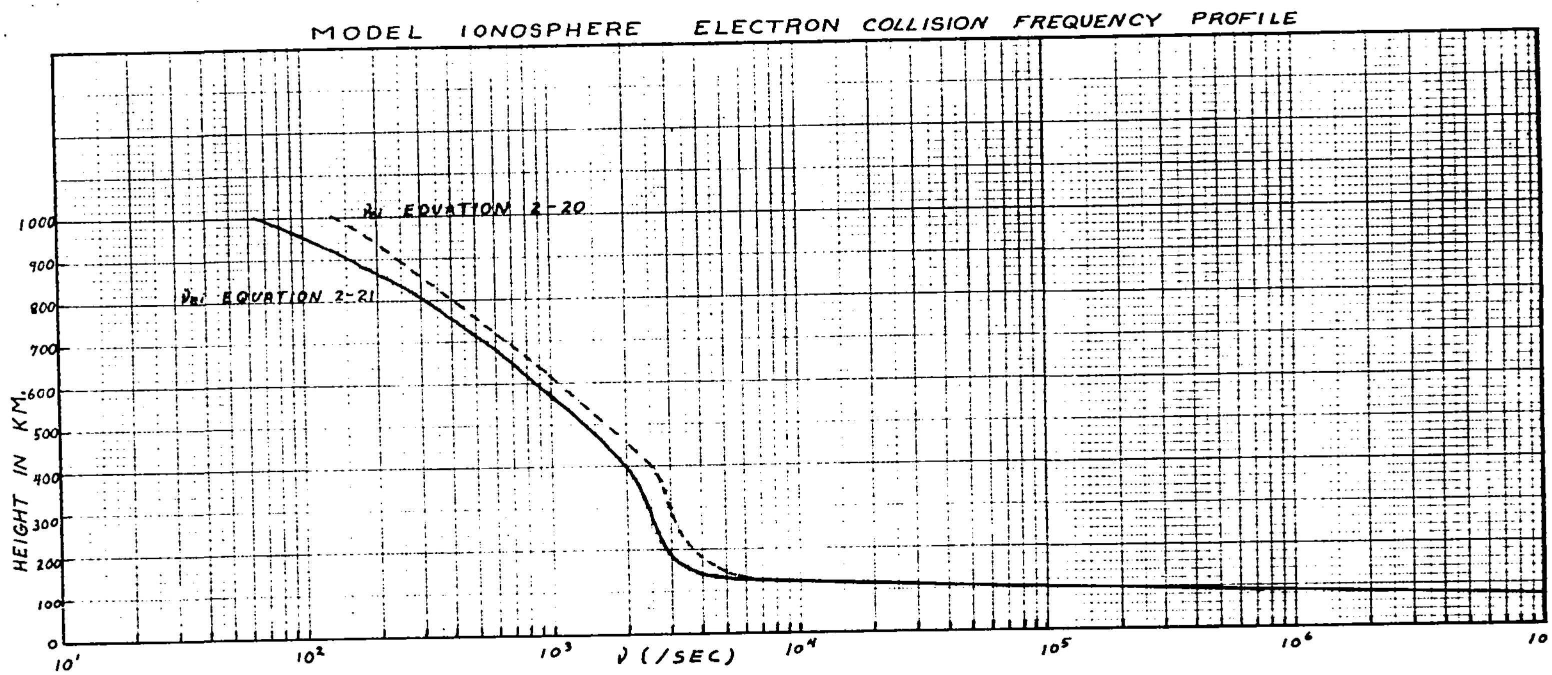
MODEL IONOSPHERE ELECTRON COLLISION FREQUENCY PROFILE
ν_{ei} EQUATION 2-20
ν_{Ei} EQUATION 2-21
HEIGHT IN KM.
1000
900
800
700
600
500
400
300
200
100
0
10^1
10^2
10^3
ν (/SEC)
10^4
10^5
10^6
10

Figure 4

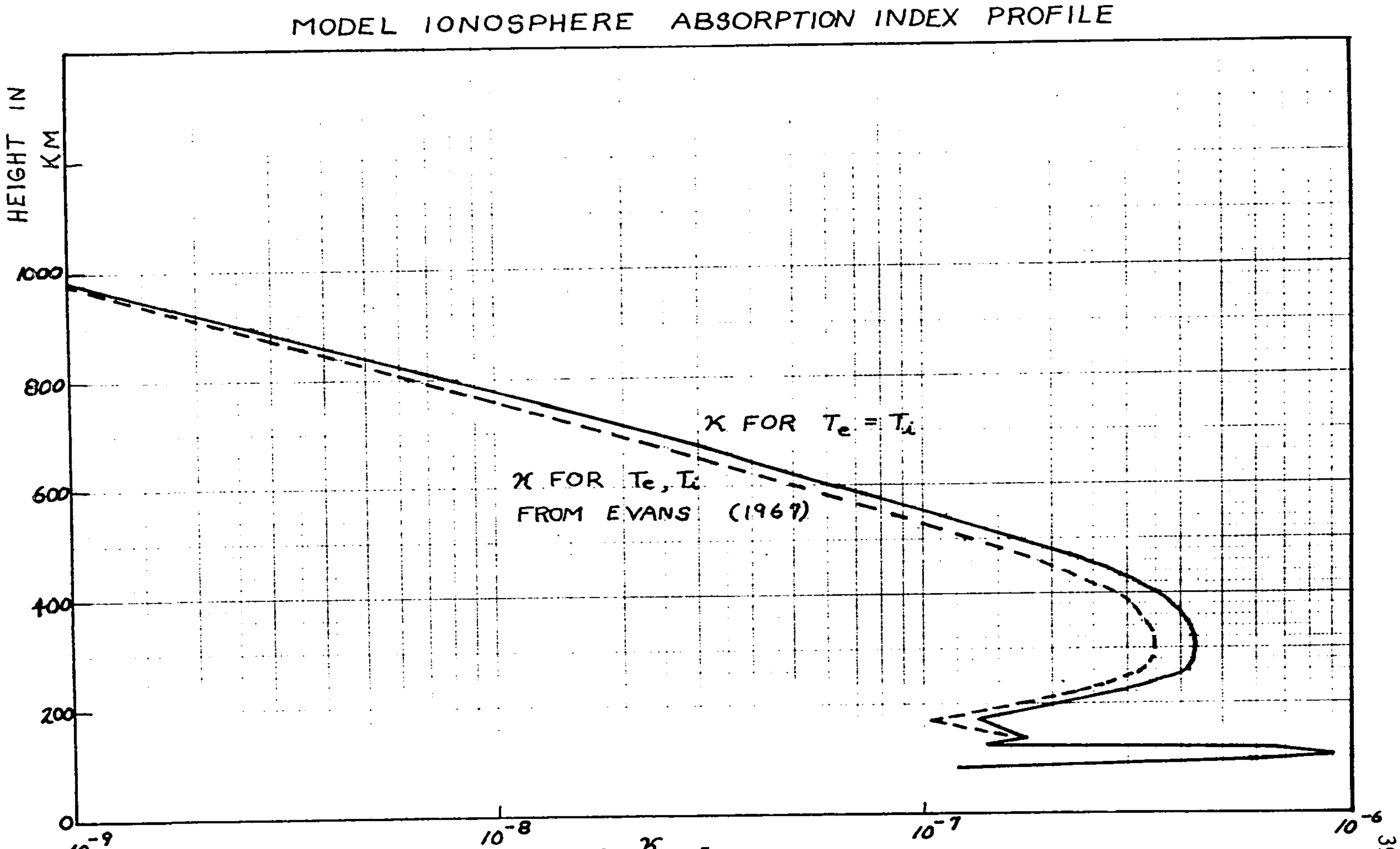
MODEL IONOSPHERE ABSORPTION INDEX PROFILE
HEIGHT IN KM
1000
800
600
400
200
0
κ FOR $T_e = T_i$
κ FOR T_e, T_i FROM EVANS (1969)
10^{-9}
10^{-8}
10^{-7}
10^{-6}
κ

Figure 5

absorption index centroid height of 365 km, for both (2-20), (2-21), with 80-84% of the total absorption occurring above 140 km. This result is compatible with those of Abdu et al. for high sunspot number years. Fig. 6 shows the dependence of the fractional absorption above 140 km and of the absorption index centroid height on the electron content below 140 km. The condition $L = 2$ corresponds to the results of Abdu, Degaonkar, and Ramanathan (1967) for sunspot minimum years.

From equations (2-16) and (2-20), above 140 km, $\bar{\nu}$ varies during a satellite pass approximately as $N_e T_e^{-3/2}$, where N_e and T_e are evaluated near the absorption index centroid. To examine the dependence of $\bar{\nu}$ on N_e and T_e let us consider the following cases:

(a) T_e is unchanged from the model but there is a fractional increase in N_e extending vertically through the ionosphere over a small horizontal range.

(b) T_e as before but the electron content irregularity is now localized at some level in the ionosphere.

(c) N_e is unchanged from the model but there is a T_e irregularity (fractional increase or decrease) extending vertically through

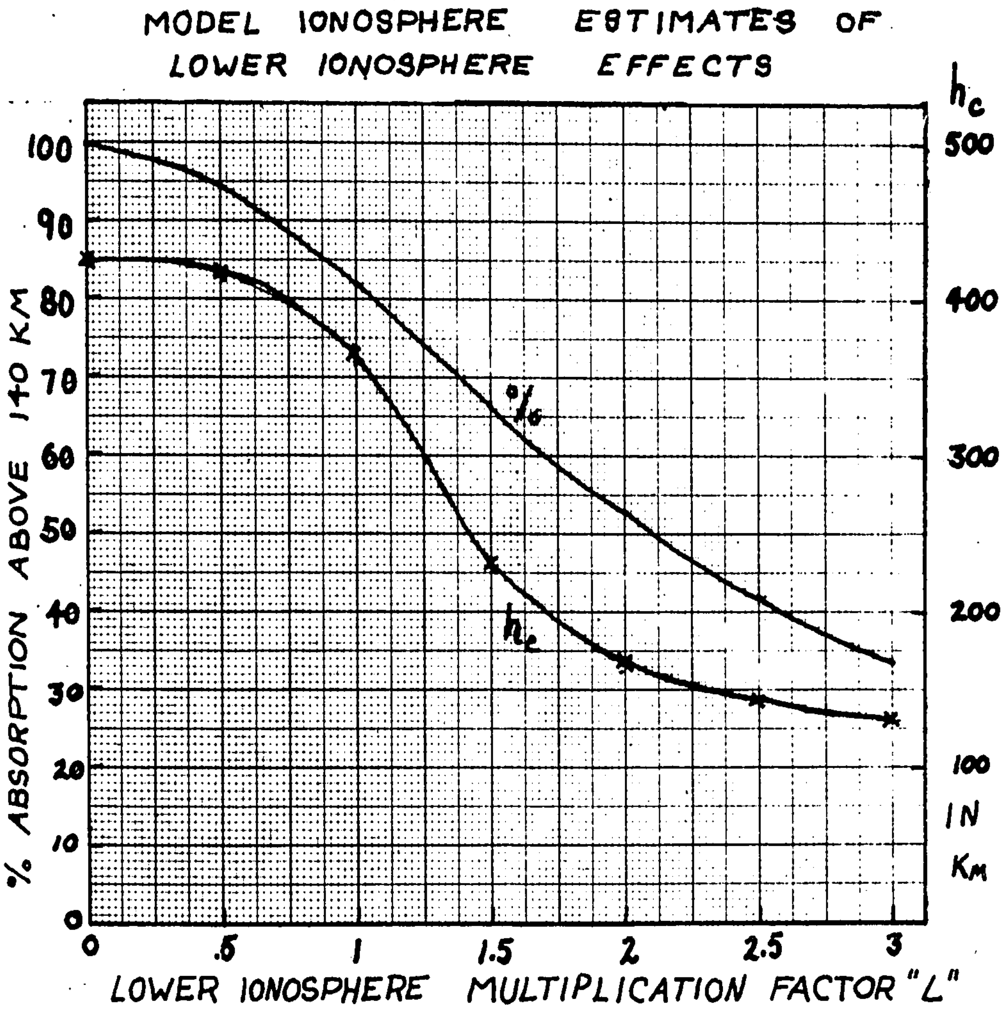
MODEL IONOSPHERE ESTIMATES OF
LOWER IONOSPHERE EFFECTS
% ABSORPTION ABOVE 140 KM
100
90
80
70
60
50
40
30
20
10
0
h_c
500
400
300
200
100
IN
KM
%
h_c
0
.5
1
1.5
2
2.5
3
LOWER IONOSPHERE MULTIPLICATION FACTOR "L"

Figure 6

the ionosphere and localized horizontally.

(d) N_e as before but there is a spatially localized T_e irregularity.

The relation between $\bar{\nu}$ and N_e in case (a) is $\frac{\Delta\bar{\nu}}{\bar{\nu}} = \frac{\Delta N_e}{N_e}$. That is, the observed fractional change in $\bar{\nu}$ is the same as the observed fractional change in N_e.

The relation between $\bar{\nu}$ and T_e in case (c) is $\frac{\Delta\bar{\nu}}{\bar{\nu}} = \frac{\Delta(T_e^{3/2})}{T_e^{3/2}}$. An increase in T_e by P % has an equivalent effect on $\bar{\nu}$ to a decrease of N_e of $3P$ %.

Cases (b) and (d) are similarly linked. Consider case (b). Let the irregularity have a horizontal scale size of 100 km, a vertical scale size of 40 km (compatible with the findings of Titherige, 1963, 1967) and an electron content of 1% of the model total electron content, $3.1 \times 10^{15}/M^2$. The new centroid height including the effect of the irregularity is

$$(2\text{-}22) \quad h'_c = \frac{h_c \int_0^{h_s} K\,dh + h_i \int_{h_1}^{h_2} \Delta K\,dh}{\int_0^{h_s} K\,dh + \int_{h_1}^{h_2} \Delta K\,dh}$$

where:

h_s is the satellite altitude.

h_c is the model absorption index centroid height (excluding the irregularity).

h_i is the height of the irregularity centroid.

h_1, h_2 are respectively the heights of the bottom and top of the irregularity.

$\Delta \kappa$ is the increase in absorption index due to the presence of the irregularity.

The variations of centroid height and $\bar{\nu}$ with irregularity position are shown in fig. 7. As can be seen, both $\bar{\nu}$ and h_c are relatively insensitive to the irregularity position (between 200 and 500 km) when the irregularity total electron content is 1% of the background. From Equation (2-22), $\frac{\Delta h_c}{h_c} = \frac{h_c - h_c'}{h_c}$ exceeds 10% only if $\frac{\int_{h_1}^{h_2} \Delta \kappa \, dh \, (1 - h_i/h_c)}{\int_0^{h_s} \kappa \, dh + \int_{h_1}^{h_2} \Delta \kappa \, dh}$ exceeds 10%. For $\int_0^{h_s} \kappa \, dh$ as given by the model and h_i = 200 km this corresponds to $\frac{\int_{h_1}^{h_2} \Delta \kappa \, dh}{\int_0^{h_s} \kappa \, dh} \geqslant .285$ --that is, irregularity total electron contents of the order of 30% or localized electron temperature irregularities $\frac{\Delta T_e}{T_e}$ of the order of 10%.

Consider now the behaviour of the mean collision frequency [Equations (2-17), (2-19)]. If the behaviour of the quantities $\int_0^S \nu X Y_L \, ds$ and $\int_0^S X Y_L \, ds$ are considered independently, Y_L in the first integral may be expressed in terms of $\bar{M} = H \cos(\theta) \sec(i)$ evaluated at the height of the absorption index centroid, while Y_L in the second integral is evaluated at the height of the electron density centroid. Rewriting Equation (2-17) to emphasize this point,

$$\bar{\nu}' = \frac{\bar{M}_\nu}{\bar{M}} \frac{\int_0^{h_s} \nu \kappa \, dh}{\int_0^{h_s} \kappa \, dh} = \frac{\bar{M}_\nu}{\bar{M}} \bar{\nu} \tag{2-23}$$

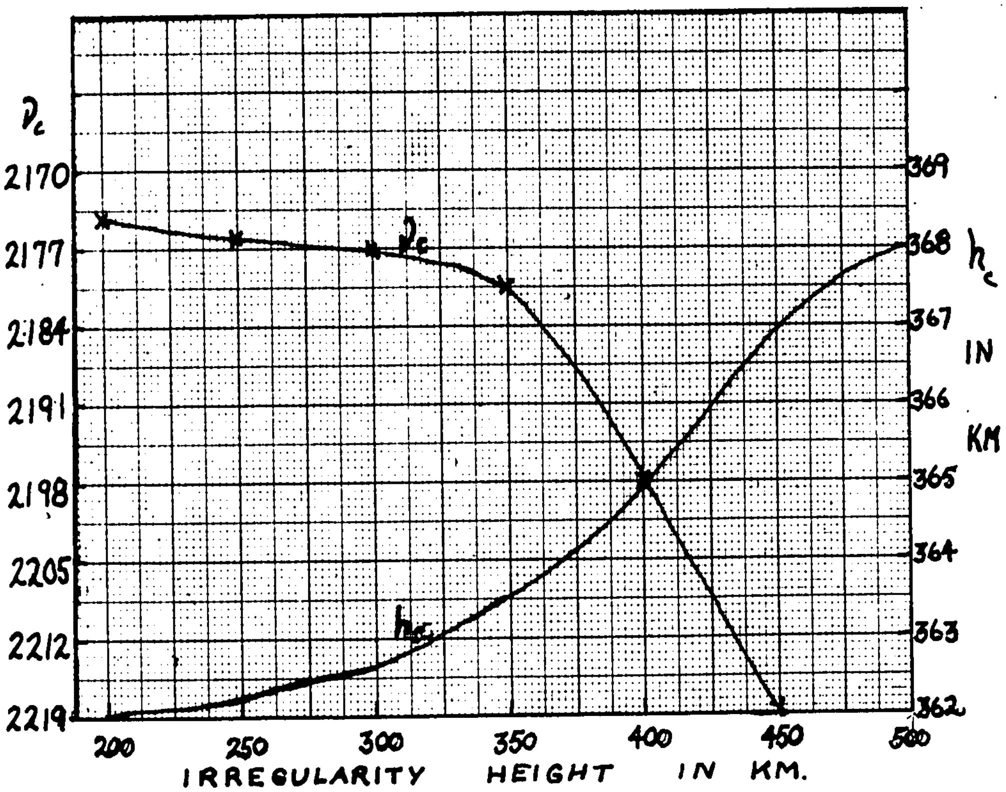

EFFECT OF A LOCALIZED 1% ELECTRON CONTENT ENHANCEMENT ON h_c, ν

Figure 7

We thus expect $\bar{\nu}' = \bar{\nu}$ only when the absorption index centroid and the electron density centroid are at the same height.

From Equations (2-18), (2-19) when $\bar{\nu}' = \bar{\nu}$ we have

$$(2\text{-}24)\quad \frac{\bar{M}_\nu}{SEC(i)_e} = \frac{2 X f \pi^3}{K_1 K_2^2} \Omega \, \rho(\Omega) \ln\left(\frac{\alpha P_x'}{\beta P_0'}\right) \Big/ \ln\left(\frac{\alpha \beta \; P'^2}{P_x' \; P_0'}\right)$$

where $SEC(i)_e$ is evaluated at the electron density centroid height. When $\bar{\nu}' = \frac{\bar{M}_\nu}{\bar{M}_e} \bar{\nu}$ [Equation (2-23)] and $\frac{\bar{M}_\nu}{\bar{M}_e} \neq 1$, $\bar{M}_\nu$ is evaluated at the absorption index centroid height and the ratio $\frac{\bar{M}_\nu}{\bar{M}_e} =$

$$\frac{\bar{M}_\nu}{SEC(i)_e} \Big/ \frac{\bar{M}_e}{SEC(i)_e}$$

is related to the separation of the two centroids.

CHAPTER 3

DATA COLLECTION AND PROCESSING

(3.1) DATA COLLECTION

From the discussions in sections 1.4, 2.4 and 2.5 it is evident that, to investigate both maximum spatial resolution of the Faraday total electron content and the behaviour of the absorption index centroid using combined differential Faraday, differential absorption measurements, the data collection (receiving) systems must be designed to meet the following criteria:

(a) The rotation of the polarization plane of the incoming satellite transmissions must be monitored continuously in time, during a satellite pass, at two frequencies 40, 41 MHz .

(b) The amplitudes of the right and left circularly polarized components of the 40 MHz transmission must also be monitored continuously in time and in such a manner that separation of the signal amplitude fluctuations from the polarization fading can be easily effected.

(c) The receivers must be in a low radio frequency noise environment.

(d) The analogue and digital analysis systems must be centrally located.

(e) The data output of the receiving system must be in a form compatible with the data transfer and/or storage device used to satisfy (c), (d).

The receiving system, whose block diagram is shown in fig. 8, was designed by the author and A. F. Dixon to meet the above criteria. The inputs A and B are fed from right and left circularly polarized antennas of the turnstile type. The signal is then amplified at the wave frequency in the corresponding front-end amplifiers and thenhetrodyned with the first local oscillator pair to 11.3 MHz.

The first local oscillator pair is critical to the operation of the system since it establishes the phase information sub-carrier. (The Faraday rotation angle is measured in terms of the relative phase of the two circular wave components.) Briefly, the oscillator pair consists of two, oven stabilized, crystal oscillators (master and slave) which are phase locked to each other at a difference frequency of 500 ± 10^{-4} Hz by the mixer, phase sensitive detector and crystal clock circuits.

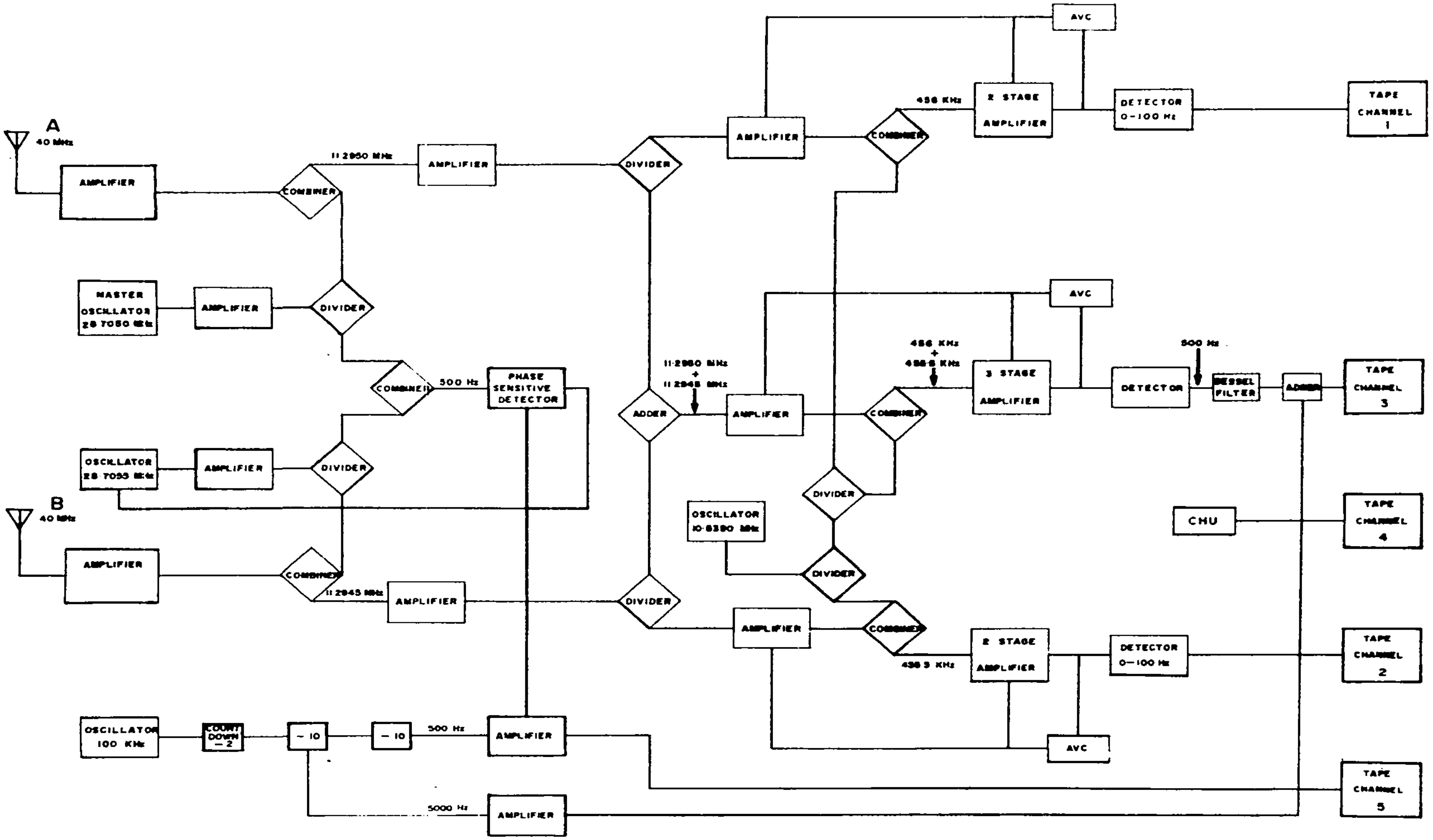

SYSTEM BLOCK DIAGRAM. Figure 8

The resulting first I. F. signals, then, have a frequency difference of $500.0000 + \omega_F$ Hz, where ω_F is the Faraday rotation rate, and absolute frequencies of 11.2950 MHz + ω_D, 11.2945 MHz + ω_D (ω_D is the Doppler shift of the satellite transmission frequency due to the motion of the satellite). These are then amplified in the corresponding first I. F. amplifiers (1st stage) and split into two branches in the signal path divider networks. One branch of each channel is fed directly to the corresponding amplitude channel first I. F. stage, hetrodyned with a common 10.8 MHz oscillator to 455 KHz, amplified, detected, filtered and recorded on magnetic tape.

The other branches of each input channel are combined in a linear adder at 11.3 MHz, amplified at 11.3 MHz, hetrodyned to 455 KHz, amplified and detected to provide the 500 Hz phase information carrier. The phase carrier is then amplified, filtered, and combined with a 5 KHz reference (derived from the crystal clock) to provide the phase information signal recorded on magnetic tape.

All three channels are amplitude controlled by independent, amplified A.G.C. control voltages applied to the second stages of the first I. F. amplifiers and to the entire second I. F. amplifier to compress the output signal level variation into a range acceptable to the tape recorder.

Two receivers of this type are used at 40, 41 MHz respectively and the following information is stored on magnetic tape: 2-40 MHz amplitudes, 1-41 MHz amplitude, Station WWV time code, 41 MHz phase information signal (500 Hz + 5 Khz rider), 500 ± 10^{-4} Hz reference, and 40 MHz phase information signal (500 Hz + 5 KHz rider).

A partial list of receiver parameters is given below:

Amplitude channel gain 93 db

Amplitude channel output passband 0-100 Hz

Amplitude channel radio frequency passband 10 KHz

Inter-channel crosstalk < -60 db

Amplitude channel maximum sensitivity $0.05 \mu V$ at 50Ω

Saturation level $\sim 100 \mu V$ into 50Ω

Phase channel gain 115 db

Constant time delay-phase band width 60 Hz centered at 500 Hz

Phase channel and phase shift radio frequency pass band 6 KHz

Phase channel maximum sensitivity for usable phase information $0.2 \mu V$ into 50Ω

Saturation level $\sim 150 \mu V$ into 50Ω

Phase variation with amplitude $< 1^\circ$ for signal amplitude change from 0.2 μV to 60 μV into 50Ω

A more detailed discussion of the receiver may be found in Dixon and Livingstone (1969).

To permit measurements of the Faraday rotation angle without contributions to the phase due to changes in the ray angle of arrival, folded dipole turnstiles of the form shown in fig. 9, with phasing networks of the form shown in fig. 10 are designed to extract both circular components from a single antenna. The phasing system is a combined hybrid network, transmission line circuit which has an impedance of 50Ω at each terminal and provides approximately 50 db isolation between the two circular modes. Impedance matching of the antenna to the phasing network is accomplished with 4:1 coaxial baluns. For further information on the antenna design and properties see Livingstone and Dixon (1968). Although, in practice, antennas of this kind have elliptic, not circular, polarizations, if sufficient care is taken in the antenna construction the eccentricity is very nearly 0.0.

TURNSTILE ANTENNA

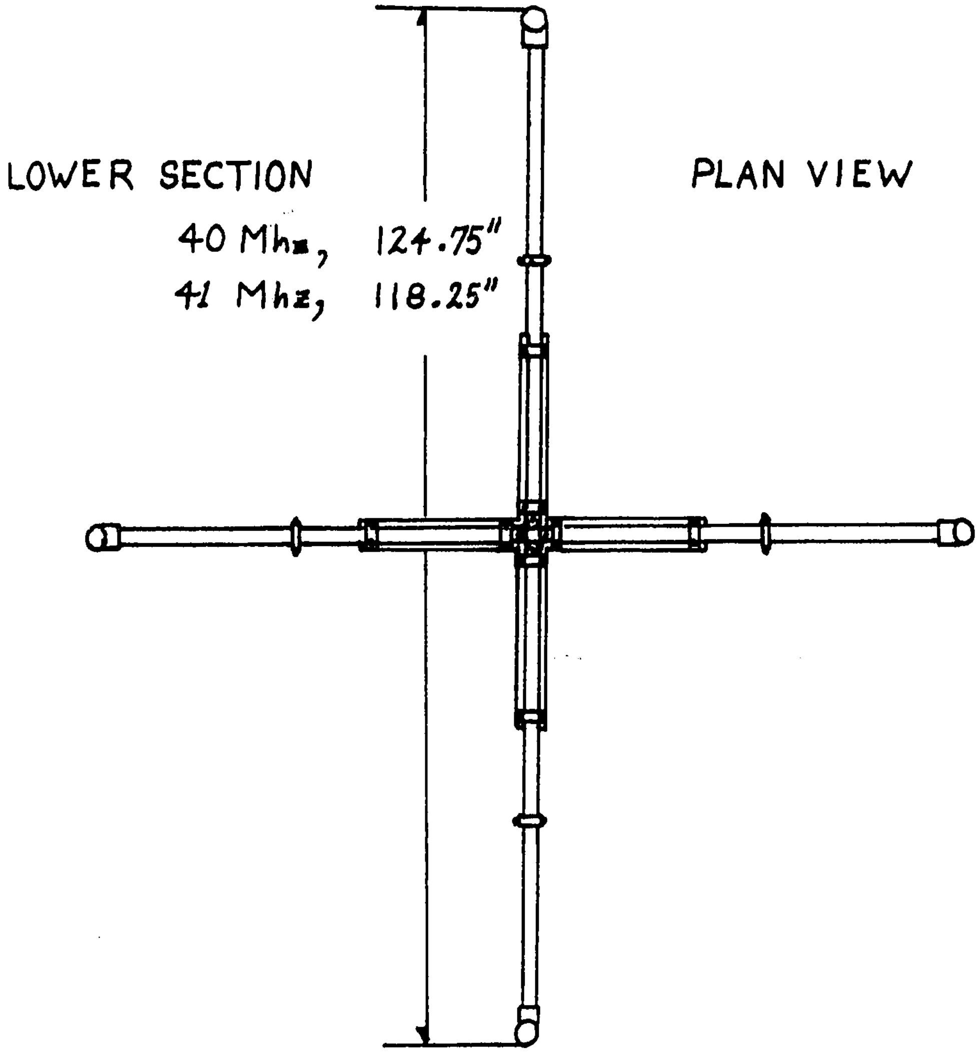

SIDE ELEVATION

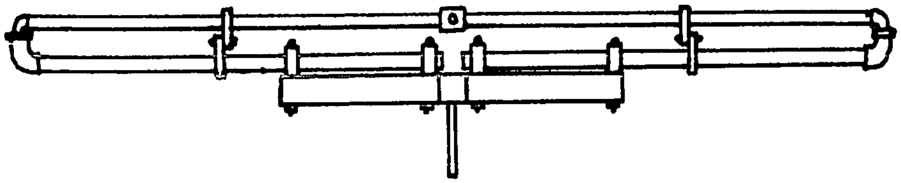

Figure 9

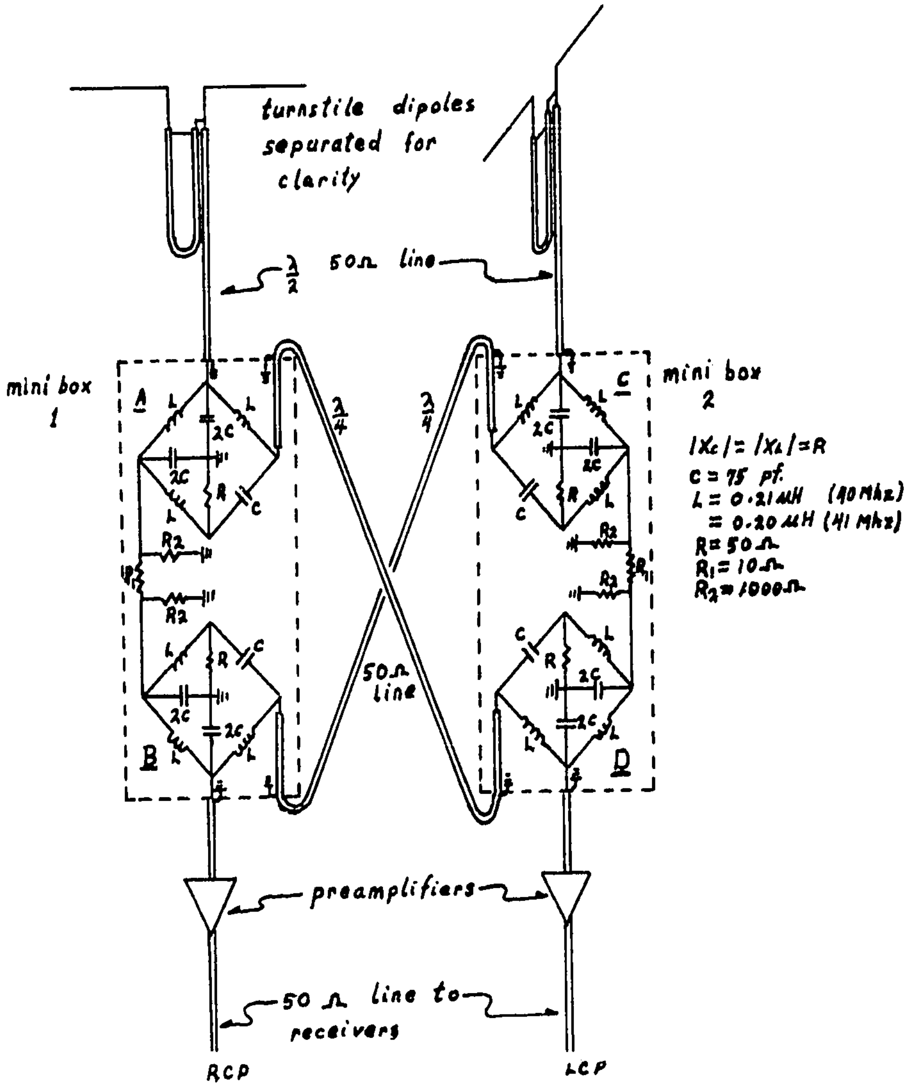
turnstile dipoles separated for clarity
λ/2 50Ω line
mini box 1
mini box 2
A
B
C
D
L
C
2C
R
R1
R2
λ/4
λ/4
50Ω line
|Xc| = |XL| = R
C = 75 pf.
L = 0.21 μH (40 Mhz)
= 0.20 μH (41 Mhz)
R = 50 Ω
R1 = 10 Ω
R2 = 1000 Ω
preamplifiers
50 Ω line to receivers
RCP
LCP

Figure 10

(3.2) DATA REDUCTION TO DIGITAL FORM

Analogue data recordings were made on a seven channel tape recorder, at a tape speed of 30 i.p.s., for each satellite pass, during the period January 1, 1968 to May 22, 1968, whose maximum elevation angle was greater than 60°.

To reduce the analogue information stored on tape to a form suitable for digital analysis, the tapes were played through an analogue data reduction system into a four track Sanborn chart recorder. Amplitude and time code information was transferred directly onto chart paper. The phase information signals and references were first processed by a tape transport correction system (Hanff, Dixon and Chess, 1968), which separated the 5 KHz rider from the 500 Hz phase information signal, counted this down to 500 Hz, compared the phases of this and the 500 Hz reference, and produced a reference signal at 500 Hz corrected for tape dropouts and tape recorder head skew. The correction system was then used to drive a phase meter. (There was an option of 0° or 180° introduced phase shift between the phase information signal and the reference.)

The phase meter output, a "rapid retrace" saw-tooth (phase ramp) voltage whose amplitude is proportional to the relative phase of the input signals (range 0°-360°), was recorded on chart paper simultaneously with the amplitudes and time code. Since the phase meter has an indecision range of 10°-15° about the 360° to 0° retrace, each phase record was replayed twice, with 0° and 180° introduced phase shifts respectively.

An overlay was prepared for the 180° shift chart and applied to the unshifted chart to span the information gap produced by the phase meter indecision range and to provide a chart-phase calibration for digital processing. The overlay technique was also used to determine the times of phase ramp correspondence at 40, 41 MHz to resolve the Faraday, $n\pi$ ambiguity.

The paper charts produced by this method were sampled digitally at one second intervals (chart time and the encoder output was punched onto computer cards for digital analysis).

To compare the (antenna and range corrected) ordinary and extraordinary mode amplitudes, an encoding sequence was devised to minimise the time parallax between the chart traces due to errors in reading the time codes--both ordinary and extraordinary mode amplitudes were recorded on a single chart and were sampled consecutively at each time point.

To permit assembly of the Faraday phase ramps into a continuous record of Faraday rotation angle the following encoding scheme was used (fig. 11).

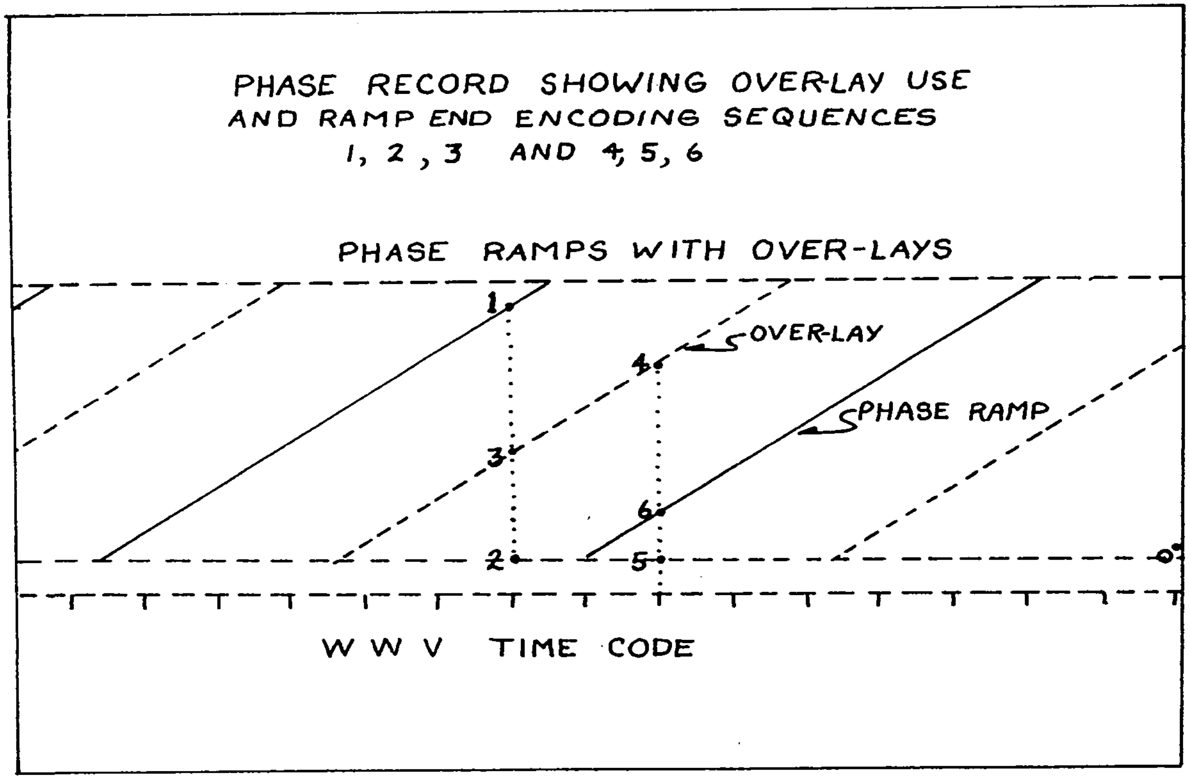
PHASE RECORD SHOWING OVER-LAY USE
AND RAMP END ENCODING SEQUENCES
1, 2, 3 AND 4, 5, 6
PHASE RAMPS WITH OVER-LAYS
1
2
3
4
5
6
0
OVER-LAY
PHASE RAMP
W W V TIME CODE

Figure 11

(a) The phase ramps were sampled digitally up to, and including, the last time mark of the ramp (point 1, fig. 11).

(b) A marker, +000, was introduced into the encoder output (point 2, fig. 11).

(c) The first point of the Overlay was sampled digitally at the same time mark (point 3, fig. 11).

(d) The overlay phase ramp was sampled up to the first point of the main ramp.

(e) The ramp-end process, a, b, c, was repeated in the sequence 4, 5, 6 (fig. 11).

A typical encoded phase record would, then, have this appearance.

$$\underbrace{010, 025, 038, 055, 070, 098, 110, 137, 150, 174}_{\text{main record}}, \underbrace{000}_{\substack{\text{point sequence}\\ 1,2,3 \text{ fig.11}}}, \underbrace{054, 079, 111}_{\text{overlay}},$$

$$000, 009$$

The point sets 174,000,054 and 11,000,009 each occur at single time marks.

Consider a time mark "S", P 000's from the start of the record, with each ramp segment (between markers) having n_j points named φ_j . Then $\sum_{K=1}^{p} n_K - p = s - n^{s}_{p+1}$ where n^{s}_{p+1} is the number of points between the start of the P + 1 ramp and "S"; and the phase at "S" is:

$$\Phi_s = \left\{ \sum_{K=1}^{P} \left[\sum_{i=1}^{n_K} \varphi_{iK} + (\varphi_{n_K,K} - \varphi_{1,K+1}) \right] + \sum_{i=1}^{n^s_{P+1}} \varphi_{i,P+1} \right\} 180R \Big/ \sum_{K=1}^{R} (\varphi_{n_K,K} - \varphi_{1,K+1})$$

where R is the number of markers in the entire record.

The second factor is simply the chart phase calibration in terms of the measured phase ramp-overlay separations at the end of each ramp segment. The sum Φ_s , is subject to two kinds of errors:

(a) Random "noise" introduced in playback and scaling ($\sim \pm 3^{\circ}$ phase).

(b) Cumulative errors caused by phase meter and chart recorder D. C. drifts.

$$\beta_e = \left\{ \sum_{K=1}^{P} (\varphi_{n_K,K} - \varphi_{1,K+1}) \, 180R \Big/ \sum_{K=1}^{R} (\varphi_{n_K,K} - \varphi_{1,K+1}) \right\} - 180P$$

The sum of all processing errors of this nature, when referred to the computed total electron content is approximately ± 0.2% of the content (fig. 12).

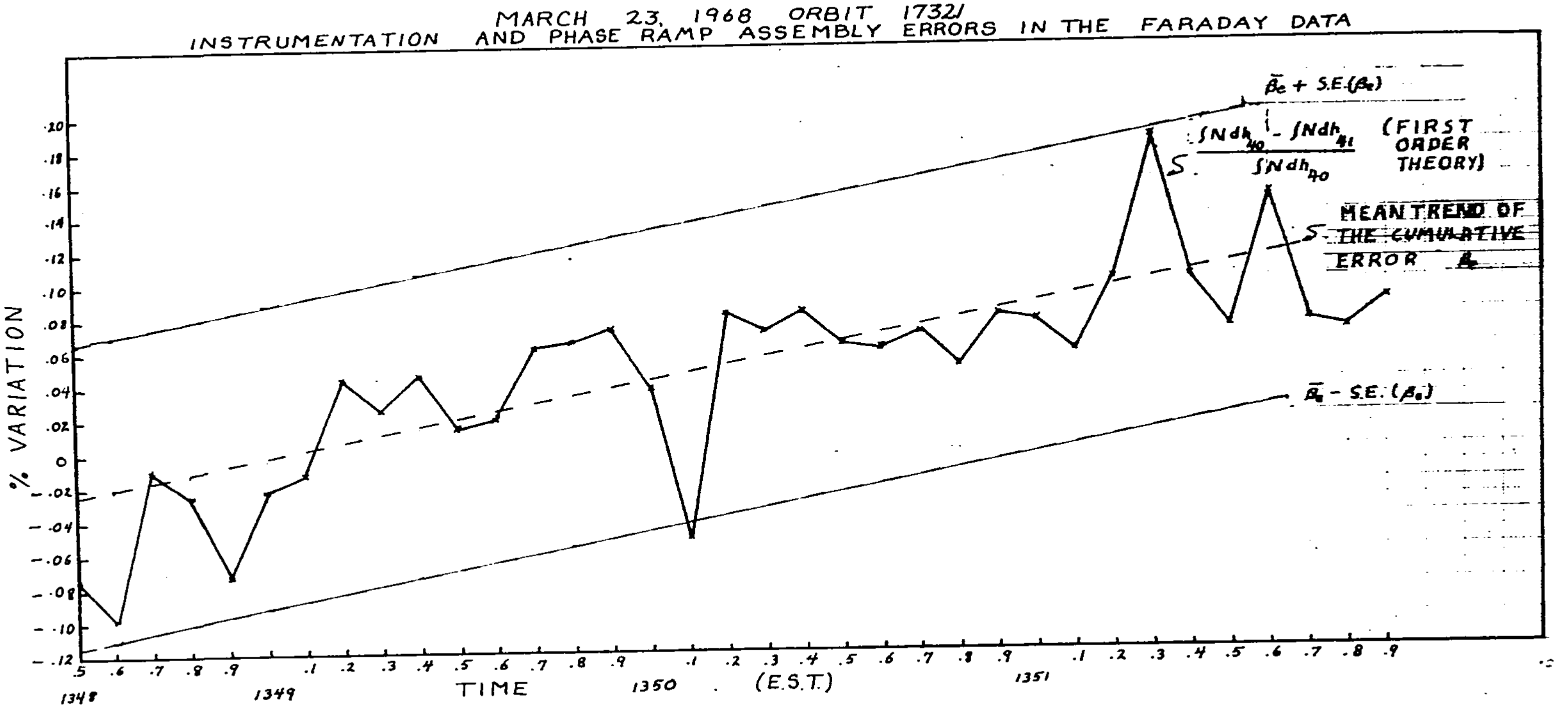
MARCH 23, 1968 ORBIT 17321
INSTRUMENTATION AND PHASE RAMP ASSEMBLY ERRORS IN THE FARADAY DATA
% VARIATION
.20
.18
.16
.14
.12
.10
.08
.06
.04
.02
0
-.02
-.04
-.06
-.08
-.10
-.12
.5 .6 .7 .8 .9 .1 .2 .3 .4 .5 .6 .7 .8 .9 .1 .2 .3 .4 .5 .6 .7 .8 .9 .1 .2 .3 .4 .5 .6 .7 .8 .9
1348
1349
1350
1351
TIME (E.S.T.)
$\bar{\beta}_e + S.E.(\beta_e)$
$\frac{\int N dh_{40} - \int N dh_{41}}{\int N dh_{40}}$ (FIRST ORDER THEORY)
MEAN TREND OF THE CUMULATIVE ERROR β_e
$\bar{\beta}_e - S.E.(\beta_e)$

Figure 12

(3.3) REDUCTION OF DIGITAL DATA

If the first order Faraday rotation approximation [Equation (2-6)] is applied to a spherically stratified ionosphere, the variation in Ω will be related only to the variation of $\bar{M}$ at the electron density profile centroid height. In terms of the relative phase of the two normal propagation modes this is

$$(3\text{-}1) \qquad \Phi_K(\bar{M}) = \frac{(\Phi_{K+1} - \Phi_{K-1})\,\bar{M}_K}{(\bar{M}_{K+1} - \bar{M}_{K-1})}$$

In general the ionosphere is not spherically stratified (section 1.3) and so, $\Omega_K(\bar{M}) = \Phi_K(\bar{M})/2$ is not a good estimate of the Faraday rotation angle. Since the ionosphere gradients are normally small ($\lesssim$ 10% of the total electron content over the satellite pass), $\Omega_K(\bar{M})$ will usually, when averaged, be of the correct order of magnitude. When $\Omega_K(\bar{M})$ is plotted against $\bar{M}$ for two frequencies (40, 41 Mhz), and the two frequency phase ramp coincidence points are plotted on the same graph parametric in n [Equation (2-10)], the best fit between the two sets of curves will select the best choice for n . Insertion of n into Equation (2-10a) then gives the total number of polarization plane rotations between the satellite and the receiving point at the first 40, 41 MHz phase ramp coincidence. Once the total value of Ω is known at one time, it is found for the entire record by shifting the origin of the relative rotation angle measured during the satellite pass. The total electron content may then be computed using Equation (2-6) to first order in X or using Equation (2-7) to second order in X.

The amplitude information is reduced to mean collision frequency estimates in a two stage computation:

(a) The digital data is calibrated in terms of power input to the receiver using the amplitude channel calibration marks stored on tape at the time the record was taken.

(b) Antenna effects are removed using the correction developed in Appendix A. Scintillations are smoothed using a 20 second running mean. Mean collision frequencies and $\bar{\nu}$, $\bar{\nu}'$ were computed using the results of section 2.3.

CHAPTER 4

EXPERIMENTAL RESULTS

(4.1) THE SPATIAL RESOLUTION OF FARADAY ELECTRON CONTENTS

From section 2.4 the expected maximum spatial resolution of Faraday electron content measurements is of the order of one to two km in the F region which corresponds to minimum record scaling interval of .5 to 1 seconds.

In the normal, inhomogenous ionosphere, small (.4 km to .1 km) scale irregularities will produce amplitude scintillations in the transmitted waves as seen at the receiving point (section 1.3.2). Since the ordinary and extraordinary rays traverse the ionosphere along separated ray paths, the time shifts between the amplitude scintillations, as seen on the two modes (fig. 13), will provide a measure of the maximum spatial resolution of the Faraday technique by providing a measure of ray separation.

The magnitude of the relative time displacements of ordinary, extraordinary mode scintillation features

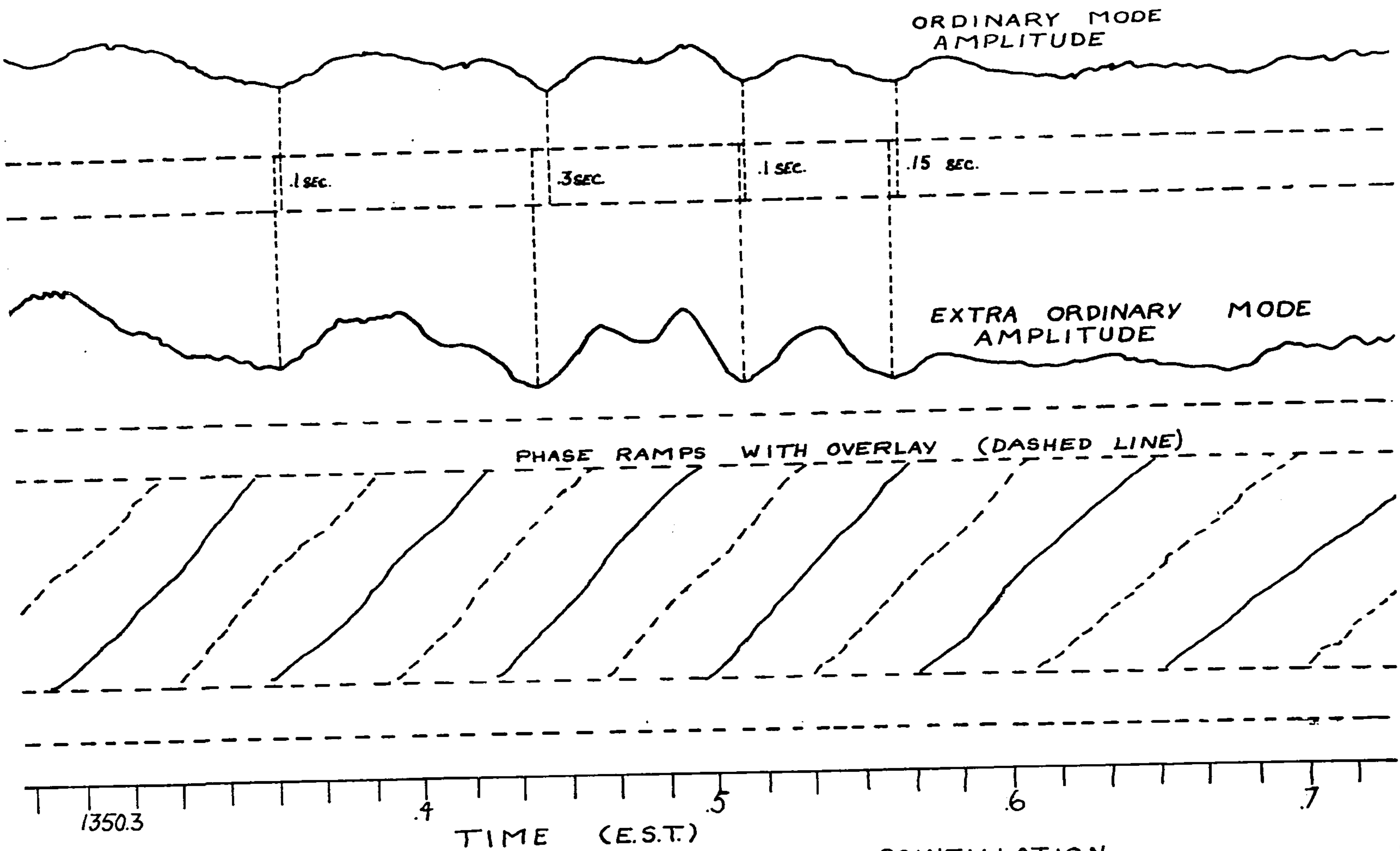

MARCH 23, 1968 ORBIT 17321 SCINTILLATION TIME SHIFTS Figure 13 were measured for eight satellite passes and grouped in twenty second intervals during each pass (a convenient, arbitrary grouping), between times corresponding to elevation angles of 40°N and 40°S.

Figure 14 is a scatter-plot showing the dependence of the time shift magnitudes greater than .1 seconds on the satellite elevation angle. There is no obvious correlation. The maximum observed time shift in 300 measurements was 0.8 seconds and this occurred once.

Figure 15 is a scatter-plot showing the dependence of the average time shift in each interval on elevation angle. There is an apparent minimum in mean time shift to the south of the receiving point at an elevation angle of 70°-75°; this appears to be a field point effect and is probably related to the occurrence of a more rapid scintillation rate near the field point masking slower variations in amplitude.

The relative occurrence of time shifts of length $n \Delta t$ ($\Delta t = 0.1$ sec) is shown in the histogram, fig. 16. From fig. 16, time shifts greater than or equal to 0.6 seconds occur in less than 1% of all cases, and thus .5-.6 seconds appear to be the shortest usable scaling interval for interpretation of variations in in terms of total electron content variations.

As the ray connecting the satellite and the

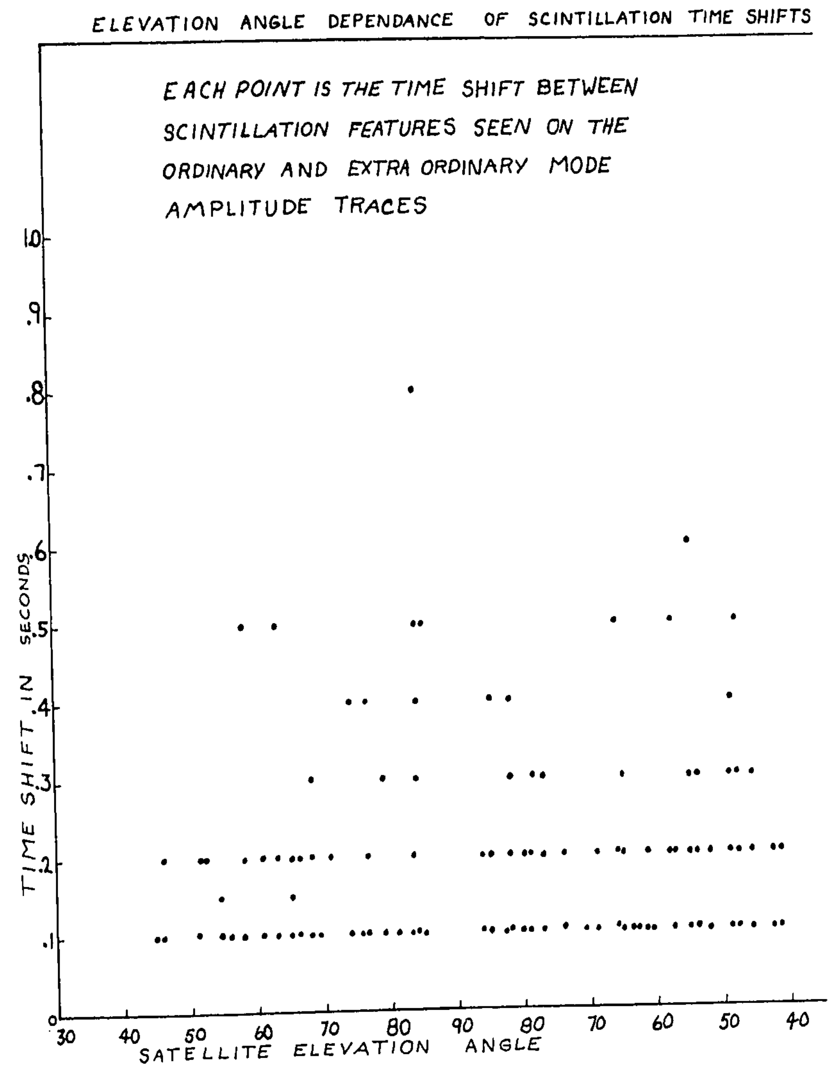
ELEVATION ANGLE DEPENDANCE OF SCINTILLATION TIME SHIFTS
EACH POINT IS THE TIME SHIFT BETWEEN SCINTILLATION FEATURES SEEN ON THE ORDINARY AND EXTRA ORDINARY MODE AMPLITUDE TRACES
TIME SHIFT IN SECONDS
1.0
.9
.8
.7
.6
.5
.4
.3
.2
.1
0
30
40
50
60
70
80
90
80
70
60
50
40
SATELLITE ELEVATION ANGLE

Figure 14

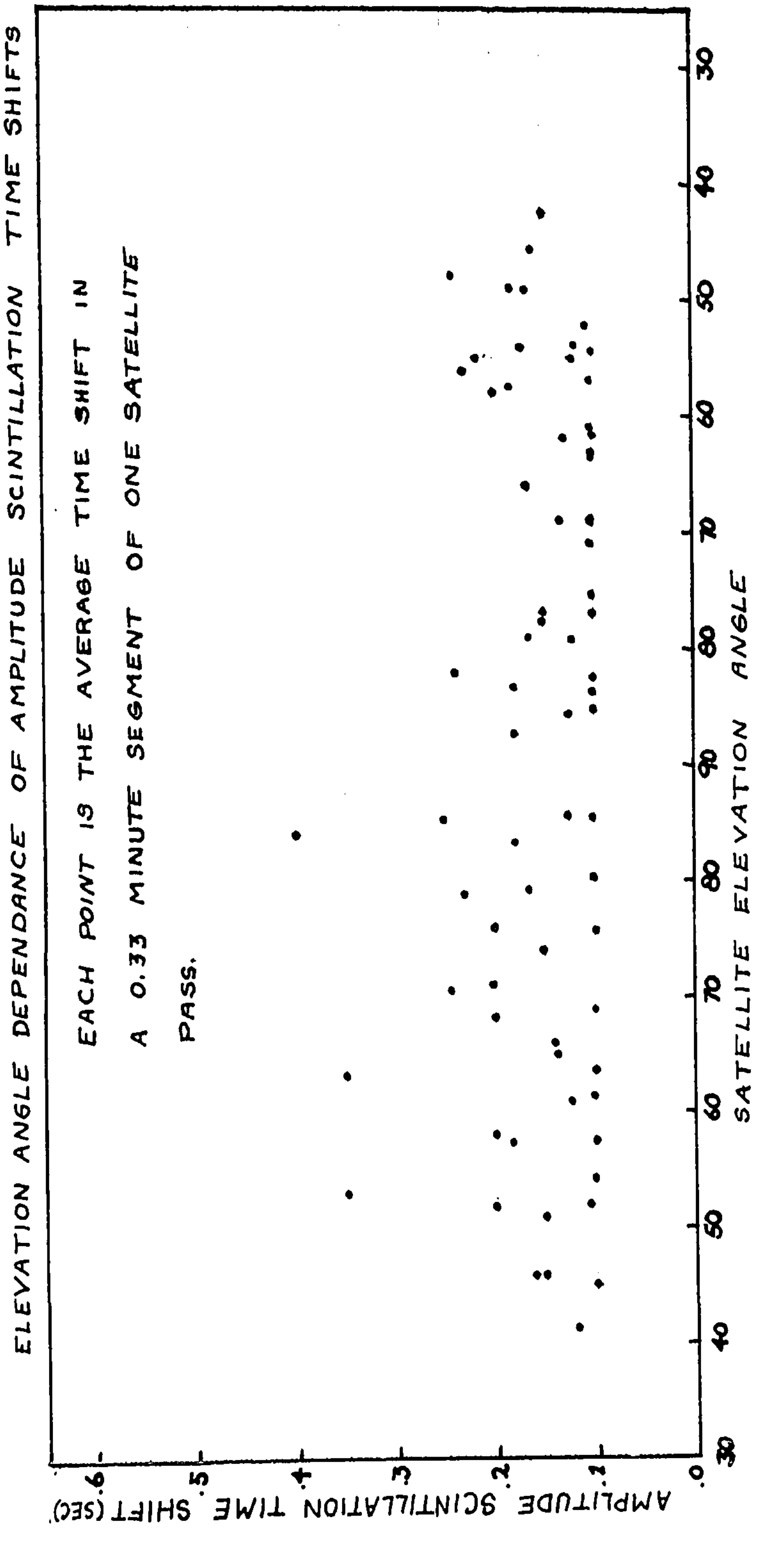
ELEVATION ANGLE DEPENDANCE OF AMPLITUDE SCINTILLATION TIME SHIFTS
EACH POINT IS THE AVERAGE TIME SHIFT IN A 0.33 MINUTE SEGMENT OF ONE SATELLITE PASS.
AMPLITUDE SCINTILLATION TIME SHIFT (SEC)
0
.1
.2
.3
.4
.5
.6
SATELLITE ELEVATION ANGLE
30
40
50
60
70
80
90
80
70
60
50
40
30

Figure 15

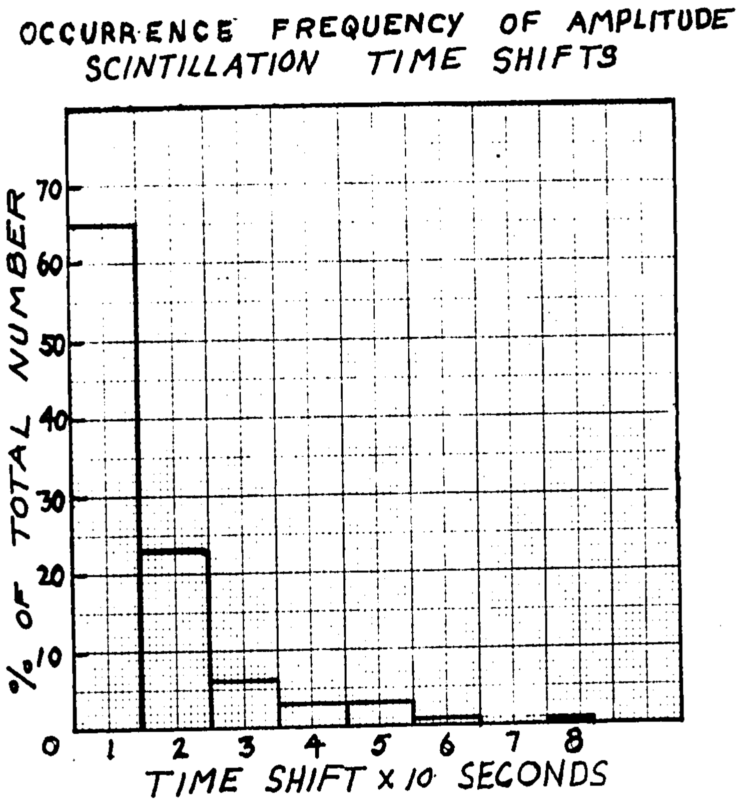
OCCURRENCE FREQUENCY OF AMPLITUDE
SCINTILLATION TIME SHIFTS
% OF TOTAL NUMBER
0
10
20
30
40
50
60
70
1
2
3
4
5
6
7
8
TIME SHIFT x 10 SECONDS

Figure 16

ground station sweeps the 350 km height shell at approximately 2 km/sec, the maximum spatial resolution (in the F region) of the Faraday electron content measurements is 1.0 to 1.2 km which is compatible with the theoretical predictions of section 2.4. It must be noted that for practical application of these results, a maximum spatial resolution of 2 km at F region altitudes may be considered "safe".

(4.2) MEASUREMENTS OF TOTAL ELECTRON CONTENT AND MEAN COLLISION FREQUENCIES

The three records selected for presentation and discussion, March 17, 1968 1434.3 EST, March 20, 1968 1413.8 EST, March 23, 1968 1350.2 EST (the times given are approximate times of pass center as observed at London, Ontario) have several common features.

They represent three consecutive, high elevation angle, North to South passes of 1964-64A/BE-B with total electron contents of greater than $3 \times 10^{17}/M^2$ (rapid rotation rates). All display some scintillation over the pass with the maximum scintillation rate occurring about the closest approach of the ray to the magnetic field direction. This time of closest approach will be called the field point. None of these records display major Faraday rotation anomalies (such as direction reversals). All three are taken at times of low world-wide indices (J.G.R. V73 #15, 5019) (magnetically quiet conditions); the Agincourt (Ontario) magnetograms for the days of interest are presented in fig. 17.

In general, the first order Faraday electron contents have a statistical uncertainty (scaling and random processing deviations accounted for) of ± 0.08% (fig. 12) with a possible consistent (instrumental drift) error of 0.12% (fig. 12) which produces an expected uncertainty of ± 0.2% from the data gathering and

STANDARD RUN MAGNETOGRAM 1500 U.T. MARCH 23 TO 1500 U.T. MARCH 24

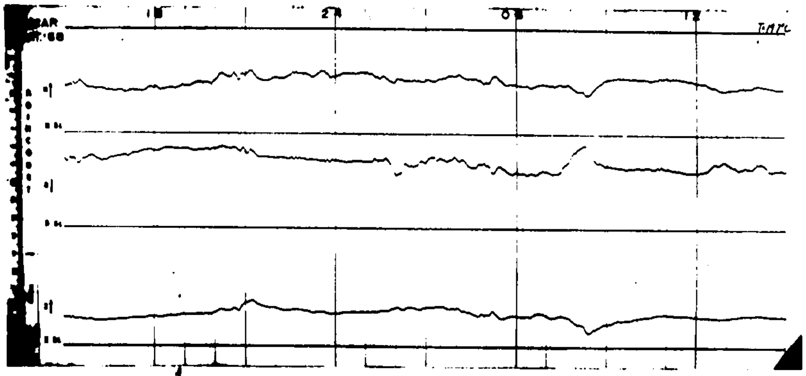

PASS CENTER ORBIT 17321

STANDARD RUN MAGNETOGRAM 1500 U.T. MARCH 20 TO 1500 U.T. MARCH 21

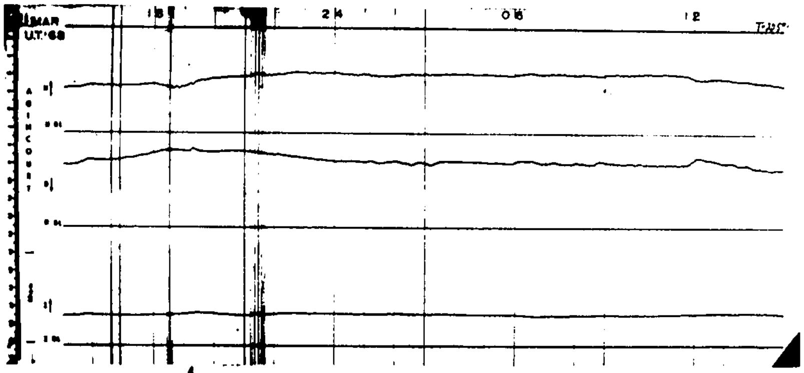

PASS CENTER ORBIT 17280

STANDARD RUN MAGNETOGRAM 1500 U.T. MARCH 17 TO 1500 U.T. MARCH 18

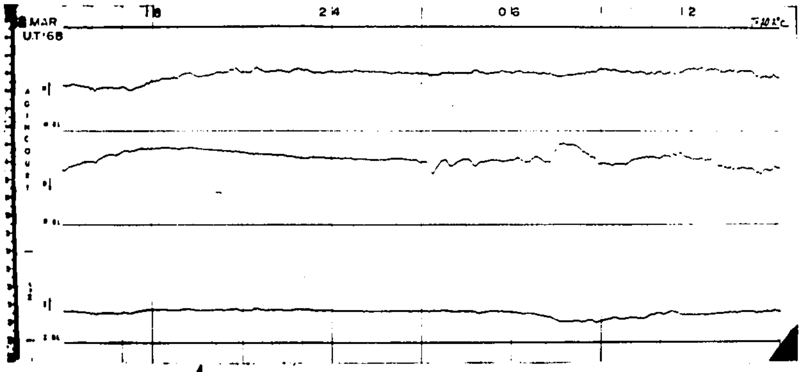

PASS CENTER ORBIT 17239

Figure 17

processing. The expected variations in $\bar{M}$ due to discrepancies between satellite position and computed satellite position will contribute a further uncertainty of magnitude 0.5% (constant shift over the pass) to the absolute value of the computed electron content.

The effect of random and consistent (scaling, instrument) uncertainties in the computation of the second order Faraday [Equation (2-7)] is to produce a random part of approximately ± 0.6% in the computed second order electron content. Combining this with the 0.5% uncertainty in $\bar{M}$ gives an uncertainty of ± 1.1% in the absolute value of the second order contents. As the same M is used for both first and second order Faraday content computations, the relative variations of the two estimates will be significant if they exceed .8% of the estimated absolute values and since the second order Faraday contents are expected to differ from the first order estimates by approximately 2% (from the ray trace calculation of Appendix B), many of the observed differences will be significant.

Computation of the expected uncertainties in $\bar{\nu}$, $\bar{\nu}'$, and $\frac{\bar{M}\nu}{\bar{M}}$ from accrued data scaling and processing errors give estimates of ± 7.5% for $\bar{\nu}$, $\bar{\nu}'$ and ± 15% for $\frac{\bar{M}\nu}{\bar{M}}$. An estimate of the statistical uncertainties involved in the use of a 20 point running mean to remove scintillation effects in the computations of $\bar{\nu}$, and in the choice of the best fit (least squares) lines, compatible to the general behaviour of $\int_0^{h_s} N' dh / \int_0^{h_s} N dh$ as computed from the first and second order electron contents, to $\bar{\nu}$, $\bar{\nu}'$ are indicated on the graphs as error bars on $\bar{\nu}$. The length of the error bar is the separation of $\bar{\nu}$ from the best fit line at which the probability of a point exceeding the error bar by chance drops to 10% according to a "t" test.

To facilitate discussion and cross comparisons of the results for the three records, the results will be presented in order of increasing complexity in the following manner:

(a) Pass information
figs. 18, 23, 29
  (i) elevation angle
  (ii) sub satellite latitude and longitude
  (iii) sub ionosphere latitude and longitude (near the electron density centroid height)

(b) Raw data--a chart record showing unprocessed right and left circular amplitudes (no correction for radial distance, antenna effects, or gain changes)
figs. 19, 24, 30

(c) First and second order electron contents

figs. 20, 25, 31

(d) $\epsilon = \dfrac{a \int_0^{h_s} N^2 dh}{f^2 \int_0^{h_s} N dh}$

figs. 21, 26, 32

(e) $\bar{\nu}$, $\bar{\nu}'$ and $\dfrac{\overline{M\nu}}{\overline{M}}$

figs. 22, 27, 33

(f) discussion

Since the satellite used is in a nearly circular orbit, the time will be used in all cases as a reference axis.

To provide a convenient comparison of F region profile shape changes, all passes will be referred to a "parabolic ionosphere" discussed in Appendix C.

The section of the second order electron content curves spanned by the error bars marks the range of validity of Equations (2-7), (2-7a) under the restrictions of Equation (2-8).

(4.3.1) MARCH 23, 1968

From the raw data (fig. 19).

The amplitude scintillation occurs over a smaller portion of the pass than either the March 17 or the March 20 passes--but over the central region, local variations in amplitude from the quiet ionosphere case are more marked. The field point scintillation depth is also greater during this pass than during the other two. From the raw data, amplitude decreases, from the expected trend of the smooth curve are found in the vicinities of pass time 1349.5, 1351.0. There appears, also, to be a marked amplitude enhancement--possibly a focusing effect in the vicinity of 1850.

Rotation rate anomalies are present in the vicinity of times 1349.5, 1350.5, 1352.

The corresponding first and second order electron contents are found in fig. 20. The upper curves are the first order electron content (with and without the coincidence point correction), the lower is the second order electron content.

The coincidence point correction is - 4% at the 1350.875 coincidence point. In this case, the first and second order contents have mean gradients of $1.36 \times 10^{13}/M^2$ km and 0 respectively. One feature of great interest is the general form of the two contents. Although both show electron content irregularities, the

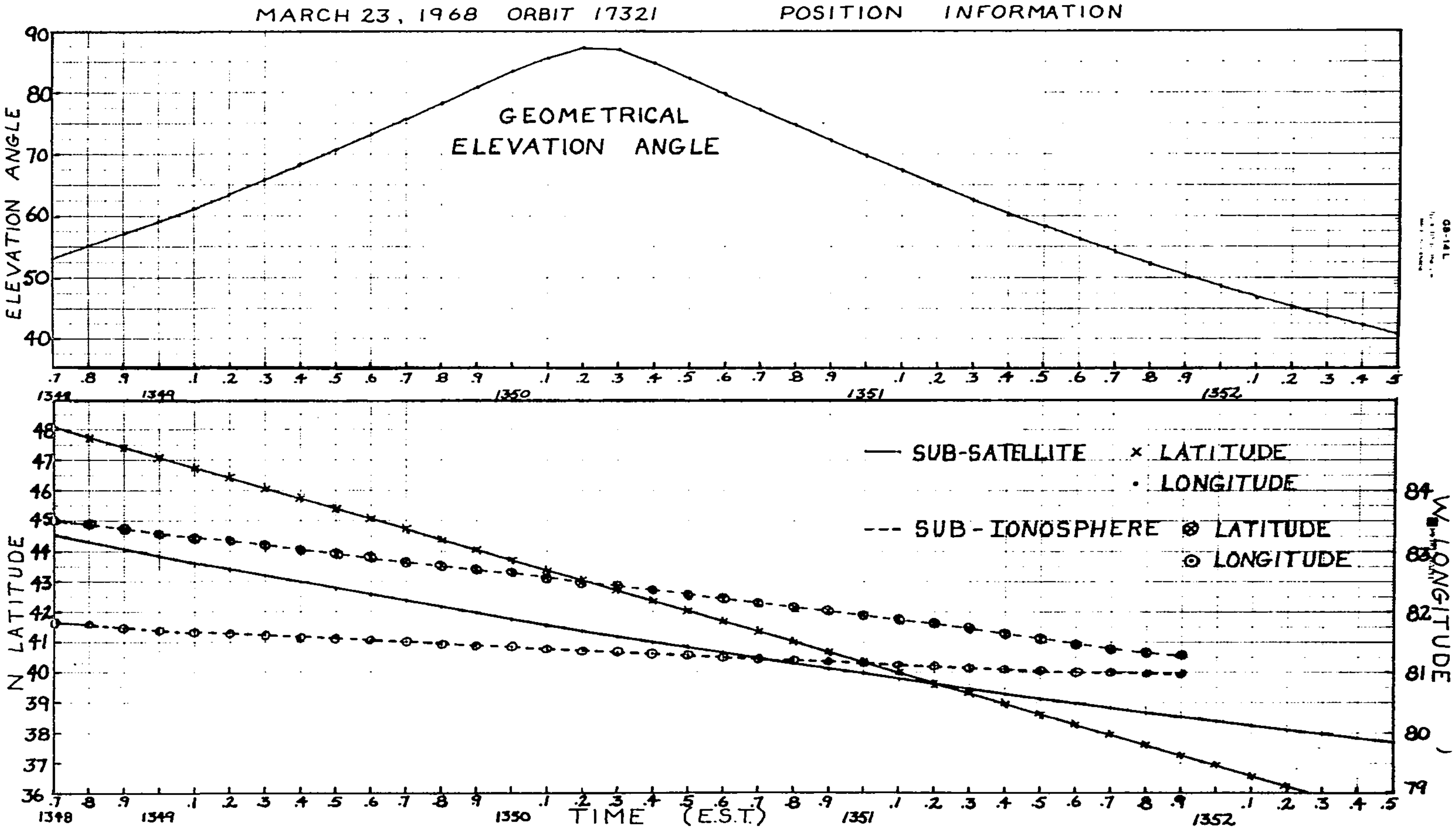
MARCH 23, 1968 ORBIT 17321 POSITION INFORMATION
GEOMETRICAL ELEVATION ANGLE
ELEVATION ANGLE
90
80
70
60
50
40
N LATITUDE
48
47
46
45
44
43
42
41
40
39
38
37
36
W LONGITUDE
84
83
82
81
80
79
— SUB-SATELLITE × LATITUDE
• LONGITUDE
--- SUB-IONOSPHERE ⊗ LATITUDE
⊙ LONGITUDE
1348
1349
1350
1351
1352
TIME (E.S.T.)

Figure 18

RAW DATA

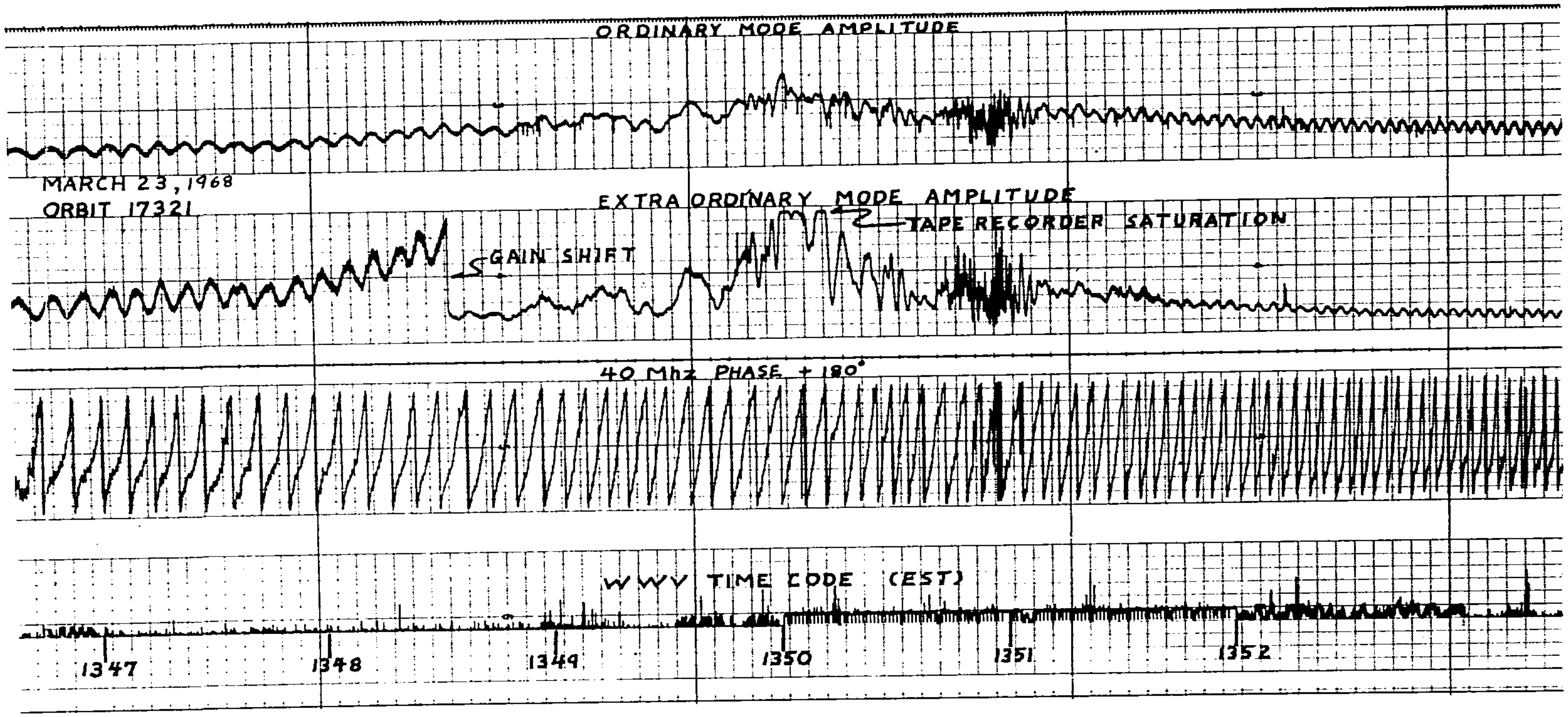

Figure 19

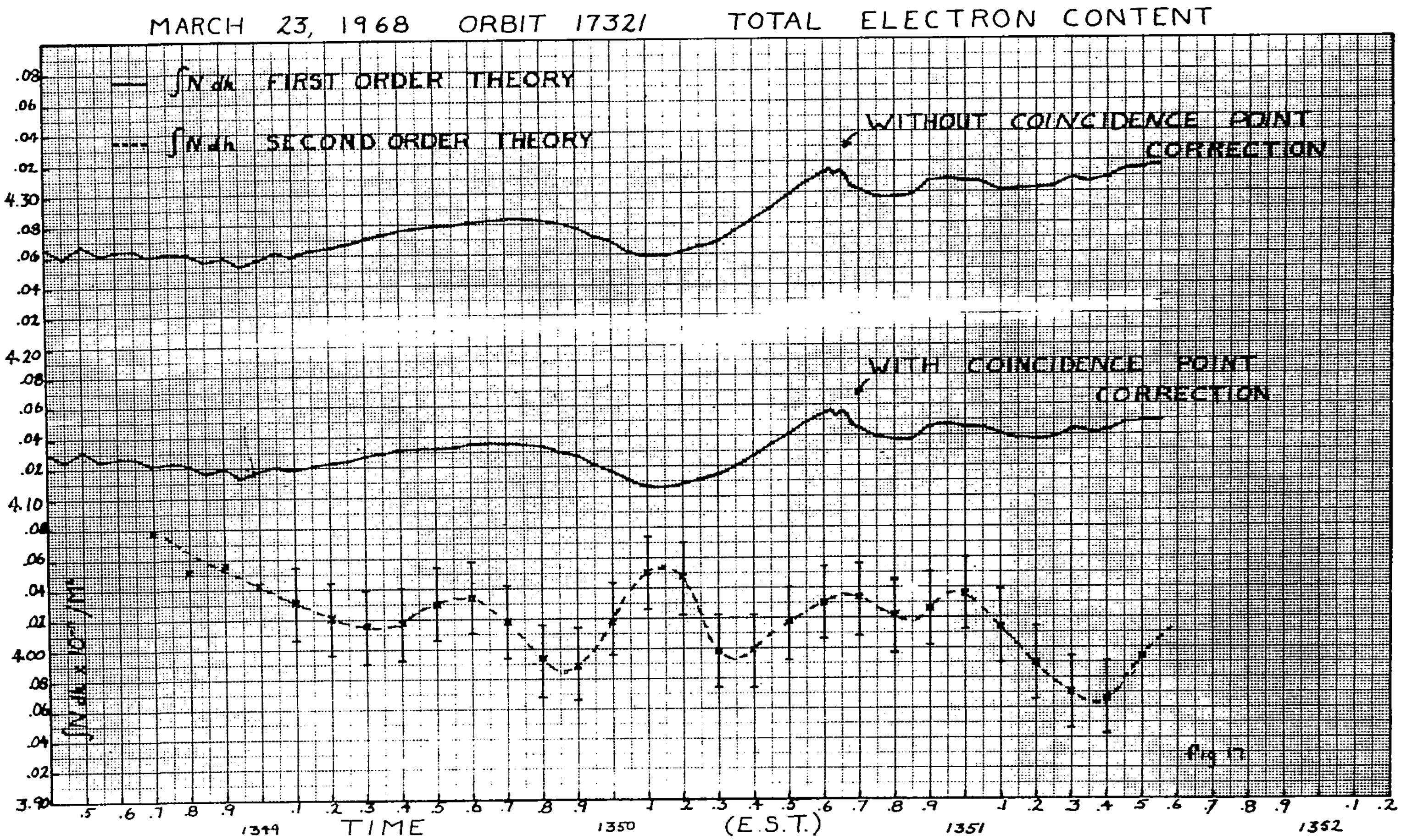
MARCH 23, 1968 ORBIT 17321 TOTAL ELECTRON CONTENT
— ∫N dh FIRST ORDER THEORY
--- ∫N dh SECOND ORDER THEORY
WITHOUT COINCIDENCE POINT CORRECTION
WITH COINCIDENCE POINT CORRECTION
∫N dh × 10¹⁷/M²
.08
.06
.04
.02
4.30
.08
.06
.04
.02
4.20
.08
.06
.04
.02
4.10
.08
.06
.04
.02
4.00
.08
.06
.04
.02
3.90
.5 .6 .7 .8 .9 .1 .2 .3 .4 .5 .6 .7 .8 .9 .1 .2 .3 .4 .5 .6 .7 .8 .9 .1 .2 .3 .4 .5 .6 .7 .8 .9 .1 .2
1349
1350
1351
1352
TIME (E.S.T.)
fig 17

Figure 20

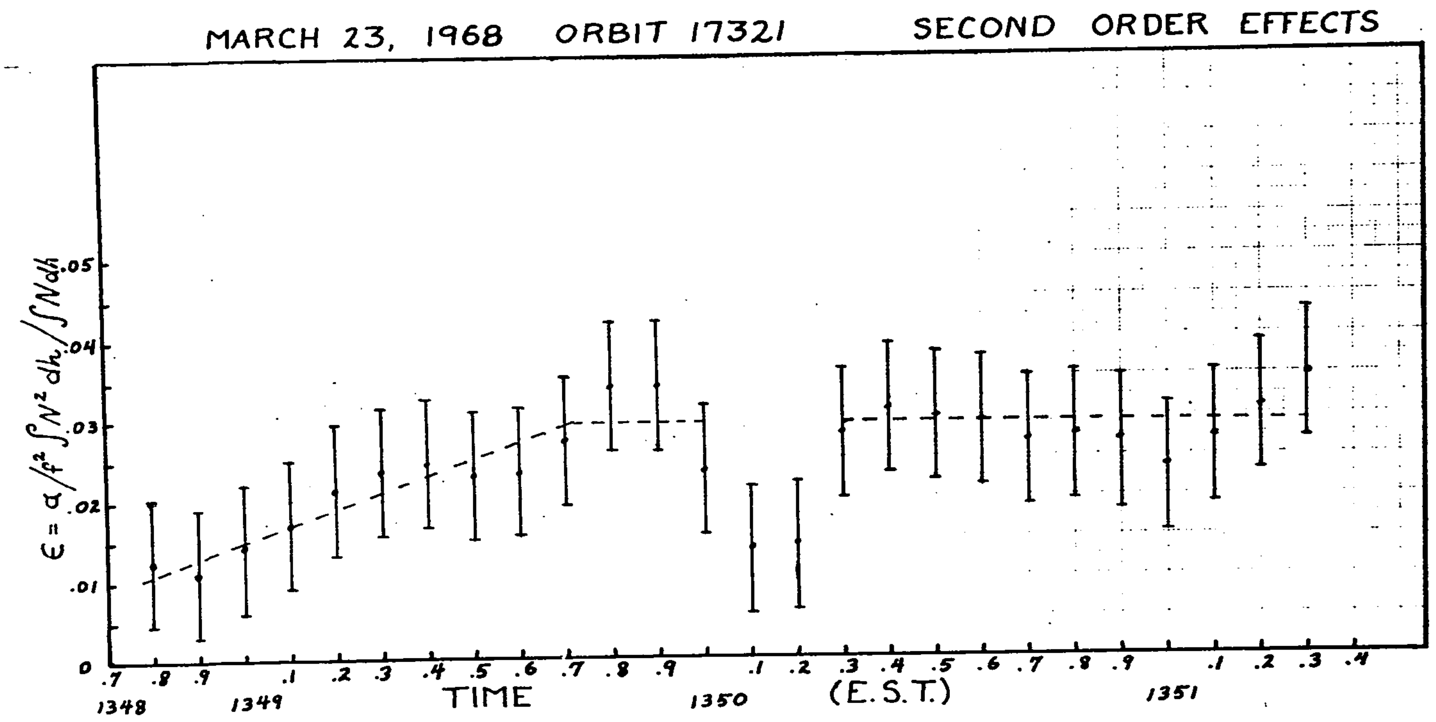
MARCH 23, 1968 ORBIT 17321 SECOND ORDER EFFECTS
$\epsilon = \alpha / f^2 \int N^2 dh / \int N dh$
.05
.04
.03
.02
.01
0
.7 .8 .9 .1 .2 .3 .4 .5 .6 .7 .8 .9 .1 .2 .3 .4 .5 .6 .7 .8 .9 .1 .2 .3 .4
1348
1349
1350
1351
TIME
(E.S.T.)

Figure 21

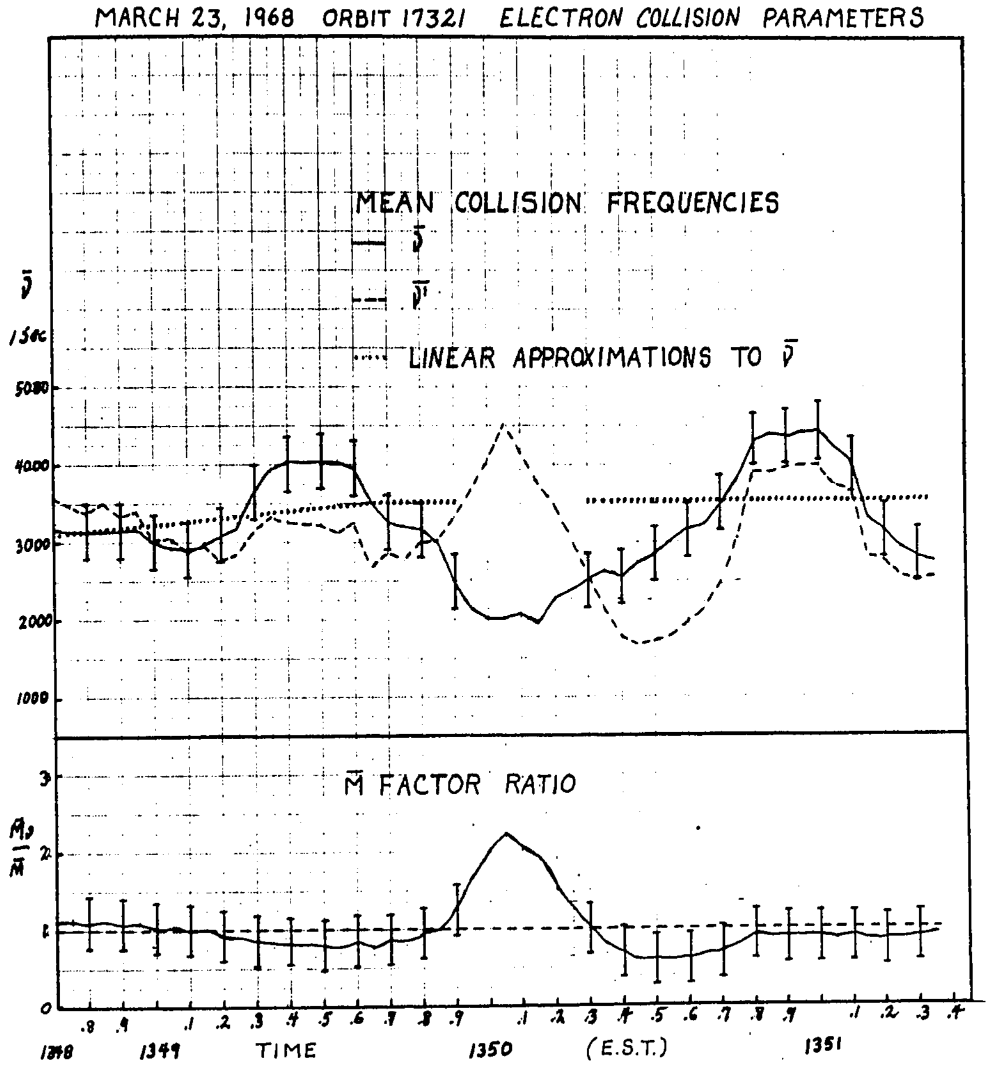
MARCH 23, 1968 ORBIT 17321 ELECTRON COLLISION PARAMETERS
MEAN COLLISION FREQUENCIES
$\bar{\nu}$
$\bar{\nu}'$
LINEAR APPROXIMATIONS TO $\bar{\nu}$
$\bar{\nu}$
/sec
5000
4000
3000
2000
1000
$\bar{M}$ FACTOR RATIO
$\frac{\bar{M}_\nu}{\bar{M}}$
3
2
1
0
.8
.9
.1
.2
.3
.4
.5
.6
.7
.8
.9
.1
.2
.3
.4
.5
.6
.7
.8
.9
.1
.2
.3
.4
1348
1349
TIME
1350
(E.S.T.)
1351

Figure 22

second order alone has a periodic structure with period 0.5 ± .05 minutes (~60 km horizontal scale size at F region heights). The peak to peak variation, however, exceeds experimental error only between 1349.85 and 1350.1, 1350.1 and 1350.75, 1351 and 1351.35.

$\epsilon = a\int_0^{h_s} N^2 dh \,/ f^2 \int_0^{h_s} N\, dh$ is plotted in fig. 21. Over the pass interval 1348.9 to 1349.7, ϵ has a positive linear gradient of 1.67 x $10^{-4}/M^3$ km ± 50% and a total increase of 55 ± 38%. Over the interval 1349.7 to 1351.3, ϵ is constant to within experimental error with the exception of the more restricted interval 1350 to 1350.3 in which ϵ decreases by 50 ± 30%.

$\bar{\nu}$, $\bar{\nu}'$ and $\frac{\overline{M_\nu}}{\bar{M}}$ are found in fig. 22. Over the pass interval 1348.9 to 1349.7 $\bar{\nu}$ may be fit with a positive linear gradient of 3.7/sec km which yields a total change in $\bar{\nu}$ of 11.4 ± 10%. Over the interval 1349.7 to 1351.3, the appropriate linear approximation to $\bar{\nu}$ is a constant with the possible exception of the interval 1349.9 to 1350.3 in which saturation of one channel of the tape recorder destroyed the usefulness of the extraordinary mode amplitude. $\bar{\nu}$ departs significantly from its best fit linear approximation by 7% in the interval 1349.3 to 1349.65, -17% in the interval 1350.4 to 1350.6, and 14% in the interval 1350.75 to 1351.1.

$\frac{\overline{M_\nu}}{\bar{M}}$ is generally within experimental error of 1.0 except for the interval 1350.45 to 1350.65 where it decreases significantly from 1.0 by 3%. The peak between 1349.9 and 1350.3 was produced by the tape recorder saturation problem mentioned earlier.

From the expected symmetry of the field point scintillation about the field point angle minimum (in terms of the angle between the magnetic field vector and the linear propagation path) the maximum height of the scintillating region is 600 ± 50 km.

Interpretation of the gross features of the data yields the following picture of the ionosphere during this pass.

From the mean behavior of $\int_0^{h_s} N\,dh$ and ϵ in the pass interval 1348.9 to 1349.7, the electron density profile is becoming sharper and the peak electron density is increasing. Over this interval $\bar{\nu}$ behaves as ϵ to within experimental error (the maximum change in $\bar{\nu}$, 21.4%, is greater than the minimum change in ϵ, 17%) and thus, no changes in electron temperature are observed. $\frac{\overline{M'}}{\overline{M}}$ is within experimental error of 1.0 which precludes major changes in the electron temperature profile and large changes in the lower ionosphere (below 140 km) contributions to the total absorption.

Using the parabolic ionosphere model of Appendix C, a semi quantitative estimate may be made of changes in the F region electron density profile. Assuming that the F region electron content changes by the same fraction as the total electron content over the pass,

$$\frac{\int_0^{h_s} N dh_{1349.7}}{\int_0^{h_s} N dh_{1348.9}} = \frac{(h' X_{MAX})_{1349.7}}{(h' X_{MAX})_{1348.9}} = 1.0 , \quad \frac{\epsilon_{1349.7}}{\epsilon_{1348.9}} = \frac{X_{MAX\,1349.7}}{X_{MAX\,1348.9}}$$

$$= 1.17 \text{ (minimum)}$$

or X_{MAX} is 14.5% smaller at 1348.9 than at 1349.7. Thus $\frac{h'_{1349.7}}{h'_{1348.9}} = 0.85$ and the F region thickness is smaller by 15% at 1349.7 than at 1348.9.

The average behavior of $\int_0^{h_s} N dh$, ϵ , $\tilde{\nu}$ and $\frac{\bar{M}_\nu}{\bar{M}}$ in the interval 1349.7 to 1351.3 is consistent with a constant electron density profile (with the exception of the interval 1350 to 1350.3), a constant or slowly declining electron temperature (any changes are still within experimental error) and a possible small upward displacement of the absorption index centroid as compared to the electron density centroid height ($\frac{\bar{M}_\nu}{\bar{M}}$ is < 1 for most of this portion of the pass but is still within experimental error of 1.0).

Examining the data in greater detail, although there is some evidence for small expansions of the F region in the vicinity of the electron content maxima, the relevant variations in ϵ are for the most part well within experimental error of the ϵ mean trend. The single exception is found in the interval 1350 to 1350.3. This irregularity in ϵ corresponds to an $\int_0^{h_s} N dh$ irregularity with a peak to peak amplitude of 1.5 ± 1.2%

of the mean electron content and to a local broadening of the F region combined with a decrease in peak density. From the parabolic profile of Appendix C, the expansion phase corresponds to $\Delta \epsilon = 0.94$, to $\Delta \int_0^{h_s} N dh = 1.015$ and thus to $\Delta h' = 1.04$. That is, a 6% decrease in peak electron density coupled with an 8% increase in F region thickness and a 1.5% increase in electron content.

Unfortunately, both $\bar{\nu}$ and $\frac{\bar{M}\nu}{\bar{M}}$ are not usable in this interval because of the previously mentioned instrumentation problem, however, examination of the raw data over this interval reveals less than normal absorption and, in the vicinity of 1350, an amplitude peak which could well be a focussing effect. Both features are compatible with the conditions above when the electron temperature is constant or rising.

The $\bar{\nu}$ irregularity in the pass interval 1349.3 to 1349.65 agrees with ϵ to within experimental error. As $\frac{\bar{M}\nu}{\bar{M}}$ at this point is within experimental error, this feature may be interpreted as an electron density irregularity in the F region with no measurable temperature change.

The $\bar{\nu}$ irregularity in the pass interval 1350.4 to 1350.6 again lies within experimental error of ϵ but corresponds to a significant variation in $\frac{\bar{M}\nu}{\bar{M}}$ of 3% below 1.0, a decrease in absorption centroid height below the electron density centroid by 60 ± 30 km. The most likely explanation for this is a decrease in absorption index below 140 km, caused by an electron temperature increase and/or electron density decrease. The remaining $\tilde{\nu}$ irregularity, 14% variation in the interval 1350.75 to 1351.1 can be explained in terms of the variation of ϵ except in the vicinity of 1351.0 where a columnar decrease in electron temperature of at least 3% is required to obtain the correct variation of $\tilde{\nu}$ with ϵ .

(4.3.2) MARCH 20, 1968

Examination of the raw data (fig. 24) reveals the presence of scintillation over most of the pass with the scintillation depth and rate increasing markedly in the vicinity of the field point. Both ordinary and extraordinary mode amplitudes show noticeable variation from the "Smooth" (spherically stratified) ionosphere case in the form of amplitude decreases in the vicinities of pass times 1413.4, 1414.2. The step discontinuities in the ordinary mode amplitude trace are caused by tape recorder input level changes made during the pass and are removed during analysis.

The only obvious anomalies in the polarization plane rotation angle, Ω , are changes in rotation rate visible from 1414 to the end of the pass. The resulting first and second order electron contents are found in fig. 25.

The two upper curves are again first order contents derived without and with the coincidence point corrections (-3.2±.2% at the ramp coincidence time 1414.55), the lower curve is the second order electron content computed from the two rotation angles using Equation (2-7a).

Over the pass interval 1412.7 to 1414.0 the second order electron content, $\int_0^{h_s} N dh$, may be fit with a mean linear gradient of $1.2 \times 10^{14}/M^2$ km while the first

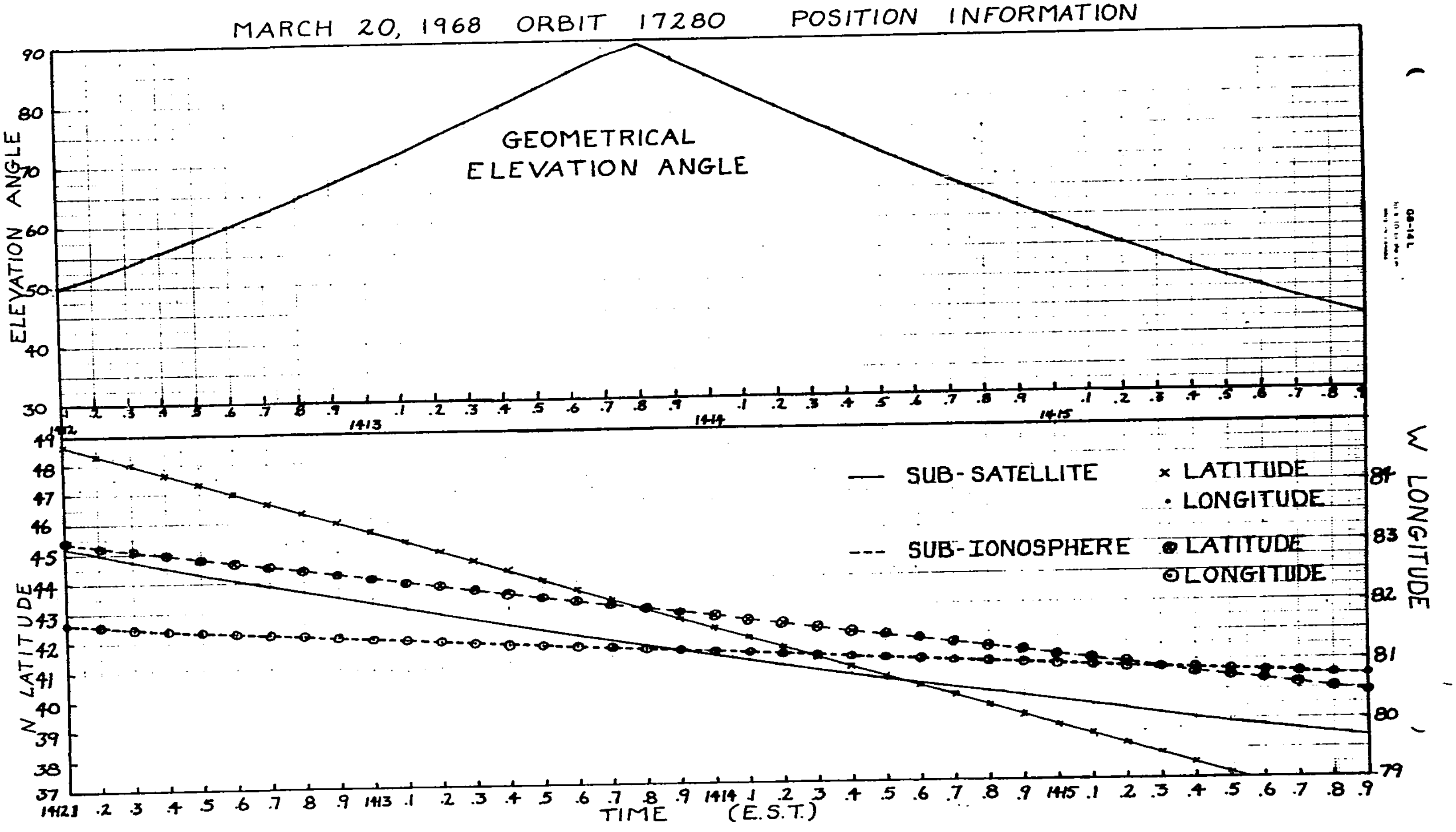
MARCH 20, 1968 ORBIT 17280 POSITION INFORMATION
GEOMETRICAL ELEVATION ANGLE
ELEVATION ANGLE
90
80
70
60
50
40
30
N LATITUDE
49
48
47
46
45
44
43
42
41
40
39
38
37
W LONGITUDE
84
83
82
81
80
79
— SUB-SATELLITE × LATITUDE
· LONGITUDE
--- SUB-IONOSPHERE ● LATITUDE
⊙ LONGITUDE
1412
1413
1414
1415
TIME (E.S.T.)

Figure 23

RAW DATA

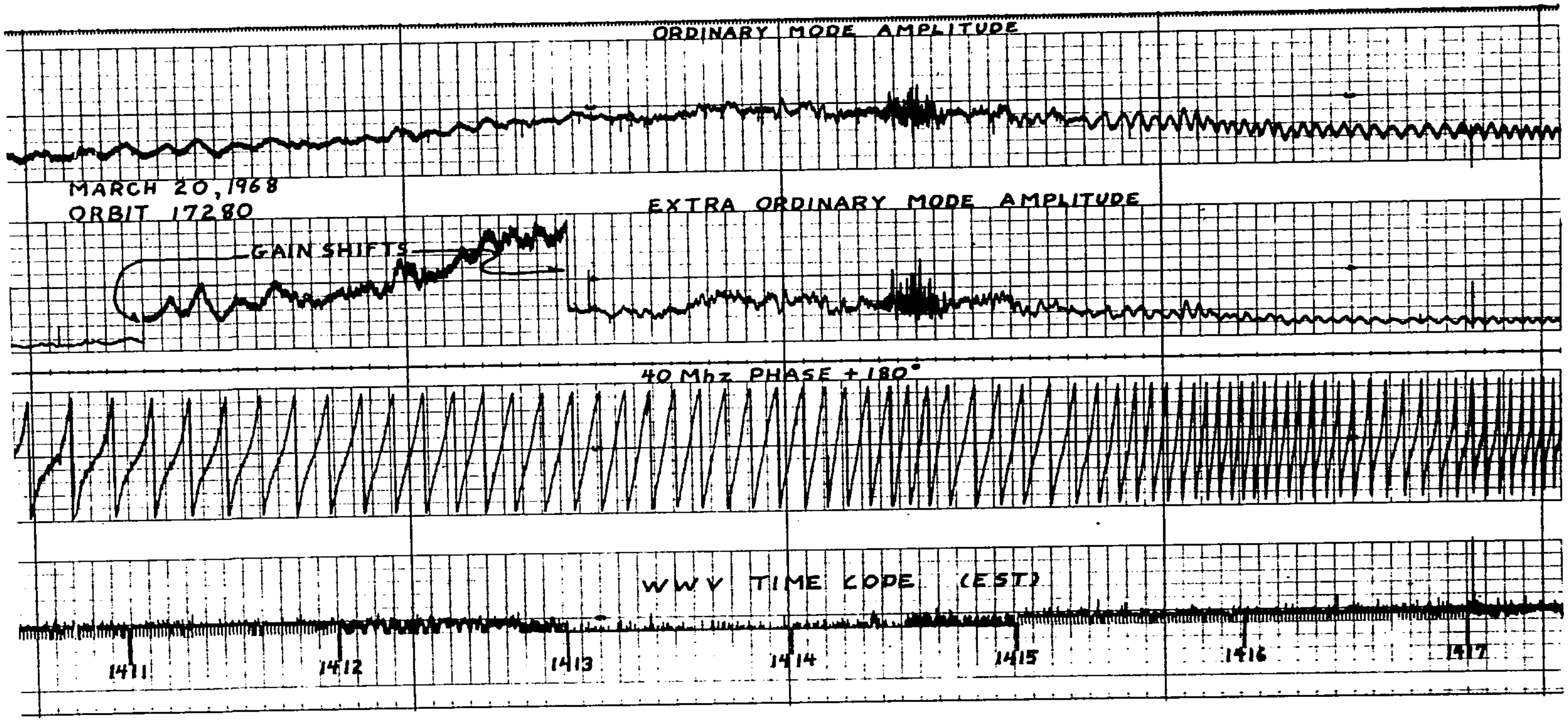

Figure 24

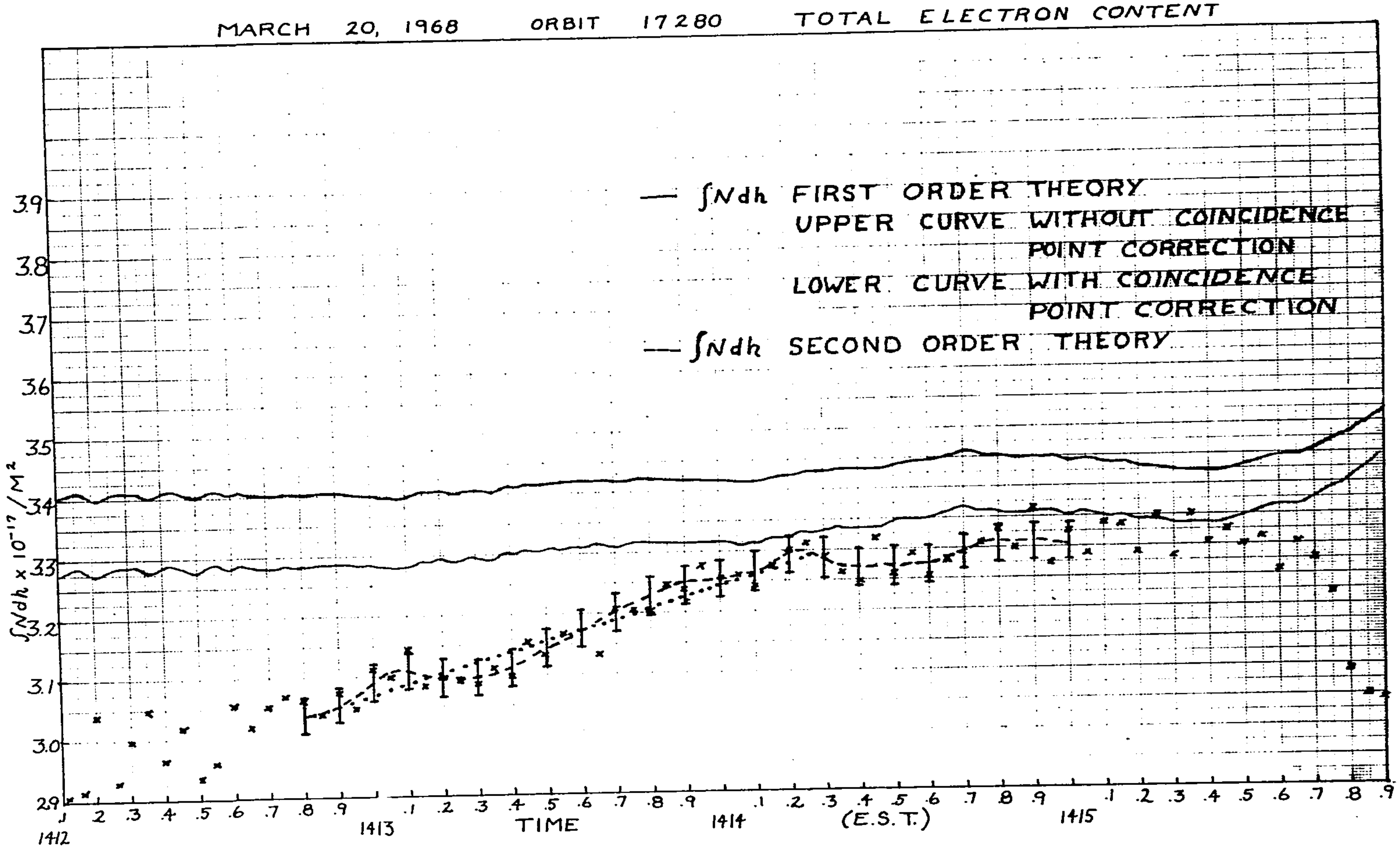
MARCH 20, 1968 ORBIT 17280 TOTAL ELECTRON CONTENT
— ∫Ndh FIRST ORDER THEORY
UPPER CURVE WITHOUT COINCIDENCE POINT CORRECTION
LOWER CURVE WITH COINCIDENCE POINT CORRECTION
— ∫Ndh SECOND ORDER THEORY
∫Ndh × 10⁻¹⁷/M²
3.9
3.8
3.7
3.6
3.5
3.4
3.3
3.2
3.1
3.0
2.9
.1 .2 .3 .4 .5 .6 .7 .8 .9
1412
1413
1414
1415
TIME
(E.S.T.)

Figure 25

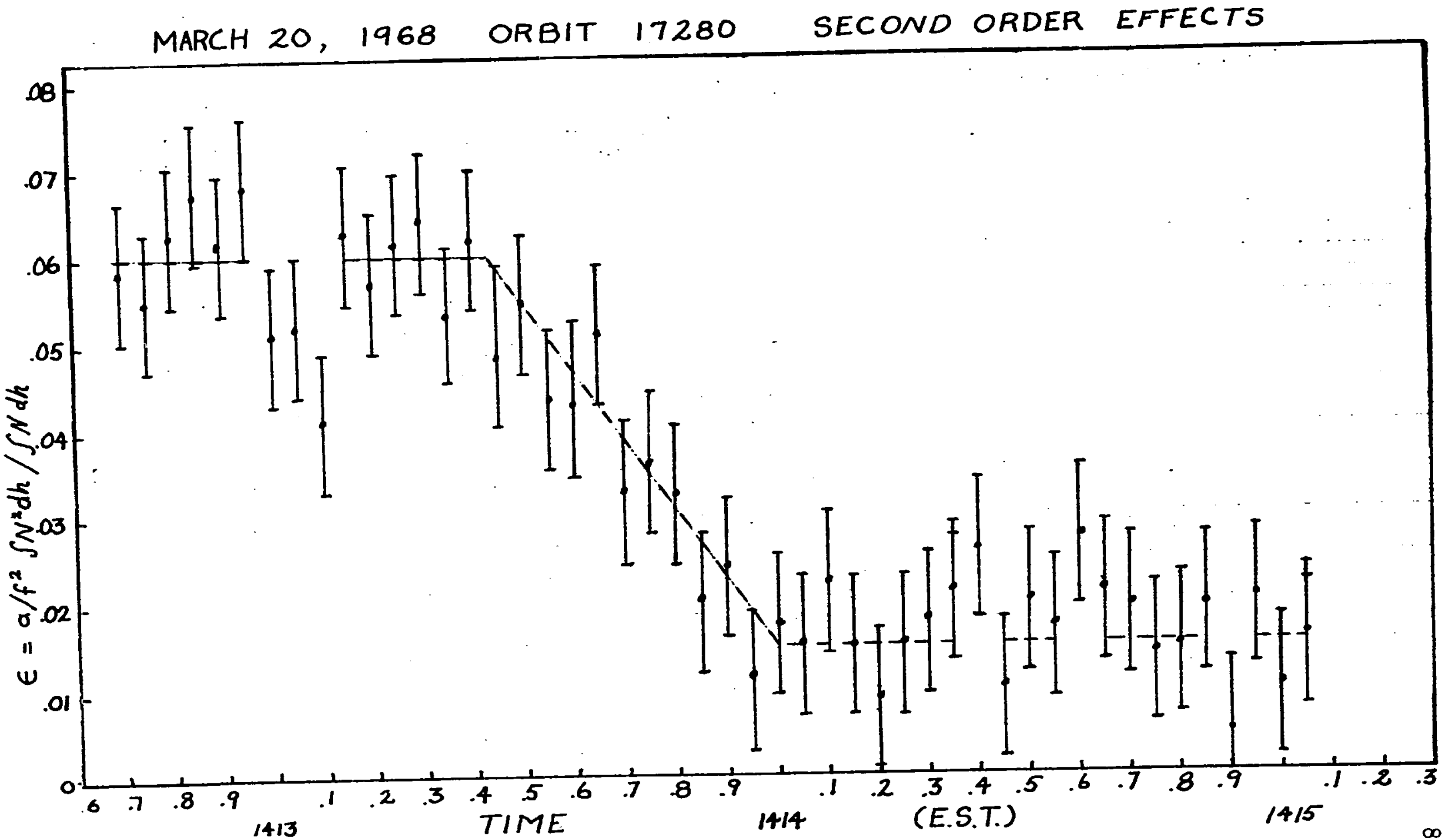
MARCH 20, 1968 ORBIT 17280 SECOND ORDER EFFECTS
$\epsilon = a/f^2 \int N^2 dh / \int N dh$
.08
.07
.06
.05
.04
.03
.02
.01
0
.6
.7
.8
.9
.1
.2
.3
.4
.5
.6
.7
.8
.9
.1
.2
.3
.4
.5
.6
.7
.8
.9
.1
.2
.3
1413
TIME
1414
(E.S.T.)
1415

Figure 26

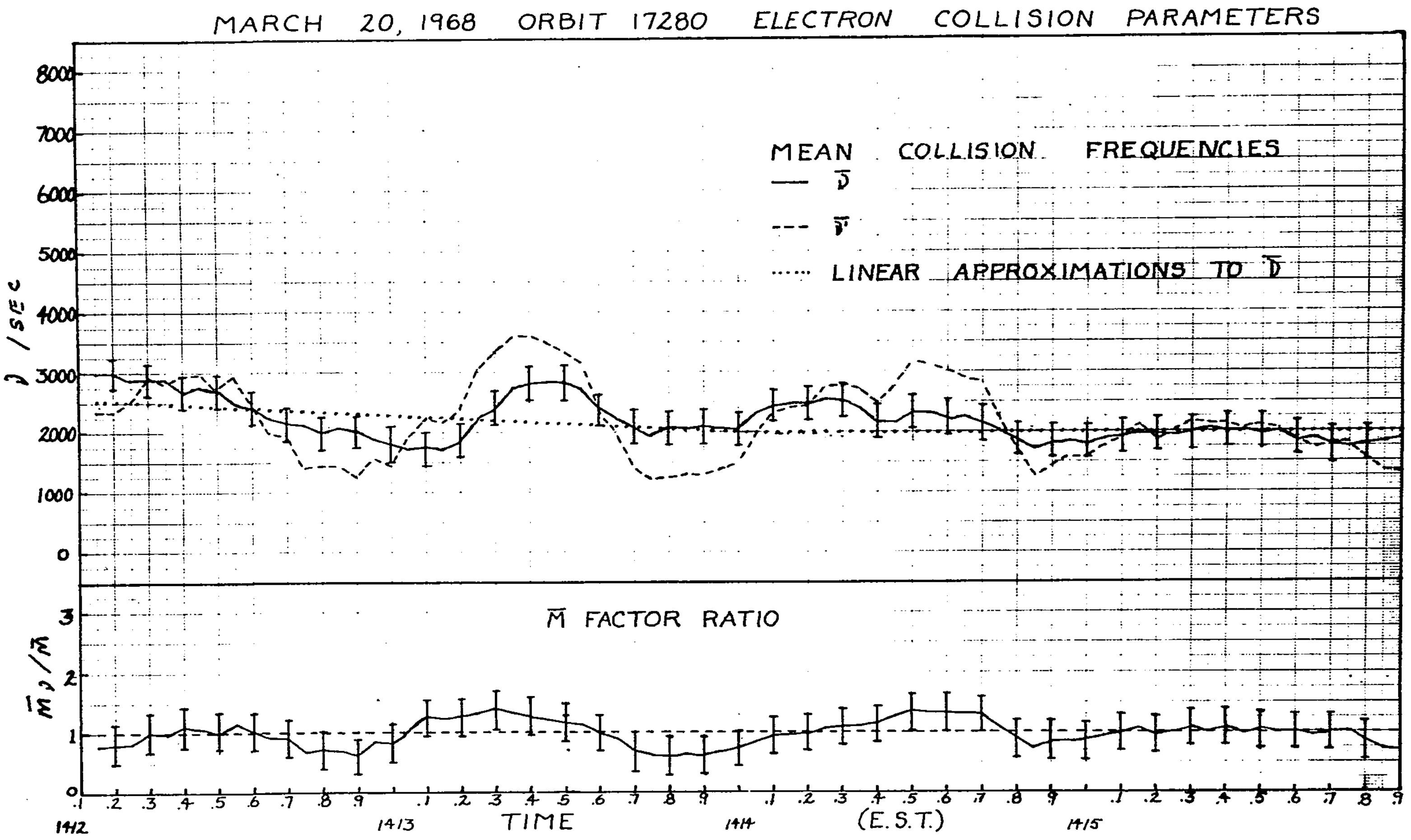
MARCH 20, 1968 ORBIT 17280 ELECTRON COLLISION PARAMETERS
MEAN COLLISION FREQUENCIES
— $\bar{\nu}$
--- $\bar{\nu}'$
····· LINEAR APPROXIMATIONS TO $\bar{\nu}$
ν /SEC
8000
7000
6000
5000
4000
3000
2000
1000
0
$\bar{M}$ FACTOR RATIO
$\bar{M}_\nu/\bar{M}$
3
2
1
0
.1 .2 .3 .4 .5 .6 .7 .8 .9
1412
1413
1414
1415
TIME
(E.S.T.)

Figure 27

order content displays a much smaller (factor of 8.8) gradient of $1.6 \times 10^{13}/M^2$ km. Over the pass interval 1414.1 to 1415, the second order electron content varies with the first order content to within experimental error. Both have a mean gradient of $4.17 \times 10^{13}/M^3$ km.

$\epsilon = \frac{a \int^{h_s} N' dh}{f^2 \int_0^{h_s} N dh}$ is displayed in fig. 26. The best linear fit over the interval 1412.8 to 1414.0 yields a decreasing gradient ∇ in the range $1.7 \times 10^{-4}/M^3 \text{ km} \leq \nabla \leq 2.5 \times 10^{-4}/M^3$ km. ϵ is significantly below the best fit line over the pass interval 1412.95 to 1413.15. In the pass interval 1414.0 to 1415 the best linear fit to ϵ is a constant.

The electron collision parameters $\bar{\nu}$, $\bar{\nu}'$ and $\frac{\bar{M}_\nu}{\bar{M}}$ are plotted in fig. 27. In the pass interval 1412.7 to 1414 the best fit line to $\bar{\nu}$ has a slope of 2.4/sec km which represents a change in $\bar{\nu}$ of 18.5% over the entire interval. In the pass interval 1414 to 1415 the trend of $\bar{\nu}$ is a constant. $\bar{\nu}$ departs significantly from its linear means only in four regions of the pass, 1412.6 to 1413.2 maximum deviation -11%, 1413.35 to 1413.55 maximum deviation 17%, 1414.05 to 1414.36 maximum deviation 12.5%, and 1414.45 to 1414.55 maximum deviation 2.5%.

$\frac{\bar{M}_\nu}{\bar{M}}$ oscillates about 1.0 over the entire pass with significant departures (average) from its mean of -3% in the interval 1412.8 to 1413.0, 0.5% in the interval 1413.2 to 1413.4, and -3% in the interval 1413.7 to 1413.4.

From the expected symmetry of the field point scintillations about the field point angle minimum, the maximum height of the scintillation region is 700 ± 50 km.

Considering the gross features of the data, in the pass interval 1412.7 to 1414.0 the electron content increases by 7.6 ± 1.2%, ϵ decreases by a factor of 4.0 ± 2.0 and in the pass interval 1414 to 1415, both $\int_0^{h_s} N dh$ and ϵ are nearly constant.

This is consistent with a broadening F region profile and declining peak electron density in the first interval, and a constant profile over the second. Once again applying the parabolic ionosphere model of Appendix C (to the first interval), we have

$$\Delta\epsilon = \frac{\epsilon_{1414.0}}{\epsilon_{1412.7}} = 0.5 \quad , \qquad \Delta \int_0^{h_s} N dh = \frac{\int_0^{h_s} N dh_{1414.0}}{\int_0^{h_s} N dh_{1412.7}} = 1.07$$

and thus

$$\Delta h' = \frac{h'_{1414.0}}{h'_{1412.7}} = 2.14$$

This implies a large change (factor of 1/2) in the peak density and a correspondingly large change (factor of 2.1) in layer thickness.

Comparison of the gross changes in $\frac{\bar{M}\nu}{M}$, $\bar{\nu}$, $\int N dh$ and ϵ for the first interval reveals a constant mean ratio (nearly identical electron density and absorption index centroid heights), a decline of 25 ± 25% in $\bar{\nu}$ and the previously mentioned decline in ϵ .

As $\frac{\bar{M}_\nu}{\bar{M}} \approx 1.0$ the fraction of the absorption above 140 km, from section 2.5, should be no less than 70%. Choosing the minimum variation in ϵ compatible with the data, 2.0, and the maximum variation in $\bar{\nu}$ compatible with the data, 50%, the minimum columnar electron temperature change required to make $\bar{\nu}$ and ϵ consistent is a decrease of 25%.

Over the second interval, $\int_0^{h_s} N dh$, $\bar{\nu}$ and ϵ are all nearly consistent which is compatible with a constant profile, constant peak electron density and a constant electron temperature.

With this general picture of the ionosphere in mind, let us now examine the data in greater detail.

In the pass interval 1412.7 to 1413.3 $\int_0^{h_s} N dh$ displays a small positive irregularity centered at time 1413.1 (2.4 ± 0.6% of the total electron content), ϵ decreases by 17±13% and $\bar{\nu}$ decreases by 11%. $\bar{\nu}$ and ϵ agree with each other to within experimental error and thus there is little or no change in electron temperature associated with the irregularity.

The minimum change in ϵ is-4% or $\Delta \epsilon = .96$, the minimum change in $\int_0^{h_s} N dh$ is 1.8% or $\Delta \int_0^{h_s} N dh = 1.018$

and thus Δh = 1.06 during the initial phase of the disturbance. All parameters return to the initial values at the end of the interval. $\frac{\bar{M}\nu}{\bar{M}}$ varies significantly from 1.0 by -3% in the more restricted interval 1412.8 to 1412.95, which corresponds to an increase in absorption index centroid height of 60 ± 30 km above the electron density centroid, but which occurs before the observed F region profile broadening and $\int_0^{h_s} N\,dh$ irregularity peak. $\bar{\nu}$ increases over this interval but the increase is small (within experimental error).

A possible interpretation of this feature is a redistribution of the total absorption above and below 140 km. An increase in the fraction of the absorption above 140 km by 11% is adequate to explain a rise in the absorption index centroid of 60 km with little or no change in the electron density centroid position (section 2.5).

Over the larger interval, $\frac{\bar{M}\nu}{\bar{M}}$ rises to a significant variation of 0.5% at 1413.3. That is, the absorption index centroid drops to 10 ± 10 km below the electron density centroid by 1413.3.

In the pass interval 1413.4 to 1414.0, ϵ decreases by a factor of 4 ± 2 while $\int_0^{h_s} N\,dh$ rises 5.4 ± 0.6%. From 1413.3 to 1413.5 $\bar{\nu}$ rises to a peak significant variation of 17% (31 ± 14%), drops to the estimated mean by 1413.6, and does not change significantly before 1414.0.

It must be noted that if the $\frac{\bar{M}\nu}{\bar{M}}$ irregularity at 1412.8 to 1412.95 is truly a lower ionosphere effect, from the ray elevation angle graph (fig. 23), it lies directly below the F region as seen at 1413.4 and thus must be considered in terms of the ionosphere parameters seen in that portion of the pass.

During the interval 1413.3 to 1413.8 $\frac{\bar{M}\nu}{\bar{M}}$ declines steadily to a minimum of -3% in the interval 1413.7 to 1413.9.

The initial rise in $\bar{\nu}$ (up to 1413.3) corresponds in time to the variation of ϵ (to within experimental error) and to a constant $\int_0^{h_s} N\,dh$. Thus, the electron density profile remains constant but T_e decreases by approximately 6%. The declining value of $\bar{\nu}$ corresponds to a decrease of ϵ by 21% and a subsequent increase in electron temperature by 1%.

The increasing trend of $\int_0^{h_s} N\,dh$ and decreasing trend of ϵ indicate a broadening F region and decreasing density as were computed from the gross record characteristics, T_e decreases by 20%.

$\frac{\bar{M}\nu}{\bar{M}}$ rises to 0.5% at 1413.3, then declines steadily to -3% in the interval 1413.7 to 1413.9. This minimum is again probably a lower ionosphere effect.

The spatial relations of the 1412.9 $\frac{\bar{M}\nu}{\bar{M}}$

irregularity, the 1413.45 $\tilde{\nu}$ irregularity, the F region spreading, and the 1413.8 $\frac{\tilde{M}\nu}{\tilde{M}}$ irregularity are shown in fig. 28 in terms of the ray path intersections with the F region and the lower ionosphere (for a plane stratified ionosphere). These features, then, appear to be part of the same ionospheric disturbance.

In the pass interval 1414 to 1415 $\tilde{\nu}$ varies as ϵ and $\int_0^{h_s} N dh$, ϵ are approximately constant as is $\frac{\tilde{M}\nu}{\tilde{M}}$. Thus the $\tilde{\nu}$ irregularities at 1414.05 to 1414.45 and 1414.45 to 1414.55 correspond to electron density increases near the peak of the electron density profile.

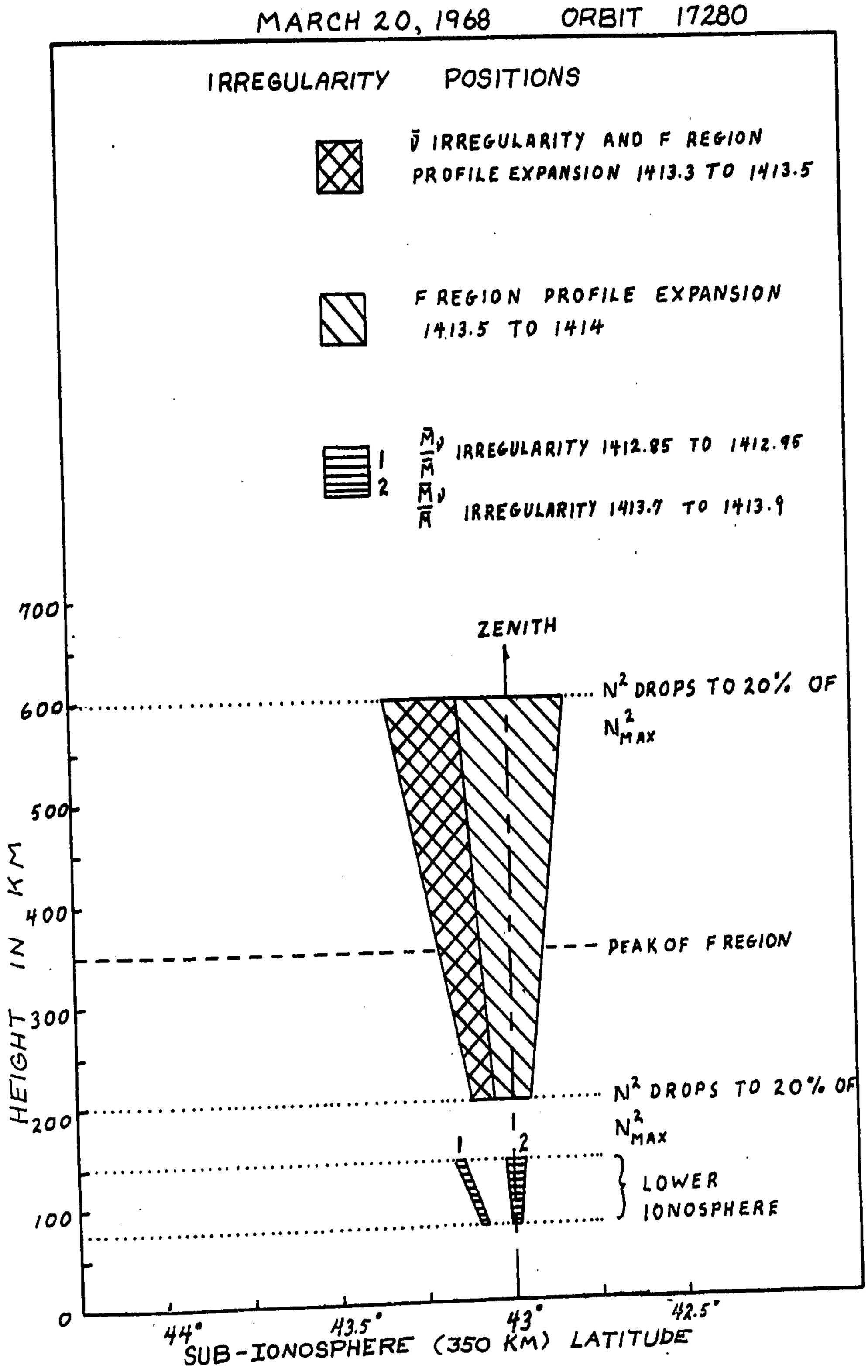
MARCH 20, 1968 ORBIT 17280
IRREGULARITY POSITIONS
$\bar{\nu}$ IRREGULARITY AND F REGION PROFILE EXPANSION 1413.3 TO 1413.5
F REGION PROFILE EXPANSION 14.13.5 TO 1414
1 $\frac{\bar{M}}{\bar{M}}$, ν IRREGULARITY 1412.85 TO 1412.95
2 $\frac{\bar{M}}{\bar{M}}$, ν IRREGULARITY 1413.7 TO 1413.9
ZENITH
N^2 DROPS TO 20% OF N^2_{MAX}
PEAK OF F REGION
N^2 DROPS TO 20% OF N^2_{MAX}
1
2
LOWER IONOSPHERE
HEIGHT IN KM
0
100
200
300
400
500
600
700
44°
43.5°
43°
42.5°
SUB-IONOSPHERE (350 KM) LATITUDE

Figure 28

(4.3.3) MARCH 17, 1968

The raw data (fig. 30) suggests a more complex ionosphere behavior on this pass than of either of the other two. Scintillation is present over most of the central portion of the pass with a pronounced change in scintillation rate in the vicinity of 14.37.8. Amplitude features which appear to be focussing effects are visible near pass times 1437.5, 1437.7. Both ordinary and extraordinary mode amplitudes are asymmetric about pass center (fig. 29) indicating greater absorption after pass center than before. The field point scintillation effects on this day are visible but the scintillation amplitude increase is not as pronounced as on either of the March 23 or March 20 records.

The amplitude discontinuities in the extraordinary mode trace are again caused by tape recorder input level changes and are removed in analysis.

The rotation rate anomalies are less evident during this pass than during the other two and are more gradual--they are found in the interval 1436.5 to 1439.

The resulting first and second order total electron contents are plotted in fig. 31. The two upper curves are the first order electron contents computed with and without the phase coincidence

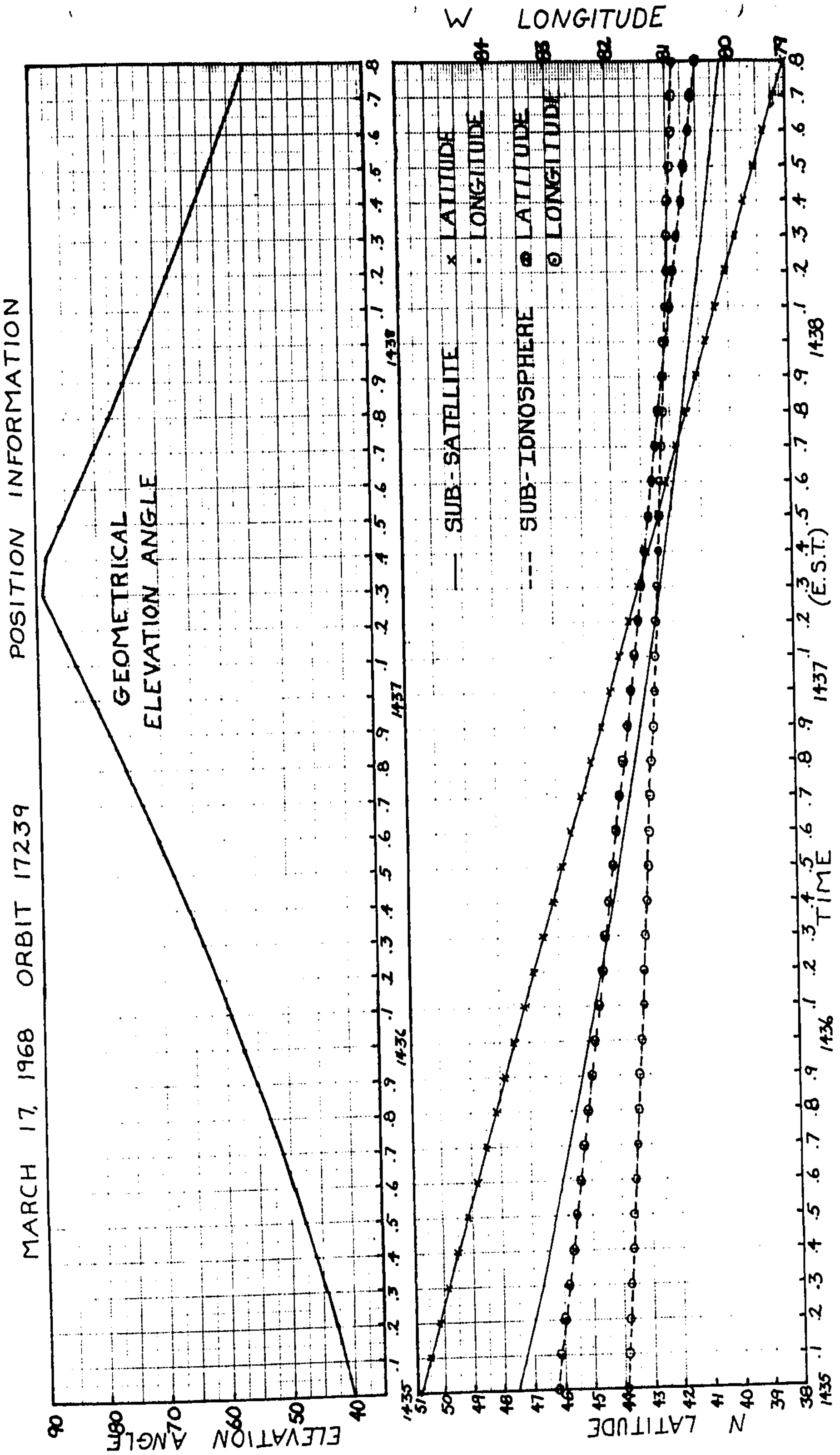
MARCH 17, 1968 ORBIT 17239 POSITION INFORMATION
GEOMETRICAL ELEVATION ANGLE
ELEVATION ANGLE
90
80
70
60
50
40
W LONGITUDE
84
83
82
81
80
79
— SUB-SATELLITE × LATITUDE
· LONGITUDE
--- SUB-IONOSPHERE ⊕ LATITUDE
⊙ LONGITUDE
N LATITUDE
51
50
49
48
47
46
45
44
43
42
41
40
39
38
1435
1436
1437
1438
.1 .2 .3 .4 .5 .6 .7 .8 .9
TIME (E.S.T.)

Figure 29

RAW DATA

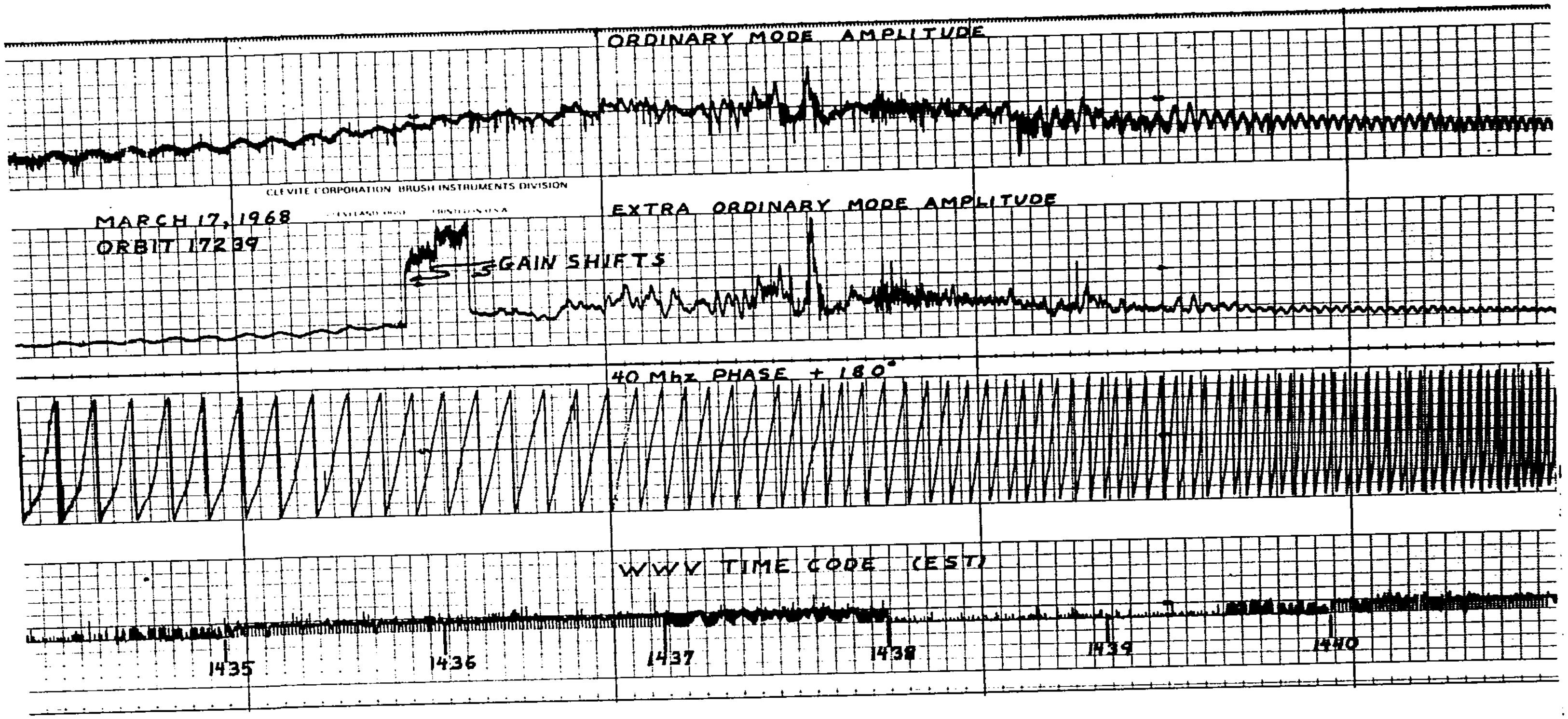

Figure 30

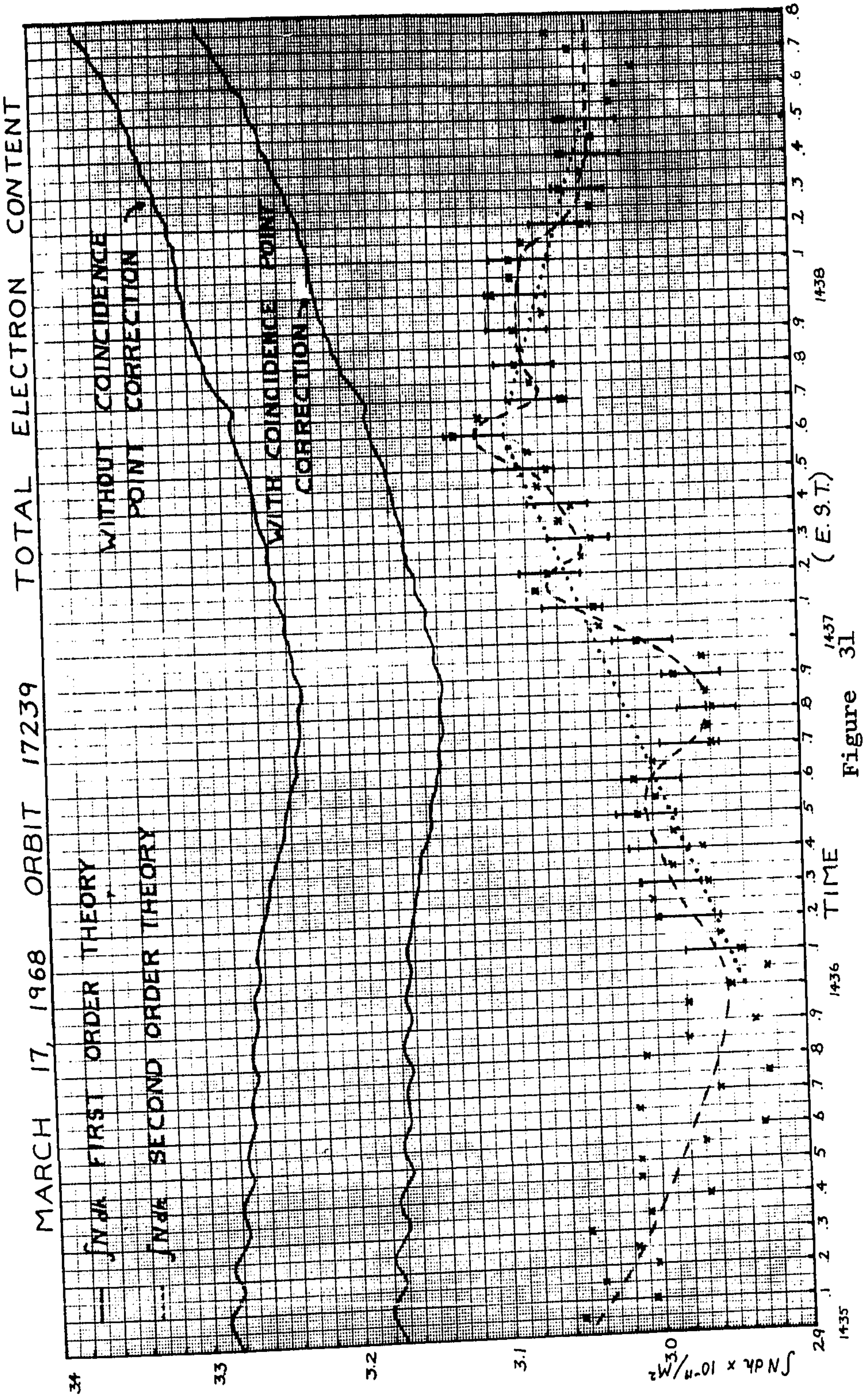
MARCH 17, 1968 ORBIT 17239 TOTAL ELECTRON CONTENT
— ∫N₁dh FIRST ORDER THEORY
---- ∫N₂dh SECOND ORDER THEORY
WITHOUT COINCIDENCE POINT CORRECTION
WITH COINCIDENCE POINT CORRECTION
3.4
3.3
3.2
3.1
3.0
2.9
∫Ndh × 10¹⁷/M²
1435
.1
.2
.3
.4
.5
.6
.7
.8
.9
1436
1437
1438
TIME (E.S.T.)

Figure 31

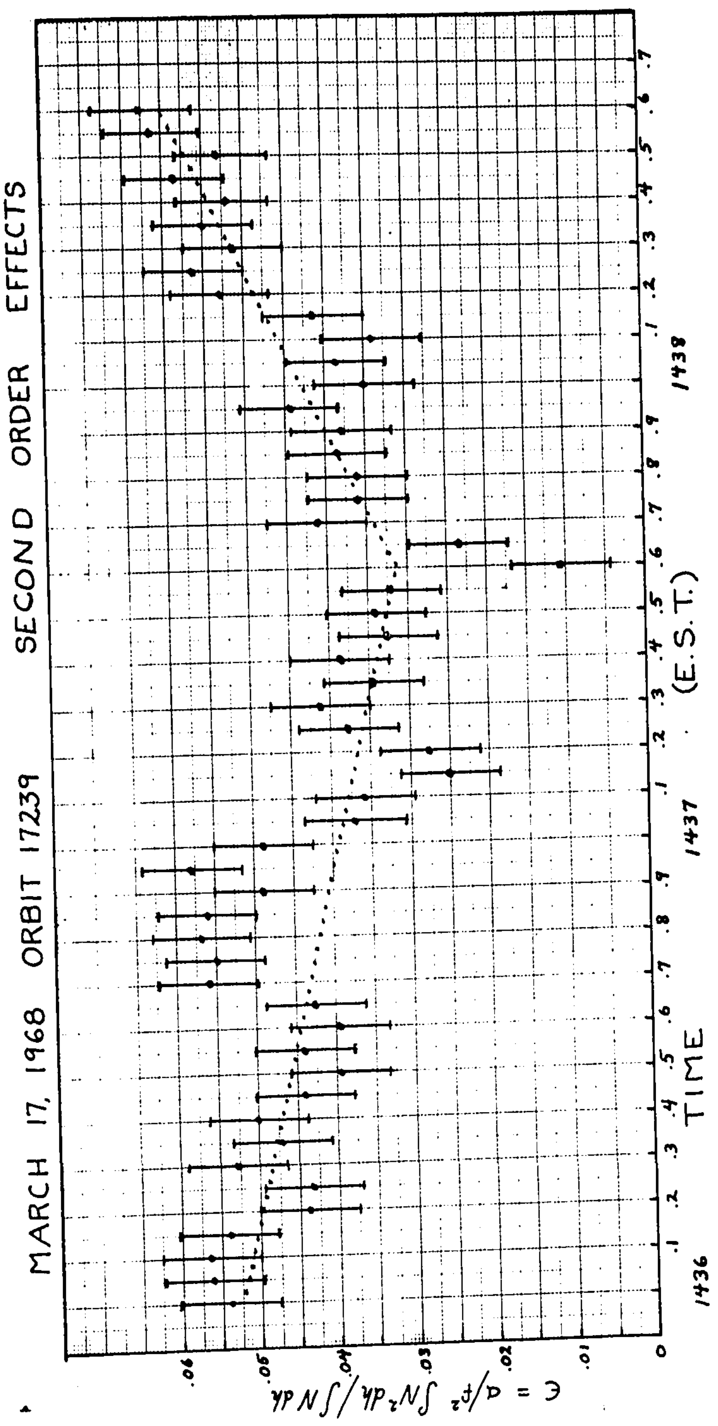
MARCH 17, 1968 ORBIT 17239 SECOND ORDER EFFECTS
$\epsilon = a/f^2 \int N^2 dh / \int N dh$
.06
.05
.04
.03
.02
.01
0
1436
.1
.2
.3
.4
.5
.6
.7
.8
.9
1437
.1
.2
.3
.4
.5
.6
.7
.8
.9
1438
.1
.2
.3
.4
.5
.6
.7
TIME (E.S.T.)

Figure 32

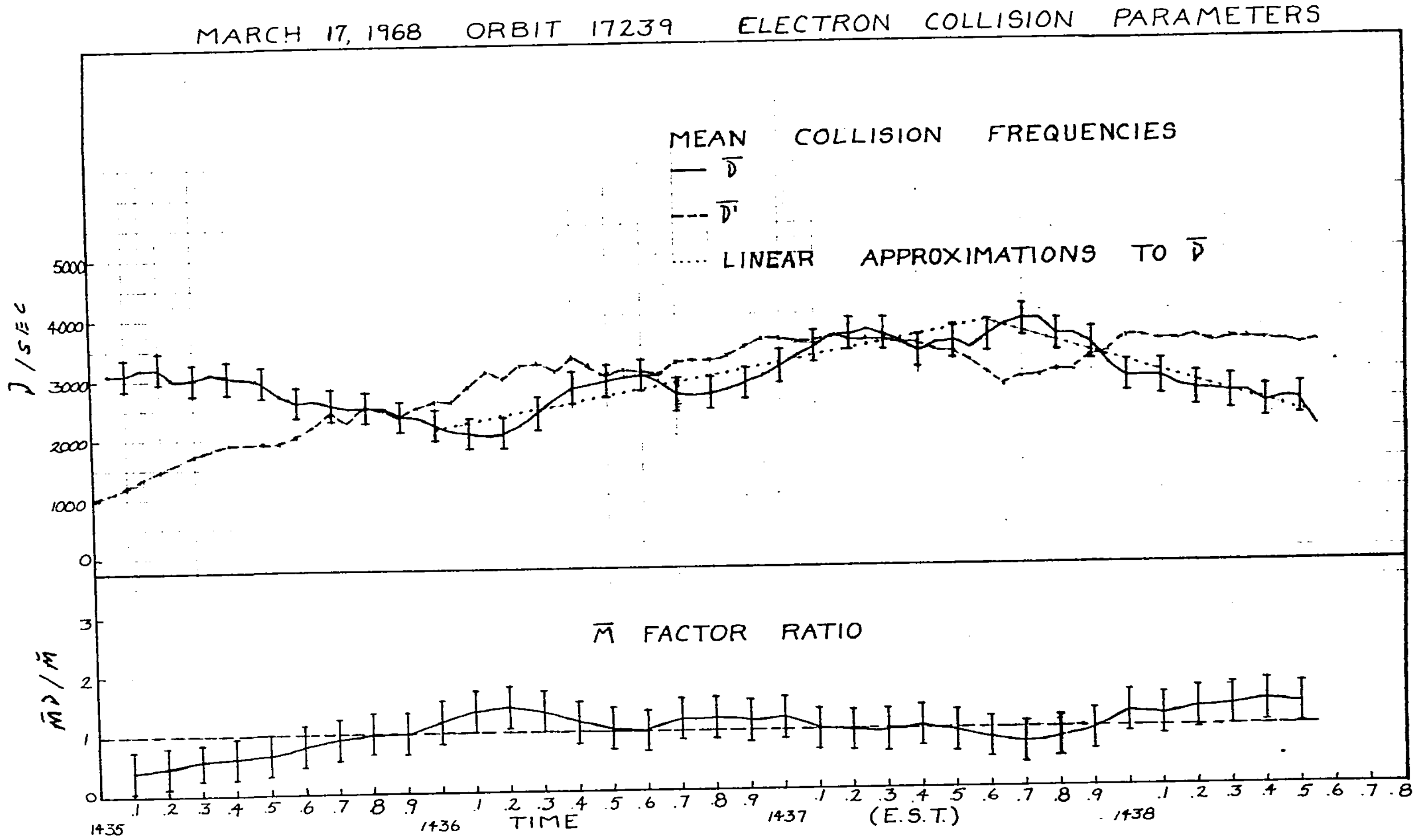
MARCH 17, 1968 ORBIT 17239 ELECTRON COLLISION PARAMETERS
MEAN COLLISION FREQUENCIES
— $\overline{\nu}$
--- $\overline{\nu}'$
..... LINEAR APPROXIMATIONS TO $\overline{\nu}$
ν/SEC
5000
4000
3000
2000
1000
0
$\overline{M}$ FACTOR RATIO
$\overline{M}\nu/\overline{M}$
3
2
1
0
.1 .2 .3 .4 .5 .6 .7 .8 .9
1435
1436
1437
1438
.1 .2 .3 .4 .5 .6 .7 .8 .9
.1 .2 .3 .4 .5 .6 .7 .8 .9
.1 .2 .3 .4 .5 .6 .7 .8
TIME (E.S.T.)

Figure 33

correction of -3.7% at the 1437.4 coincidence point. The lower curve is the second order electron content computed from Equation (2-7a).

The onset of the field point scintillation is too poorly defined to make a maximum height estimate.

Over the pass interval 1436 to 1437.6 the second order content may be fit with a linear gradient of $4.2 \times 10^{14}/M^2$ km and over the interval 1437.6 to 1438.6 with a linear gradient of $-9.5 \times 10^{13}/M^2$ km. The first order content may be fit with linear gradients of $-3.2 \times 10^{13}/M^2$ km in the interval 1436 to 1436.8 and of $2.8 \times 10^{14}/M^2$ km in the interval 1436.8 to 1438.6

Figure 32 may also be fit with a pair of linear gradients, $-1.1 \times 10^{-4}/M^3$ km in the interval 1436 to 1437.6 and $2.4 \times 10^{-4}/M^3$ km in the interval 1437.6 to 1438.6. Both $\int_0^{h_s} N\,dh$ and ϵ depart significantly from their mean trends but examination of the electron content data reveals a better approach to the discussion of the data.

The collision parameters $\bar{\nu}$, $\tilde{\nu}'$, $\frac{\bar{M}\nu}{\bar{M}}$ are found in fig. 33. They may be approximated with linear gradients to within experimental error. In the interval 1436 to 1437.6 the gradient is 9.2/sec km and in the interval 1437.6 to 1438.6 the gradient is -12.5/sec km. $\frac{\bar{M}\nu}{\bar{M}}$ has a declining trend over the interval 1436 to 1437.7 which lies within experimental error of 1.0, however, in the intervals 1436.1 to 1436.3 and 1438.3 to 1438.5 $\frac{\bar{M}'}{\bar{M}}$ is significantly greater than 1.0 by 2%.

Inspection of the second order electron content reveals the presence of at least two electron content irregularities--one in the interval 1436 to 1436.8 (horizontal scale size of 100 km at F region heights) with a peak electron content enhancement of 1.5 ± 0.6% and the other in the interval 1436.8 to 1438.4 (220 km horizontal scale size at F region heights) with a peak content enhancement of 4.5%. The smaller scale (20 km horizontal scale size) structure found in the intervals 1437.1 to 1437.25 and 1437.5 to 1437.7 (enhancements of 0.7 ± 0.6 % and 1.4 ± 0.6% respectively) may be considered to be separate irregularities superposed upon the large one.

A qualitative comparison of the $\int_0^{h_s} N dh$ and ϵ gradients reveals that the gradients diverge from pass time 1436 and converge towards pass time 1438.6. That is, an increase in $\int_0^{h_s} N dh$ corresponds to a decrease in ϵ --an expanding F region (up to 1437.6) and the decrease in $\int_0^{h_s} N dh$ corresponds to an increase in ϵ , a contracting F region.

A more detailed examination of the behavior of $\int_0^{h_s} N dh$ and ϵ reveals the same basic results for the 1438 to 1436.8 irregularity alone and suggests an independent existence for the two small electron content irregularities, again with the same basic behavior.

A qualitative comparison of $\bar{\nu}$, $\frac{\bar{M}\nu}{\bar{M}}$, $\int_0^{h_s} N dh$, and ϵ reveals that the collision frequency varies in the same manner as $\int_0^{h_s} N dh$, not as ϵ as in the other passes, and that $\frac{\bar{M}\nu}{\bar{M}}$ varies in the same manner as ϵ , as expected.

The corresponding quantitative results are as follows. The electron content and F region thickness maxima correspond to a drop in electron temperature (from initial conditions) of approximately 7% in the interval 1436 to 1436.8, and 14% in the interval 1436.8 to 1438.6.

Applying the model of Appendix C to the electron content irregularity in the interval 1436 to 1436.8, $\Delta \epsilon = 0.92$, $\Delta \int_0^{h_s} N dh = 1.015$, and thus $\Delta h' = 1.1$ (trough to peak estimate). The F region expands throughout the irregularity to its peak and then contracts. The electron content maximum corresponds to an electron density minimum.

Applying the Appendix C model to the large irregularity in the interval 1436.8 to 1438.6, $\Delta \epsilon = 0.78$, $\Delta \int_0^{h_s} N dh = 1.045$ and thus $\Delta h' = 1.34$ (trough to peak estimate). Again the F region expansion is synchronized with the electron content variations.

The $\frac{\bar{M}\nu}{\bar{M}}$ irregularities in the intervals

1436.1 to 1436.3 and 1438.3 to 1438.5 correspond to absorption index centroid height shifts of 40 ± 20 km below the electron density centroid height. As neither of these correlate with the other measured parameters, they are probably lower ionosphere effects. If so, their spatial positions (estimated in terms of their defining ray paths), fig. 34, show them to be vertically below the two small electron content irregularities in the vicinities of 1437.15 and 1437.6. The large irregularities do not correlate with $\frac{\bar{M}'}{\breve{M}}$ variations and thus are located in the F region, centered near the F region peak.

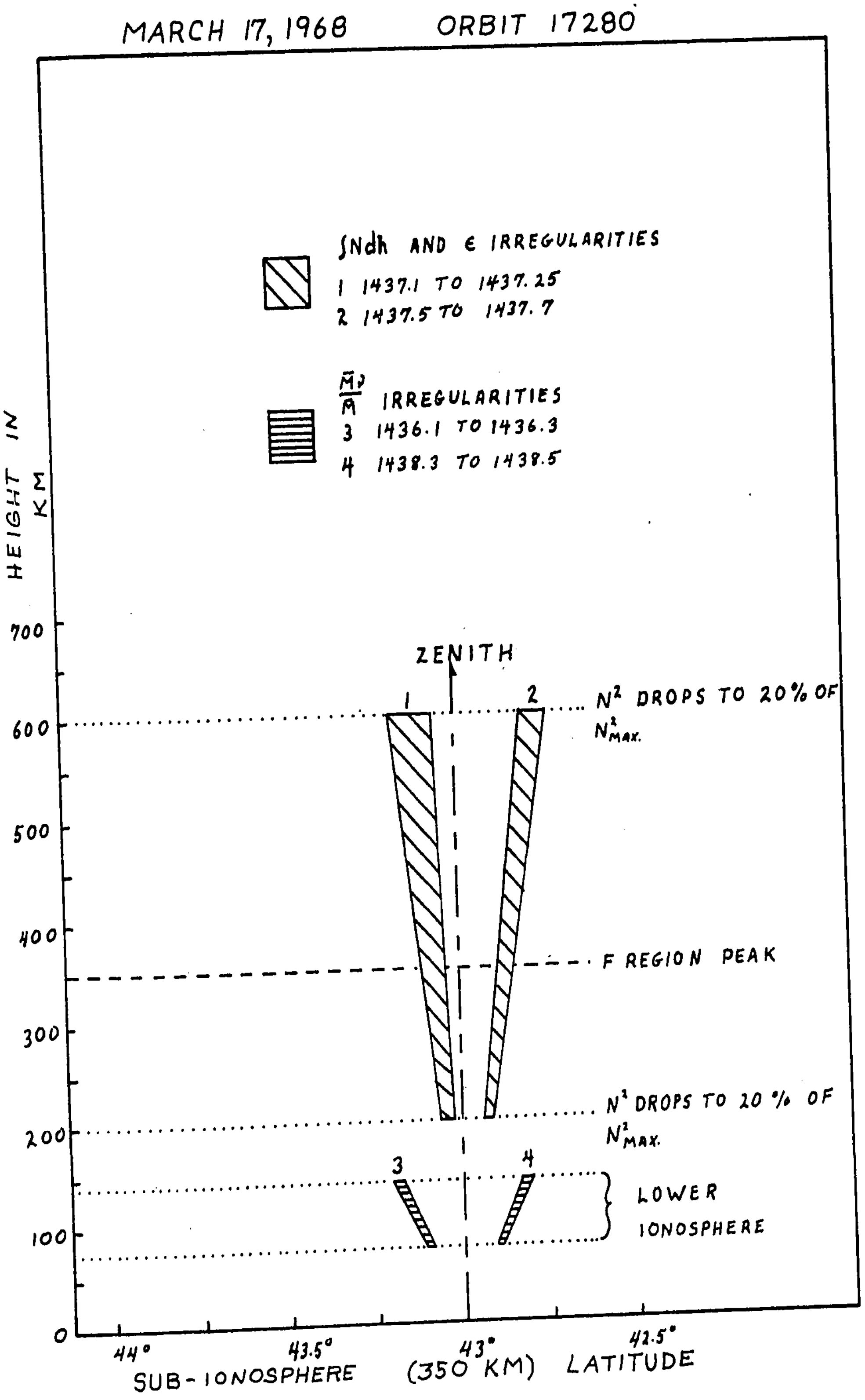
MARCH 17, 1968 ORBIT 17280
∫Ndh AND ε IRREGULARITIES
1 1437.1 TO 1437.25
2 1437.5 TO 1437.7
M̄J/M̄ IRREGULARITIES
3 1436.1 TO 1436.3
4 1438.3 TO 1438.5
HEIGHT IN KM
700
600
500
400
300
200
100
0
ZENITH
1
2
N² DROPS TO 20% OF N²MAX.
F REGION PEAK
N² DROPS TO 20 % OF N²MAX.
3
4
LOWER IONOSPHERE
44°
43.5°
43°
42.5°
SUB-IONOSPHERE (350 KM) LATITUDE

Figure 34

(4.4) SUMMARY

Measurements of the ordinary, extraordinary mode ray path splitting using amplitude time shifts have established that fluctuations in Faraday rotation angle with F region scale sizes of less than one kilometre may not simply be interpreted in terms of total electron content variations. This is in agreement with the theoretical calculations of section 2.4.

Since the three passes used in this experiment to evaluate the combined differential Faraday, differential absorption technique represent a biased sample of the available data (they were selected as moderately disturbed records with no large Faraday rotation anomalies, little large amplitude scintillation, and greater than average electron contents) the results are not indicative of the general properties of the ionosphere, but are representative of the kinds of information that may be extracted using this method of measurement and analysis.

The measurement of Faraday rotation angle variations in terms of the relative phase of the two circularly polarized components of the incoming wave permits a correction to be made to the first order theory coincidence point relations as well as permitting arbitrarily fine rotation angle measurement spacings. The interpretation of the Faraday angles in terms of electron content is subject to the ray path splitting conditions above.

From the passes selected for evaluation, the field point correction results in a 3% to 4% decrease in the total electron content as computed using the first order theory [Equation (2-6)]. The measurement and data reduction errors are of the order of 0.2%.

When total electron contents are computed to second order in X as well, two general points of interest emerge; (a) The electron content irregularities as observed using both the first and second order theories can differ both in scale size and peak enhancements and the differences can be considerable. This has also been observed by Rao and Yeh (1968). The first order electron content variations are usually smaller and the scale sizes estimated from the first order electron contents are often larger than the same parameters as measured using the second order theory. (b) Computation of the second order term ϵ from the first and second order electron contents reveals that associated with irregularities in total electron content there are often changes in electron density profile shape. These changes when referred to a parabolic layer suggest thickness and peak electron density changes as large as a factor of 2.

When the ordinary and extraordinary mode amplitudes are used with the Faraday information to compute the mean electron collision parameters $\bar{\nu}$, $\bar{\nu}'$, and $\frac{\bar{M}_\nu}{\bar{M}}$, several complementary features are observed.

(a) Large changes in electron density profile shape are often correlated with changes in F region temperature. While both increases and decreases in electron temperature have been observed, F region expansions on the days measured are most commonly associated with decreasing electron temperature. (Decreases as large as 25% over 72 km distances at F region altitudes have been observed.)

(b) On many occasions $\tilde{\nu}$ and ϵ agree with each other to within experimental error as expected from the theory for conditions of constant electron temperature and unchanging electron temperature profile.

(c) $\frac{\bar{M}_\nu}{\bar{M}}$ provides a measure of the vertical position of electron density irregularities in the ionosphere and may upon occasion be used to select lower ionosphere absorption events.

(d) In at least one case, March 20, 1968, a decrease in lower ionosphere absorption correlates with a spreading F region, a $\int N dh$ increase and an electron temperature decrease, thus suggesting the presence of a disturbance extending through a large (vertical) portion of the ionosphere.

A confirmation of geographically varying F region electron densities is provided by Roger (1964, fig. 2). From spaced ionosonde measurements at a given time, N_{MAX} was found to vary by 33% over a sub-ionosphere distance of 1^{o} geomagnetic latitude (equivalent to 0.6 minutes pass time) on a typical day of greater than normal F region disturbance.

Scintillation studies by Kamas and Jesperson (1964) have revealed changes by factors of 3 to 4 in the thickness of scintillating regions over comparable intervals but this may or may not be indicative of F region broadening.

The mean collision frequencies as measured in this experiment are of the correct order of magnitude when compared to the results of Setty, Jain and Vyawahare (1969).

A possible mechanism for the F region expansion is given by Rishbeth (1966) and Brace, Mayr, and Findlay (1969) on a global scale.

Rishbeth has shown that for the vertical drift parameter $W = v \frac{H_i}{D}$ where:

v is the vertical plasma drift velocity

H_i is the ion scale height

D is the diffusion constant at the F region peak

z is the reduced height $\frac{h-h_0}{H_i}$

$\frac{dw}{dz} > 0$ corresponds to an expanding F region and decreasing N_{MAX}

$\frac{dw}{dz} < 0$ corresponds to a contracting F region and increasing N_{MAX}, and $-\frac{\Delta N}{N} \approx 0.3 \frac{dw}{dz}$

The vertical displacement of the F region peak is not greatly affected by changes in $\frac{dw}{dz}$. Brace et al. have noted that an upwards drift implies increases in H_i, a downward drift implies decreases in H_i.

An upward drift of plasma into regions of smaller loss rate could account for the increase in total electron content observed in conjunction with an expanding layer.

The drop in electron temperature with constant average electron ion collision frequency, possibly indicates an increase in ion-neutral partical collision frequency caused by transport of other species into the F region which would, then, indirectly act as an energy sink for the thermal energy of the electrons.

Thus a qualitative description of the ionosphere may be formulated in terms of ionosphere vertical drifts.

From the data at hand, only $\frac{dw}{dz}$ may be conveniently computed. The remainder of the parameters require extensive model calculations.

For the F region contraction observed on March 23, the corresponding value of $\frac{dw}{dz}$ is -.6. For the F region expansion observed on March 20, the corresponding value of $\frac{dw}{dz}$ is 1.7. And for the electron content irregularities of March 17, the corresponding values of $\frac{dw}{dz}$ are 0.3, 0.7.

It must be noted that although the qualitative behavior of parameters is, as mentioned, compatible with vertical motions of the neutral gas, the effect observed is local not global.

CHAPTER 5

CONCLUDING REMARKS

The results in the preceding chapter clearly establish the combined differential Faraday, differential absorption approach to the analysis of beacon satellite transmissions as a powerful tool for investigations of spatial changes in several ionospheric parameters during a satellite pass.

The use of the phase comparison method of Faraday rotation angle measurements provides an experimental estimate of the maximum spatial resolution of Faraday electron contents, and permits a correction to the total rotation angle for the neglect of second order effects in the differential Faraday phase coincidence point relations.

Particular results of interest are as follows:

(a) The maximum spatial resolution of Faraday rotation derived electron contents in the vicinity of 40 Mhz is 1 km.

(b) The coincidence point corrections to the total electron contents are typically 3% to 4% of the measured content.

(c) The first order Faraday theory is misleading for both electron content gradient measurements and electron content scale size measurements under some conditions (as was noted by Rao and Yeh, 1968).

(d) Total electron content irregularities are often associated with changes in shape of the electron density profile in the F region and with corresponding changes in N.

(e) The mean collision frequencies computed by the differential absorption technique are of the correct order of magnitude when compared with the results of other workers.

(f) Electron temperature changes are at times associated with electron content irregularities.

(g) Lower ionosphere absorption events are at times detectable and sometimes coincide spatially with F region irregularities.

(h) The electron content, layer thickness, peak electron density and electron temperature changes measured in this experiment qualitatively behave as expected from the theories of vertical drifts of neutral particles. The effects, however, are local and not global, showing significant change in the required drift velocity over distances of the order of seventy km and thus require a different driving mechanism than the global temperature gradients. The rapid horizontal variation of parameters argues in favor of propagating disturbances but the rate at which the satellite scans the ionosphere is too great to permit computation of propagation velocities or directions using single point measurements.

It is the author's belief that continued experiments of this kind, combined with riometer absorption measurements and angle of arrival measurements using a slowly moving source (possibly solar interfurameter measurements) would be of value for examining the observed processes.

Local ionosonde measurements would also be of value to establish the bottom side profile for a more detailed examination of the variation of .

It is here proposed that an ionosonde be acquired by the Centre for Radio Science for use with experiments of this kind to provide the necessary auxiliary data for further computations.

APPENDIX A

CORRECTIONS TO AMPLITUDE MEASUREMENTS FOR ANTENNA EFFECTS OF TURNSTILE ANTENNA

Within a cone of 30° about the zenith, the Faraday rotation angle (Ω_f) may be related to the relative phase (φ_f) of the two circularly polarized components of the incoming plane wave by $\Omega_f = \frac{\varphi_f}{2}$ (Livingstone and Dixon, 1968).

Consider the ray path coordinate system $\hat{i}', \hat{j}', \hat{k}$ shown in figure A-1.

$\hat{i}'$ lies on a spherical shell concentric with the earth.

$\hat{j}'$ lies in the plane of the wave propagation direction and the zenith.

$\hat{k}$ is in the direction of propagation.

$\hat{i}, \hat{j}, \hat{k}$ is the ground coordinate system with $\hat{i}$ pointing east, $\hat{j}$ pointing north and $\hat{k}$ pointing down.

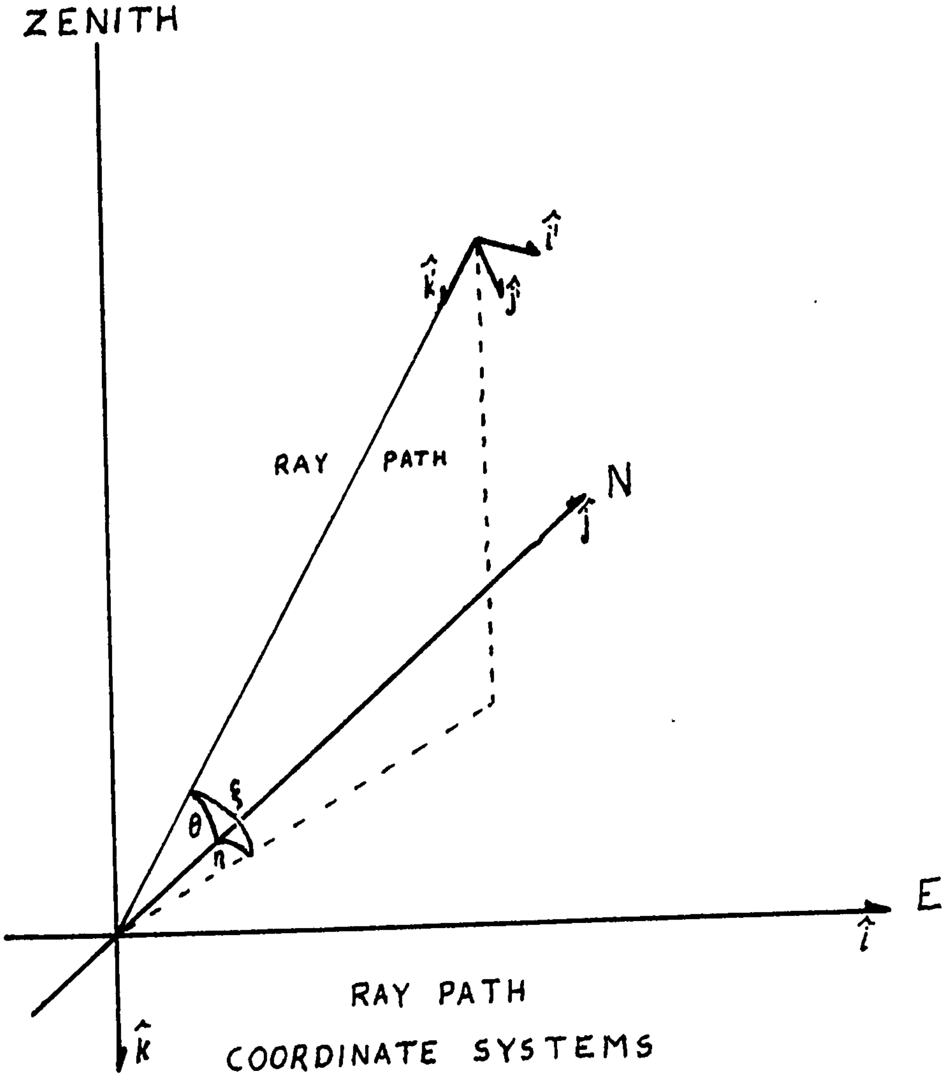

Figure A-1

In the ray path coordinate system $\hat{i}', \hat{j}', \hat{k}$ the two circular components of the wave field can be expressed as

$$\vec{E}_R = E_o \left(\hat{i}' \cos(\omega t + \varphi_f/2) + \hat{j}' \sin(\omega t + \varphi_f/2) \right)$$

(A-1)

$$\vec{E}_L = E_o \left(\hat{i}' \cos(\omega t - \varphi_f/2) - \hat{j}' \sin(\omega t - \varphi_f/2) \right)$$

where ω is the wave angular frequency, t is the time in seconds and E_o is a constant.

Transforming coordinates from the $\hat{i}, \hat{j}, \hat{k}$ system to the $\hat{i}', \hat{j}', \hat{k}$ system we have:

$$(A-2)\quad \begin{pmatrix} \hat{i}' \\ \hat{j}' \\ \hat{k}' \end{pmatrix} = \begin{pmatrix} \cos(\eta) & -\sin(\eta) & 0 \\ \sin(\xi)\sin(\eta) & \sin(\xi)\cos(\eta) & \cos(\xi) \\ -\cos(\xi)\sin(\eta) & -\cos(\xi)\cos(\eta) & \sin(\xi) \end{pmatrix} \begin{pmatrix} \hat{i} \\ \hat{j} \\ \hat{k} \end{pmatrix}$$

and thus the ground projections of $\vec{E}_R$ and $\vec{E}_L$ are given by:

$$\vec{E}_R = E_0 \{ \hat{i} [\cos(\eta)\cos(\omega t + \varphi_f/2) + \sin(\xi)\sin(\eta)\sin(\omega t + \varphi_f/2)] + \hat{j} [-\sin(\eta)\cos(\omega t + \varphi_f/2) + \sin(\xi)\cos(\eta)\sin(\omega t + \varphi_f/2)] \}$$

$$(A-3)\quad \vec{E}_L = E_0 \{ \hat{i} [\cos(\eta)\cos(\omega t - \varphi_f/2) - \sin(\xi)\sin(\eta)\sin(\omega t - \varphi_f/2)] - \hat{j} [\sin(\eta)\cos(\omega t - \varphi_f/2) + \sin(\xi)\cos(\eta)\sin(\omega t - \varphi_f/2)] \}$$

Assuming that the turnstile antennas are constructed from two ideal crossed dipoles, oriented in the $\hat{i}, \hat{j}$ directions respectively; the dipole gains are

$$(A-4)\quad g_i = \frac{\cos(\pi/2 \cos(\xi)\cos(\eta))}{\sqrt{1 - \cos^2(\xi)\cos^2(\eta)}}$$

and

$$(A-5)\quad g_j = \frac{\cos(\pi/2 \cos(\xi)\sin(\eta))}{\sqrt{1 - \cos^2(\xi)\sin^2(\eta)}}$$

The antenna output is proportional to the received power, so that

$$(A-6)\quad P_R = \{ g_i^2 [\cos(\eta)\cos(\omega t + \varphi_f/2) + \sin(\xi)\sin(\eta)\sin(\omega t + \varphi_f/2)]^2 + g_j^2 [-\sin(\eta)\cos(\omega t + \varphi_f/2) + \sin(\xi)\cos(\eta)\sin(\omega t + \varphi_f/2)]^2 \} P_0$$

and $$P_L = \{ g_i^2 [\cos(\eta)\cos(\omega t - \varphi_f/2) - \sin(\xi)\sin(\eta)\sin(\omega t - \varphi_f/2)]^2 + g_j^2 [\sin(\eta)\cos(\omega t - \varphi_f/2) + \sin(\xi)\cos(\eta)\sin(\omega t - \varphi_f/2)]^2 \} P_0$$

where P_R and P_L are the two instantaneous powers.

As $\omega >> \varphi_f/2$ $(\omega = 2\pi \times 4 \times 10^7 Hz, \varphi_f < 1 Hz)$ the detected receiver output will be

$$\begin{aligned} P_R = P_L = \{ & g_l^2 [\cos(\eta)\cos(\varphi_f/2) + \sin(\xi)\sin(\eta)\sin(\varphi_f/2)]^2 \\ & + g_j^2 [-\sin(\eta)\cos(\varphi_f/2) + \sin(\xi)\cos(\eta)\sin(\varphi_f/2)]^2 \} \\ & \times P_0 \end{aligned} \tag{A-7}$$

The antenna function is $f(\xi, \eta, \Omega) = P_R / P_0$ (figure A-2).

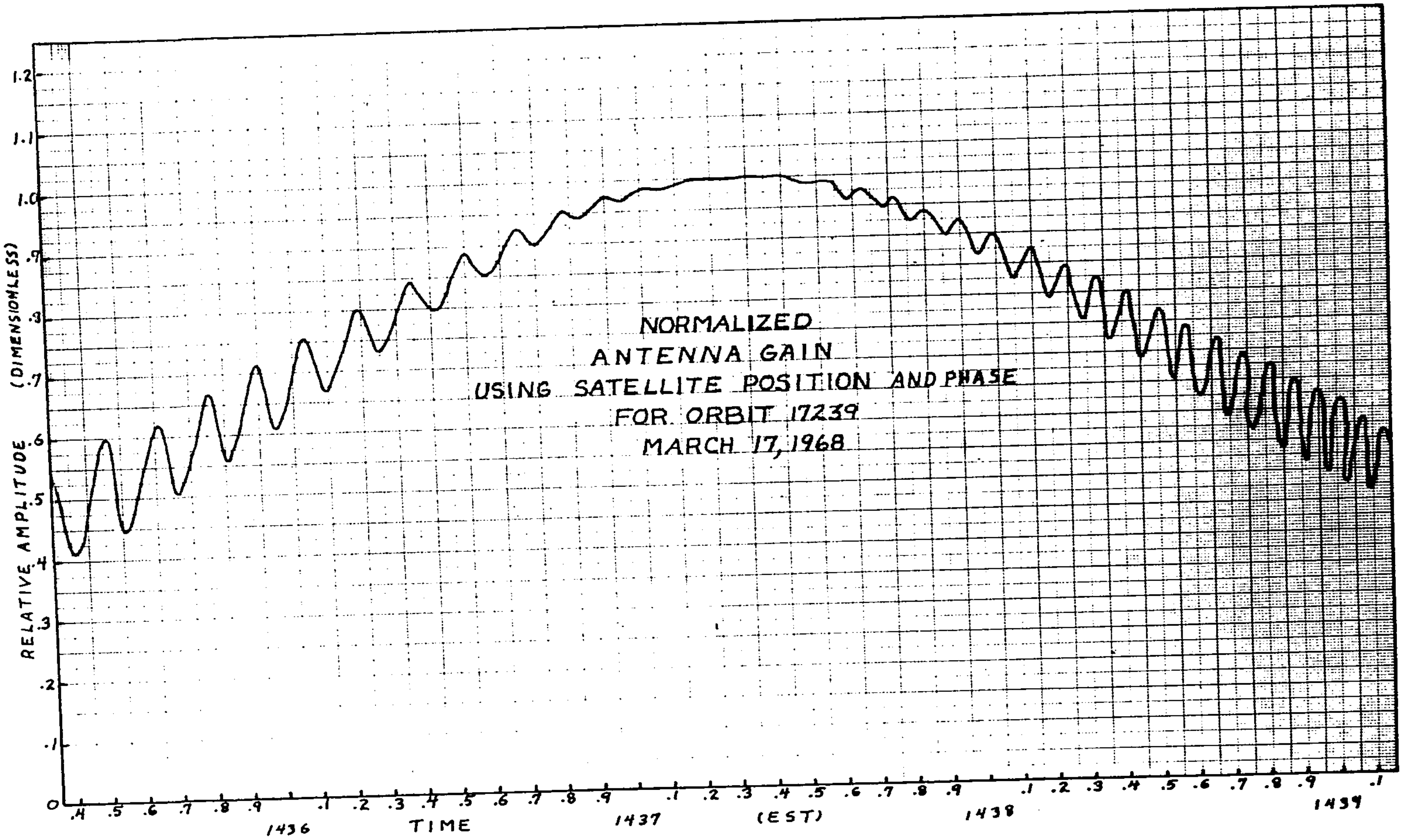
NORMALIZED
ANTENNA GAIN
USING SATELLITE POSITION AND PHASE
FOR ORBIT 17239
MARCH 17, 1968
RELATIVE AMPLITUDE (DIMENSIONLESS)
0
.1
.2
.3
.4
.5
.6
.7
.8
.9
1.0
1.1
1.2
TIME (EST)
1436
1437
1438
1439
.4 .5 .6 .7 .8 .9 .1 .2 .3 .4 .5 .6 .7 .8 .9 .1 .2 .3 .4 .5 .6 .7 .8 .9 .1 .2 .3 .4 .5 .6 .7 .8 .9 .1

Figure A-2

APPENDIX B

MODEL IONOSPHERE RAY TRACE

To estimate the refractive properties of the ionosphere in an ideal case consider a model ionosphere as follows:

(a) The model is spherically stratified with relative layer thickness chosen to produce approximately equal phase path lengths in each layer for radial propagation.

(b) The radial variation of electron density is an average midday profile at the peak of the sunspot cycle (Satellite Environments Handbook) with the bottom side of the profile adjusted to correspond to Ottawa ionosonde data (March 23/68 1400 EST). The radially integrated electron density is normalized to the total electron content measured at London, Ontario on March 23/68 1400 EST (fig. 1).

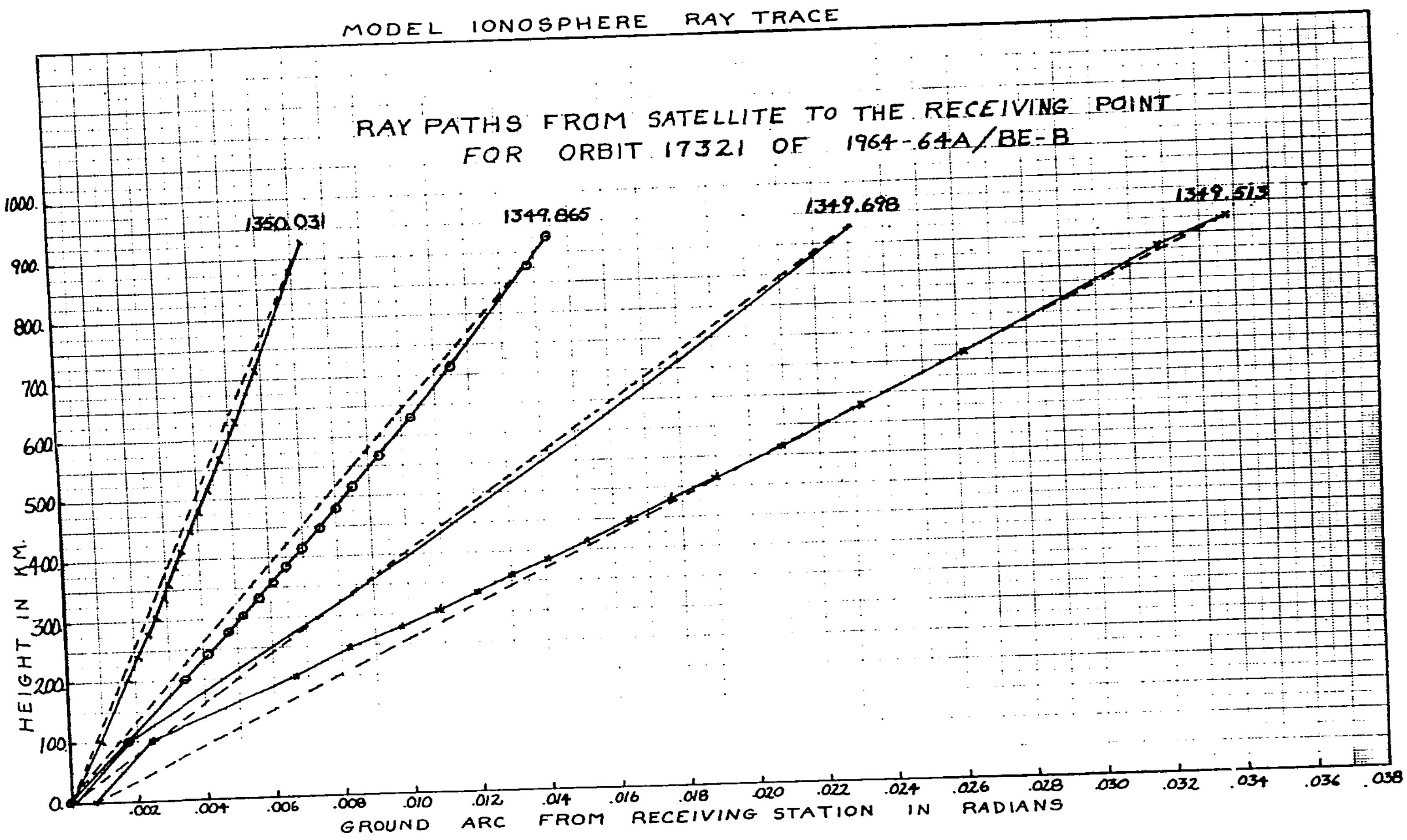
MODEL IONOSPHERE RAY TRACE
RAY PATHS FROM SATELLITE TO THE RECEIVING POINT
FOR ORBIT 17321 OF 1964-64A/BE-B
1350.031
1349.865
1349.698
1349.513
HEIGHT IN KM.
1000.
900.
800.
700.
600.
500.
400.
300.
200.
100.
0.
.002
.004
.006
.008
.010
.012
.014
.016
.018
.020
.022
.024
.026
.028
.030
.032
.034
.036
.038
GROUND ARC FROM RECEIVING STATION IN RADIANS

Figure B-1

(c) The earth's magnetic field is computed from a 48 coefficient spherical harmonic expansion.

Then, by tracing the ordinary and extraordinary rays through the model ionosphere, from the satellite to the receiving point for several satellite positions, we can estimate:

(a) The behavior of the rays in the ionosphere as a function of satellite position (fig. B-1).

(b) The variations of the Appleton-Hartree variables X, Y_L along the ray path, in an undisturbed ionosphere, containing no horizontal electron density gradients.

Starting at the satellite position (layer 1, height H, above the earth) with ray departure angle R_1, towards the next lower shell we have the situation shown in fig. B-2.

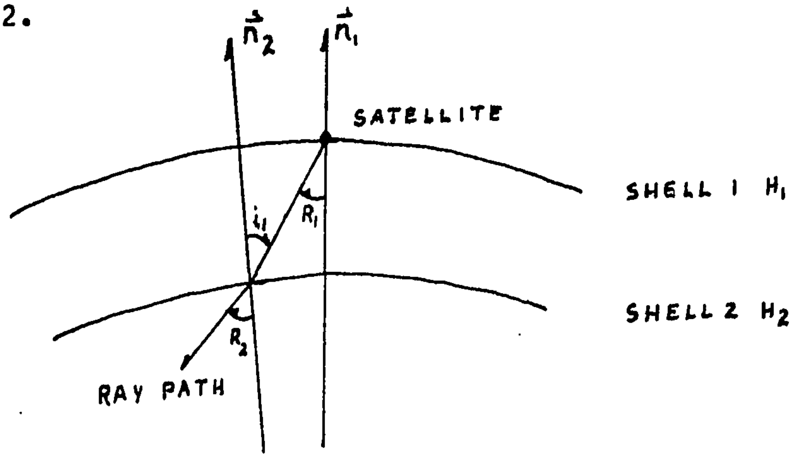

RAY TRACING A SLAB

Figure B-2

$\vec{n}_1$ is the earth normal (assuming a spherical earth) through the satellite position, $\vec{n}_2$ is the earth normal through the ray intersection with shell 2, the angle between $\vec{n}_1$, $\vec{n}_2$ at the center of the earth is

$$(B\text{-}1) \quad d\alpha_1 = \frac{(H_1 - H_2)\,\mathrm{TAN}\,(R_1)}{H_R + H_2 - H_1}$$

where H_R is the radial distance of shell 1 from the center of the earth. Then $i_1 = R_1 + d\alpha_1$ is the incidence angle of the ray on the next shell (shell 2). The ionosphere refractive indices in the high frequency, quasi longitudinal approximation are:

(a) ordinary mode

$$(B\text{-}2) \quad \mu_o^j = \sqrt{1 - \frac{X}{1 + Y_L}}$$

where the superscript j refers to the model layer considered and Y_L is computed at the ray intersection with the layer boundary.

(b) extraordinary mode

$$(B\text{-}3) \quad \mu_x^j = \sqrt{1 - \frac{X}{1 - Y_L}}$$

The neglect of ray curvature within a shell (due to variation of Y_L with height and central angle) introduces less error (in the high frequency approximation) than the shell model itself and so is a reasonable approximation. Snell's law may now be applied to the interface of the first and second shells to give

(B-4) $$R_{\substack{x\\o}}^{(2)} = \mathrm{SIN}^{-1}\left(\mu_{\substack{x\\o}}^{(1)}\,\mathrm{SIN}(R_1)/\mu_{\substack{x\\o}}^{(2)}\right)$$

In general, to perform the ray trace, the refractive indices $\mu_{\substack{x\\o}}$ must be known along the ray path. As this is not feasible at the outset of the calculation, preliminary estimates of Y_L are made along a linear ray path joining the satellite and the ground station. As each shell is considered in turn these estimates are refined by an iterative calculation involving the ray intersection position with the next shell.

Since the ray departure angle from the satellite was determined by the linear ray approximation, we do not expect that either of the rays traced will intersect the earth's surface at the receiving station. Since the ordinary, extraordinary ray refractive indices are not equal we do not expect that both rays will intersect the earth's surface at the same point. The ray trace must then proceed iteratively with each ray traced through the model ionosphere individually and the initial departure angle recomputed until the ray intersects the earth at the receiving point.

Consider a ray of either mode departing from the $j-1$ shell at an angle R_j --it intersects the shell at $j+1$ at an angle i_j where

(B-5) $$i_j = R_j + d\alpha_j \quad ,$$

(B-6) $$d\alpha_{j+1} = \frac{(H_j - H_{j+1})\,TAN(R_j)}{H_R - H_1 + H_{j+1}}$$

and $\vec{n}_j$ is in the plane of the ray path and the receiving station normal at a central angle

(B-7) $$\delta_j = \alpha - \sum_{K=1}^{j} d\alpha_K$$

(α is the central angle from the satellite to the receiver) from the receiving station. The ray path length in the j shell is

(B-8) $$S_j = \frac{H_j - H_{j+1}}{COS(R_j)}$$

At $\vec{n}_{j+1}$, Y_L and thus $\mu^{(j)}$ are recomputed and Snell's law is applied to the $j, j+1$ layer boundary using the corrected $\mu^{(j)}$ in the j layer and the linear ray path estimate of $\mu^{(j+1)}$

(B-9) $$R_{j+1} = SIN^{-1}(\mu^{(j)} SIN(i_j) / \mu'^{(j+1)})$$

(where the $'$ denotes first approximation). $Y_{L_{j+1}}$ is now recomputed for the angle R_{j+1} at $\vec{n}_{j+1}$ and $\mu^{(j+1)}$ is re-evaluated. We return to Snell's law and recompute R_{j+1}. Iteration continues until a preset internal consistency estimate is reached for μ^{j+1}.

The computation proceeds stepwise to the earth's surface (m shell) where the residual $\delta_m = \alpha - \sum_{K=1}^{m} d\alpha_K$ is examined to determine the initial departure angle correction.

If ξ is the ground elevation angle of the linear ray path, R its length and R_0 the radius of the earth, the angle subtended at the satellite by the receiving station and the ray impact point is

(B-10) fig. B-3 $\Delta \approx \delta_m \frac{R_0}{R} \sin(\xi)$

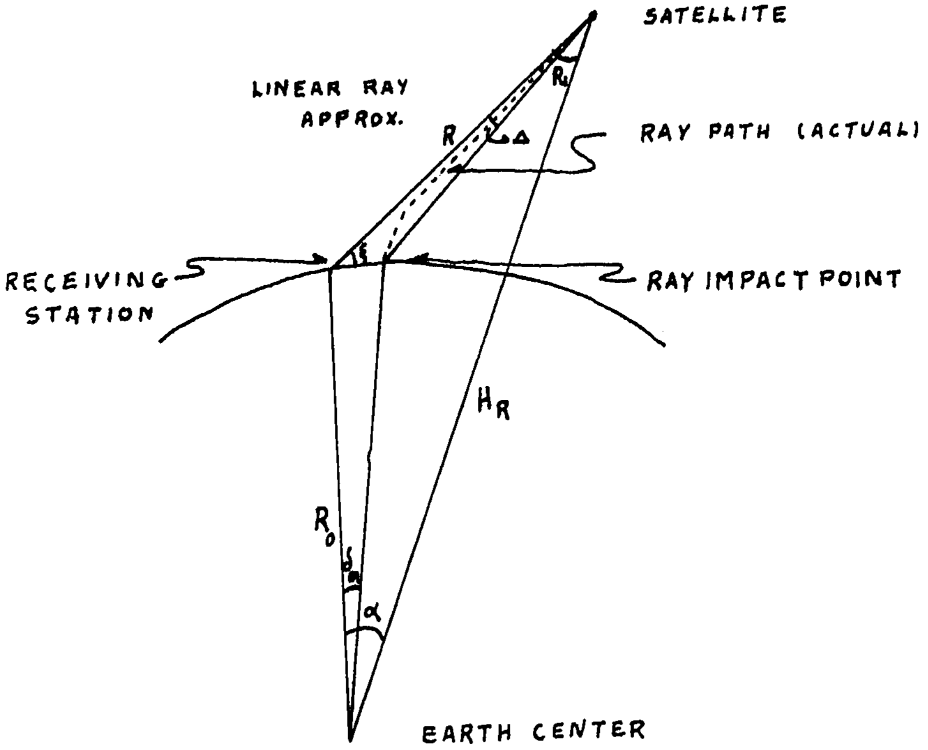

Figure B-3

The initial angle is then corrected to $R_1' = R_1 + \frac{\Delta}{2}$ and the ray trace is redone. Iteration continues until $\delta_m R_0$ comes within a specified range of the receiving station.

APPENDIX C

To consider the qualitative behavior of the terms $\int_0^{h_s} X\,dh$, $\int_0^{h_s} X^2\,dh$ (c_T and δ) of the discussion at the end of section 2.3, let us consider a simple minded model of the F region of the ionosphere. Let the F region of the ionosphere have a parabolic electron density distribution with a peak at height h_0 and a half width at $X=0$ of h' (fig. C-1), and let z be $h-h_0$ for some point on the profile.

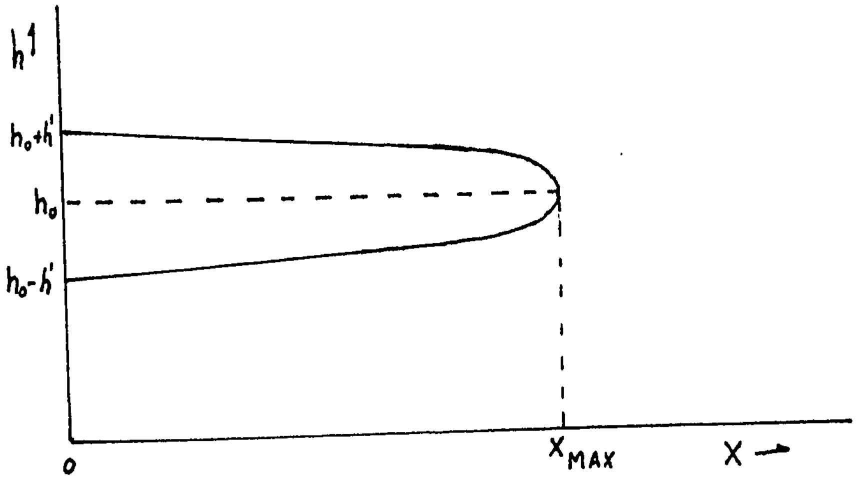

Figure C-1

then $X = az^2+b$ where $b = X_{MAX}$ and $a = -X_{MAX}/h'^2$. The total electron content of such a layer is $\int_0^{h_s} N\,dh \propto \int_{h_0-h'}^{h_0+h'} (az^2+b)\,dh$

or $\int_0^{h_s} X\,dh = 4/3\ X_{MAX}\ h'$. Similarly $\frac{1}{2}\int_0^{h_s} X^2 dh = \frac{8}{15}\ X^2_{MAX}\ h'$.

If we write $X_{MAX}\,h' = \bar{c}$,

(C-1) $\frac{1}{2}\int_0^{h_s} X^2 dh = \bar{c}\ (8/15\ X_{MAX})$

and the ratio

(C-2) $\frac{1}{2}\int_0^{h_s} X^2 dh \Big/ \int_0^{h_s} X\,dh = \frac{2}{5}\ X_{MAX}$

depends solely on the behavior of X_{MAX} .

This model, it must be reiterated, may not be used for quantitative estimates of actual X_{MAX} and layer thickness changes in the ionosphere--it should, however, suffice to provide a basis for comparison of the behavior of these quantities during different satellite passes.

REFERENCES

Abdu, M. A., and Degaonkar, S. S., J. Geophys. Res. 72(21), 5559 (1967).

Abdu, M. A., Degaonkar, S. S., and Ramathan, K. R., J. Geophys. Res. 72(5), 1547 (1967).

Aikin, A. C., and Blumle, L. J., Geophys. Res. 73(5), 1617 (1968).

Aitchison, G. J., and Weekes, K., J. Atmosph. Terr. Phys. 14, 236 (1959).

Allen, R. S., J. Atmosph. Terr. Phys. 31, 289 (1969).

Blackband, W. T., et al., Nature 183, 1 (1959).

Bowhill, S. A., J. Atmosph. Terr. Phys. 13, 175 (1958).

Brace, L. H., Mayr, H. G., and Findlay, J. A., J. Geophys. Res. 74(11), 2952 (1969).

Brace, L. H., and Spencer, N. W., J. Geophys. Res. 68(19), 5397 (1963).

Briggs, B. H., and Parkin, I. A., J. Atmosph. Terr. Phys. 25, 339 (1963).

Browne, I. C., Evans, J. V., Hargreaves, J. K., and Murray, W. A. S., Proc. Phys. Soc. 69, 901 (1956).

Canadian Department of Transport, Canadian Ionospheric Data, Ottawa, 1968.

Degaonkar, S. S., and Abdu, M. A., J. Atmosph. Terr. Phys. 30, 555 (1968).

Dixon, A. F., Ph.D. Thesis, Centre for Radio Science, University of Western Ontario, August, 1969.

Dixon, A. F., and Livingstone, C. E., University of Western Ontario Center for Radio Science Report HA-13 (1969).

Dyson, P. L., J. Atmosph. Terr. Phys. 29, 857 (1967).

Evans, J. V., J. Geophys. Res. 73(11), 3489 (1968).

Evans, J. V., J. Geophys. Res. 72(13), 3343 (1967).

Evans, J. V., J. Atmosph. Terr. Phys. 11, 259 (1957).

Garriot, O. K., J. Geophys. Res. 65, 1139 (1960).

Garriot, O. K. and de Medonca, F., J. Geophys. Res. 68(17), 4917 (1963).

Hanff, E. S., Dixon, A. F., and Chess, G. F., C.A.S.I. Transactions 1(2), 68 (1968).

Jespersen, J. L., and Kamas, G., J. Atmosph. Terr. Phys. 26, 457 (1964).

Jolley, L. E. W., "Summation of Series." Dover Publications Inc., New York (1961).

Kaiser, A. B., and Preddy, G. F., J. Atmosph. Terr. Phys. 30, 285 (1968).

Kane, J. A., J. Atmosph. Terr. Phys. 23, 338 (1962).

Kent, G. S., J. Atmosph. Terr. Phys. 22, 225 (1961).

Kushnir, V. M., M.Sc. Thesis, University of Western Ontario (1966).

Liszka, L., Radio Science 1(10), 1135 (1966).

Liszka, L., and Taylor, G. N., J. Atmosph. Terr. Phys. 27, 843 (1965).

Little, C. G., and Lawrence, R. S., J. Res. Nat. Bur. Standards 64D(4), 335 (1960).

Livingstone, C. E., and Dixon, A. F., University of Western Ontario Center for Radio Science Report HA-10 (1968).

Lyon, G. F., Can. J. Phys. 43, 1059 (1965).

Maude, A. D., and Pramanik, M. A. H., J. Atmosph. Terr. Phys. 29, 1311 (1967).

Muldrew, D. B., J. Geophys. Res. 68(19), 5355 (1963).

Münther, C., Radio Science 1, 1141 (1966).

Murray, W. A. S., and Hargreaves, J. K., Nature 13, 944 (1954).

Parkin, I. A., J. Atmosph. Terr. Phys. 29, 1135 (1967).

Piggot, W. R., and Thrane, E. V., J. Atmosph. Terr. Phys. 28, 311 (1966).

Rao, N. Narayana, J. Geophys. Res. 72(11), 2929 (1967).

Rao, N. Narayana, and Yeh, K. C., J. Geophys. Res. 73(7), 2447 (1968).

Ratcliffe, J. A., Magneto-ionic Theory and its Applications to the Ionosphere, Cambridge University Press (1959).

Ratcliffe, J. A., Reports on Progress in Physics 19, 188 (1956).

Rishbeth, H., Rev. Geophys. 6(1), 33 (1968).

Rishbeth, H., J. Atmosph. Terr. Phys. 29, 225 (1967).

Roger, R. S., J. Atmosph. Terr. Phys. 26, 499 (1964).

Roger, R. S., J. Atmosph. Terr. Phys. 26, 475 (1964).

Ross, W. J., and Kuntman, D., J. Geophys. Res. 72(3), 1041 (1967).

Setty, C. S. G. K., Jain, A. R., and Vyawahare, M. K., J. Atmosph. Terr. Phys. 31, 883 (1969).

Singleton, D. G., J. Geophys. Res. 74(7), 1772 (1969).

Singleton, D. G., and Lynch, G. J. E., J. Atmosph. Terr. Phys. 24, 375 (1962).

Thrane, E. V., and Piggot, W. R., J. Atmosph. Terr. Phys. 28, 721 (1966).

Titheridge, J. E., J. Geophys. Res. 68, 3399 (1963).

Titheridge, J. E., J. Atmosph. Terr. Phys. 30, 73 (1968).

Titheridge, J. E., J. Geophys. Res. 73(9), 2985 (1968).

Yeh, K. C., J. Geophys. Res. 65(8), 2548 (1960).

Yeh, K, C., and Flaherty, B. J., J. Geophys. Res. 71(19), 4557 (1966).

Yeh, K. C., and Gonzalez, V. H., J. Geophys. Res. 65(10), 32-09 (1960).

Yeh, K. C., and Swenson, G. W. Jr., J. Geophys. Res. 66(4), 1061 (1961).